

Forschungszentrum Karlsruhe
Technik und Umwelt

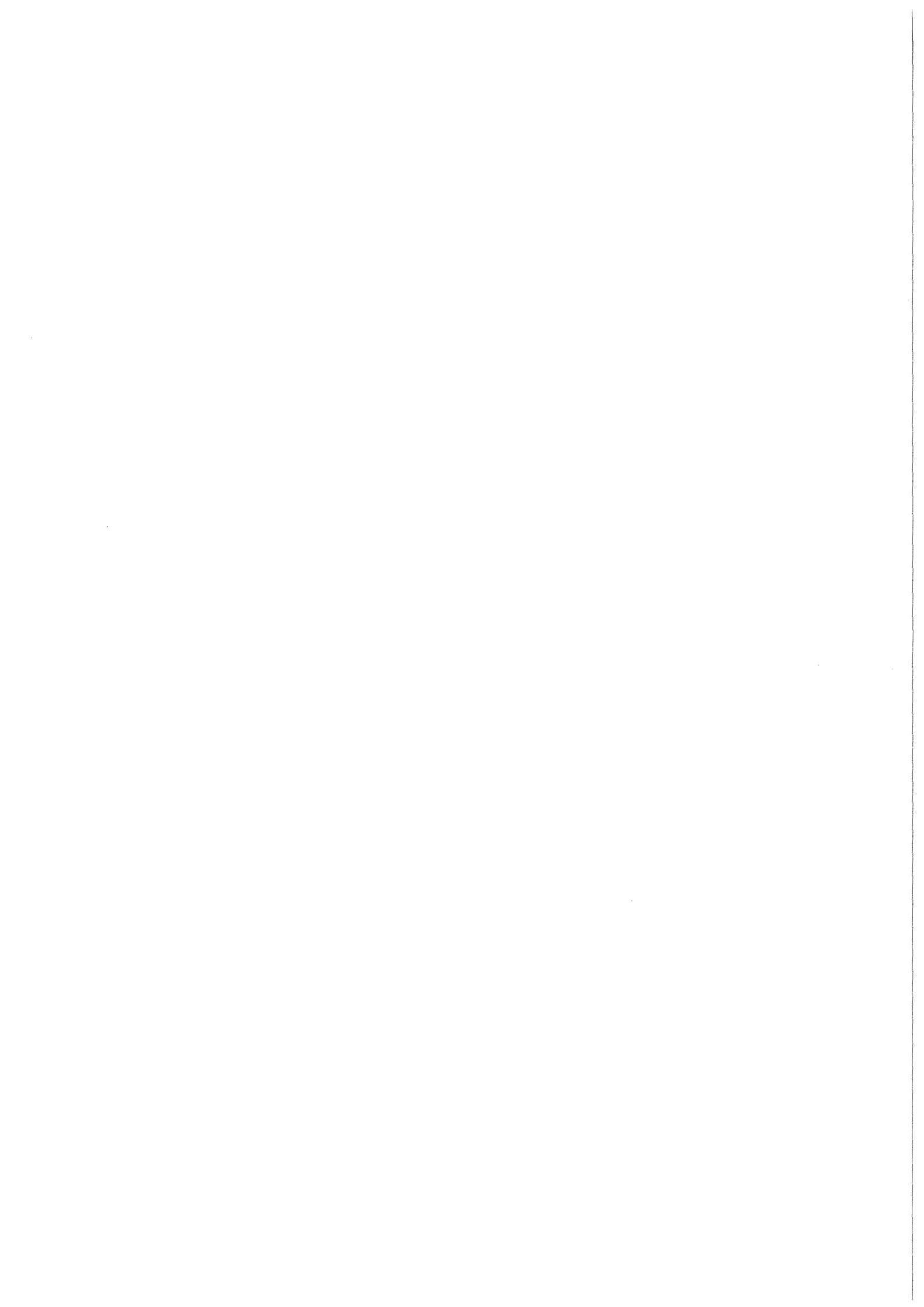
Wissenschaftliche Berichte
FZKA 5821

**The MEKKA-facility a
Flexible Tool to Investigate
MHD-flow Phenomena**

L. Barleon, K.-J. Mack, R. Stieglitz

Institut für Angewandte Thermo- und Fluidodynamik
Projekt Kernfusion

September 1996



FORSCHUNGSZENTRUM KARLSRUHE
Technik und Umwelt
Wissenschaftliche Berichte
FZKA 5821

The MEKKA-facility
a flexible tool to investigate MHD-flow
phenomena

L. Barleon, K.-J. Mack, R. Stieglitz

Institut für Angewandte Thermo- und Fluidodynamik
Projekt Kernfusion

Forschungszentrum Karlsruhe GmbH, Karlsruhe
1996

Als Manuskript gedruckt
Für diesen Bericht behalten wir uns alle Rechte vor

Forschungszentrum Karlsruhe GmbH
Postfach 3640, 76021 Karlsruhe

ISSN 0947-8620

Das MEKKA Labor- eine flexible Einrichtung zur Untersuchung von MHD-Strömungsphänomenen

Zusammenfassung:

Dieser Bericht beschreibt den Aufbau der Versuchsanlage MEKKA (Magneto-hydrodynamische Experimente in Natrium Kalium Karlsruhe) im Institut für Angewandte Thermo- und Fluidodynamik (IATF) am Forschungszentrum Karlsruhe Technik und Umwelt.

Die ursprüngliche Motivation für den Bau der MEKKA-Anlage war die Untersuchung magnetohydrodynamischer Strömungen bei hohen Magnetfeldern, wie sie in der Kernfusion auftreten. Daneben werden andere Themengebiete der Magnetohydrodynamik (MHD) angesprochen, die in Zukunft verstärkt Beachtung finden werden. Zum besseren Verständnis der in der Magnetohydrodynamik auftretenden Effekte und Phänomene erfolgt in diesem Bericht zunächst eine kleine Einführung in die Gedankenwelt der MHD. Anschließend wird der Prozeß der Auswahl geeigneter Flüssigmetalle sowohl im Hinblick auf den Betrieb wie auch umwelttechnischer Aspekte beleuchtet. Den größten Raum innerhalb dieses Berichtes nimmt die Auslegung und der Aufbau der flüssigmetallbetriebenen Kreisläufe inklusive der zugehörigen Komponenten ein. In einem weiteren Abschnitt werden Wirkprinzipien und Meßverfahren, die in der MHD benutzt werden, aufgezeigt und diskutiert. Abschließend werden aus der Vielzahl der in der MEKKA-Anlage durchgeführten Experimente einige besonders wichtige Ergebnisse aufgezeigt und deren Konsequenzen in Hinblick auf den Einsatz in technischen Komponenten diskutiert.

Dieser Bericht gibt den Stand des MEKKA-Labors im Juli 1996 wieder.

Abstract:

This report describes the design of the MEKKA facility of the Institute of Applied Thermo- and Fluidynamics (IATF) at the Research Centre Karlsruhe.

Besides the original motivation of the MEKKA laboratory to measure fusion relevant magnetohydrodynamic (MHD) flows other possible MHD topics which may gain importance in the future are outlined. After a short introduction into the basics of magnetohydrodynamics the major MHD flow problems appearing in liquid metal cooled fusion blankets are addressed. Later the selection process of the liquid metal used in the experimental facility is discussed under operational and environmental aspects. The main description is focussed on the design and the construction of the liquid metal loops including all relevant components. Another section deals with the discussion of the measurement techniques commonly used in MHD and their accuracy and applicability to specific configurations. Finally some of the major experimental results obtained in the MEKKA-facility are outlined and their consequences with respect to the use in technical components are discussed.

This report represents the state of the MEKKA facility in July 1996.



Table of Content

1 Introduction.....	5
1.1 Technical background of MHD research	5
1.2 A view beyond fusion blanket applications	6
1.3 Aims and limitations of the experimental facility.....	7
2 Magnetohydrodynamics (MHD).....	9
2.1 Derivation of a simple pressure drop correlation in a duct flow	9
2.2 Transport equations, characteristic numbers and boundary conditions	11
2.3 Fully developed MHD duct flows	14
2.4 Three-dimensional MHD-Phenomena	19
3 Fusion reactor blankets with liquid metal as coolant.....	21
3.1 The principle of the fusion process.....	21
3.2 Blanket concepts and design limitations	23
3.3 Flow configurations and flow geometries appearing in blankets.....	29
4 The MEKKA-program and the design formulation	31
5 Coolant/operating liquid	33
5.1 Commonly available liquids and formulation of requirements	33
5.2 Transferability of experimental results.....	33
5.2 Velocity distribution and pressure drop.....	37
5.3 Operation procedures	39
5.3.1 Operation technology.....	39
5.3.2 Safety aspects.....	41
5.4 Determination of the coolant material	42
6 The magnets.....	43
6.1 General.....	43
6.2 The MA-magnet	43
6.2.1 The power supply	44
6.2.2 The water-cooling system	45
6.2.3 Magnetic field strength and field distribution of the MA-magnet.....	46
6.3 The super-conducting CELLO-magnet	48
6.3.1 The liquid helium supply	49
6.3.2 The vacuum system	52
6.3.3 Operation/control/security systems.....	54
6.3.4 Magnetic field strength and field distribution of the CELLO magnet.....	55
7 The sodium-potassium loop	58
7.1 Mechanical setup	58
7.2 The loop scheme.....	59

7.2.1	The operational loop.....	61
7.2.2	The inertgas system	67
7.2.3	The purification loop	68
7.3	Control and operation of the sodium-potassium loop	70
8	The gallium-indium-tin loop (GALINKA).....	73
8.1	The design features of the gallium-indium-tin loop	73
8.2	The pump design	75
8.3	The heat exchanger.....	78
9	Measurement techniques in liquid metal MHD	79
9.1	General remarks	79
9.2	Flow rate measurement devices.....	79
9.3	Pressure difference measurement methods	81
9.4	Surface potential measurement method	85
9.5	Temperature measurement principle and error sources	86
9.5.1	The Nernst-Ettingshausen effect	88
9.5.2	The Righi-Leduc effect	89
9.5.3	The Seebeck-effect	89
9.5.4	Galvano-magnetic effects.....	90
9.6	Local measurements within the liquid metal	90
9.6.1	Some general remarks.....	90
9.6.2	The potential probe (LEVI-probe) and the applicability in MHD-flows	93
9.6.3	The hot wire anemometer	96
9.6.4	The temperature pulse method	98
9.6.5	The pitot tube.....	100
9.6.6	Fibre-mechanical method	100
9.6.7	Ultrasonic measurement probes.....	100
9.6.8	Traversing mechanisms	101
10	The data acquisition system	102
10.1	The steady state system SPECTRA.....	102
10.2	The fast acquisition system DT and DAS.....	104
11	MHD-experiments performed in MEKKA	106
11.1	Fully developed MHD-flows	106
11.2	Three-dimensional MHD-flows.....	109
12	Summary and future program.....	128
13	References.....	132
	Appendix A.....	137
	Abbreviations, Variables and characteristic numbers.....	139

1 Introduction

1.1 Technical background of MHD research

At the Research Center Karlsruhe (FZK) breeder blankets for fusion power reactors like the planned ITER and in a later stage DEMO are being developed as part of the European blanket development program.

Fusion blankets are essential components of fusion power reactors in which the high neutron and γ -radiation energy from the plasma is transferred to utilisable thermal energy and where, moreover, the fuel component for nuclear fusion tritium is bred by the reaction of neutrons with lithium. The location of the blanket in the fusion reactor and a brief description of the working principle of a fusion reactor is given in section §3.1.

For several technical reasons liquid metals are considered as breeder material and coolant. Pure lithium or lead-lithium alloys are attractive breeder materials in fusion power reactor blankets since they are immune to irradiation damage and additionally offer tritium self-sufficiency without any additional neutron multiplier. These so called self-cooled liquid metal blankets are particularly attractive because the high thermal conductivity of liquid metals facilitates robust and rather simple blanket designs. Using liquid metals a fusion blanket can be designed in form of a simple and robust self-supporting structure of coolant channels.

As the blankets have to be placed within the plasma-confining strong magnetic fields (4-7 Tesla) of a Tokamak reactor, the electrically well conducting coolant encounters strong electromagnetic forces which may give rise to pressure losses intolerable with regard to the structural stresses and may generate local flow distributions in the channels unfavourable for uniform cooling of the plasma facing first wall. Therefore, a detailed knowledge of the magnetohydrodynamic (MHD) characteristics of liquid metal flows in coolant channels and systems is of crucial importance for the proper design of self-cooled blankets.

There are numerous ideas, concepts and research activities dealing with the above issues. During the past ten years a lot of work has been dedicated to investigate both experimentally and theoretically MHD-problems associated with the design of liquid metal fusion breeder blankets (Hua et al. 1994, Malang et al. 1988, 1994, Smith et al. 1985). The Forschungszentrum Karlsruhe (FZK) in collaboration with the Argonne National Laboratory (ANL) and the Institute of Physics of the Latvian Academy of Science in Riga (LAS) is actively taking part in the design of self-cooled blankets and the related MHD-research. An overview over the main flow configurations which has to be solved for technically viable fusion blanket designs is given in section §3.2 of this report.

1.2 A view beyond fusion blanket applications

The detailed knowledge of the specific properties of magnetohydrodynamic flows is not of particular interest to fusion applications only. MHD-effects are frequently used in industrial and manufacturing processes where we are mostly unconsciously taking advantage of the specific features of these components. However, not only in technology but also in nature magnetohydrodynamic phenomena appear. In this section the authors give you a small view of the already used and the possible use of MHD-means to control technical processes or to describe phenomena taking place in nature in order to outline the necessity to investigate both experimentally and theoretically MHD flow phenomena.

The most commonly used MHD-device is probably the electromagnetic flow meter, which measures the average flow rate of an electrically conducting fluid through a duct. Even weakly electrically conducting fluids like water can be measured using this technique. In the chemical and metallurgical industry MHD induction and conduction pumps are utilised to transport aggressive, chemical reactive or extremely hot ($> 1800^{\circ}\text{C}$) fluids without contact to pressure bearing walls or rotating mechanical compression parts. MHD-means are also used for homogenising glass, contactless mixing of alloy materials into molten steel and pressure casting of titanium.

A gate to a new field for MHD research is opened by the computer industry, which needs large silicon crystals of rather high homogeneity. Since molten silicon owns a high electrical conductivity magnetic fields (steady and oscillating ones) can be used to control the crystallisation process at the fluid-crystal interface. The implementation of MHD-means in this technology facilitates the opportunity to control the convection in a desired way in the bath upon the crystal, and moreover, offers the possibility to realise a defined dotation of the crystal and an enlargement of the crystal size. In order to study the applicability of MHD-means in this field currently an experimental facility (SIKKA) is built at the Institute of Thermo- and Fluidynamics (IATF) of the Forschungszentrum Karlsruhe.

But MHD is not only of relevance with respect to technical applications. The interaction of electromagnetic and rotational forces is responsible for sun spots and the development of polar light. Also the existence of the earth magnetic field is based on MHD-effects. The convection driven by the temperature difference between the earth inner core and outer mantle, the rotational forces and Eckmann forces lead to a flow pattern in which any magnetic perturbation is amplified. In order to demonstrate this phenomenon experimentally, which is called the "*homogeneous dynamo-effect*", an experimental facility (GEODYNAMO, Stieglitz et al. 1996) is being built up in the Institute for Applied Thermo- and Fluidynamics (IATF) of the Forschungszentrum Karlsruhe.

1.3 Aims and limitations of the experimental facility

The strongest electromagnetic-viscous and electromagnetic-inertial interactions in MHD-flows appear in the field of fusion technology. Therefore, these technology forms the highest demands on an experimental facility.

In order to conduct fusion blanket relevant MHD experiments two essential components are required. First a magnet which owns a sufficiently large experimental volume of high and rather homogeneous magnetic field strength and second a liquid metal loop, which is capable covering the whole fusion relevant parameter range.

To meet these demands at the IATF the experimental facility MEKKA (Magneto-hydrodynamik Experimente in Natrium-Kalium Karlsruhe) has been designed and built up in the IATF. This report describes the main ideas of the design considerations on which MEKKA is based on and the setup of the facility MEKKA in its current state (April 1996).



2 Magnetohydrodynamics (MHD)

The expected pressure drop and the related velocity distribution of a MHD duct flow in a fusion blanket are of significant importance for a self-cooled liquid metal blanket concept. The combined tasks to be fulfilled by the blanket have already been outlined in the introduction. Nevertheless the reader should keep in mind in this chapter, that the main task of a self-cooled blanket is to remove the heat from the plasma facing hot wall within acceptable pressure drops tolerable to available structural materials. In this section first a simple pressure drop correlation is derived, before the main transport equations, boundary conditions and scaling parameters are described. Since velocity distribution as well as the pressure drop reveals features unknown in conventional hydrodynamics the principle physics of magnetohydrodynamic phenomena are described in section §2.3.

2.1 Derivation of a simple pressure drop correlation in a duct flow

The magnetohydrodynamics is located at the border between two fields of the classical physics, the electrodynamics and the fluid dynamics. The complete formulation of a MHD flow demands the coupling of the electrodynamic terms given by the Maxwell equations with the Navier-Stokes equation of ordinary hydrodynamics. In order to introduce the reader in the world of MHD and to outline the principle differences between a hydrodynamic and a magnetohydrodynamic flow a simple derivation of a pressure drop correlation is deduced below.

Consider a duct of the height $2a$, the width $2b$, the wall thickness t_w and the length l placed in an uniform constant magnetic field of the strength B_0 , as shown in figure 2.1. Through this duct a liquid metal with the specific electrical conductivity σ flows with a slug flow profile of the average velocity v_0 . The assumption of a slug flow velocity profile is for the following deduction necessary and for large magnetic fields, not too high velocities and well conducting fluids justified.

Due to the fluid motion perpendicular to the magnetic field lines an electric field according the "*three-finger-rule*" is induced. The induced voltage U_{ind} can be calculated with equation 2.1.

$$U_{ind} = 2 b v_0 B_0 \quad (2.1)$$

Because of this potential difference an electric current I is driven, which can short circuit via the liquid metal and the electrically conducting duct walls. These electric currents themselves lead to Lorentz-forces which are perpendicular to the externally applied magnetic field.

In the so-called core of the duct flow the Lorentz-forces are opposite to the applied

external pressure gradient produced by the pump. In the boundary layers at walls normal to the magnetic field the Lorentz-forces act in flow direction. These walls are called Hartmann walls and the adjacent boundary layers are the Hartmann layers. In the Hartmann layers exists an equilibrium of Lorentz and viscous forces. Walls aligned in magnetic field direction are named side walls.

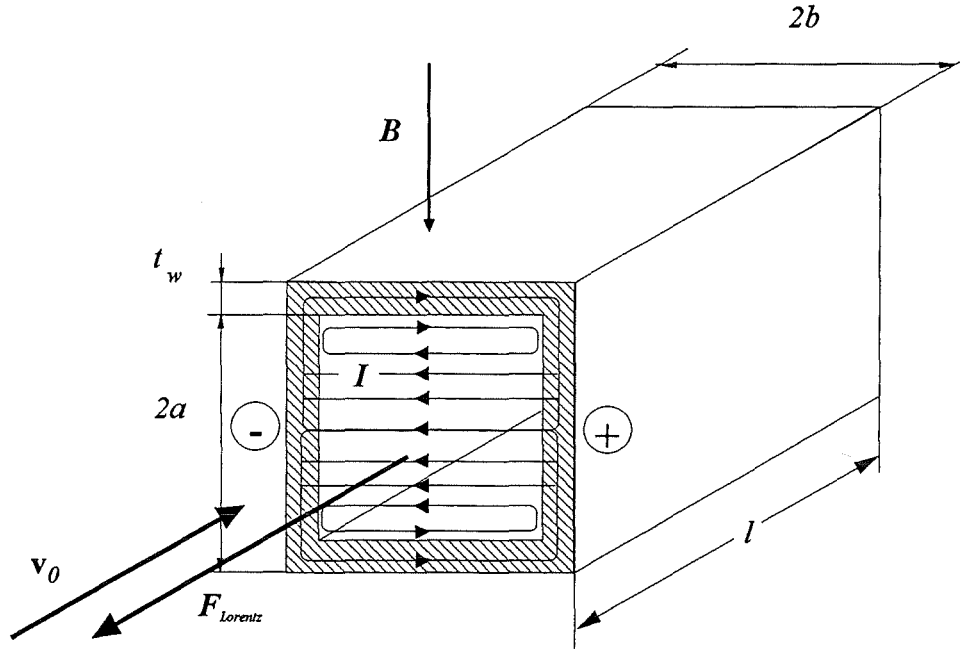


Figure 2.1: Sketch of MHD-duct flow in a rectangular duct with electrically conducting walls.

In the following considerations the electrical resistance of the boundary layers is considered to be negligible, so that an electrical circuit for the flow problem as shown in figure 2.2b can be assumed. The magnitude of the electric currents, which determines Lorentz forces in the *core* of the duct, depends on the ohmic resistances in the circuit. The resistance of the fluid R_f and the resistances of the walls R_w are:

$$R_f = \frac{2 b}{\sigma a l} ; R_w = \frac{2 b}{\sigma_w t_w l} \quad (2.2)$$

Using Ohms law for the electric current I in the fluid yields equation 2.3.

$$I = \frac{U_{ind}}{R_f + R_w} \quad (2.3)$$

The Lorentz-force acting on the ducts cross section opposite the applied pressure gradient is then:

$$F_{Lorentz} = I B_0 2 b \quad (2.4)$$

A force balance of pressure and Lorentz-forces $F_{Lorentz}$ leads finally to an expression for the pressure drop in the following way.

$$\Delta p = \frac{F_{Lorentz}}{2ba} = \sigma v_0 B_0^2 l \frac{c}{1+c} \quad (2.5)$$

Herein, c is the wall conductance ratio. c describes the ratio between the electric resistance of the fluid and that of the wall and is defined by

$$c = \frac{\sigma_w t_w}{\sigma a} \quad (2.6)$$

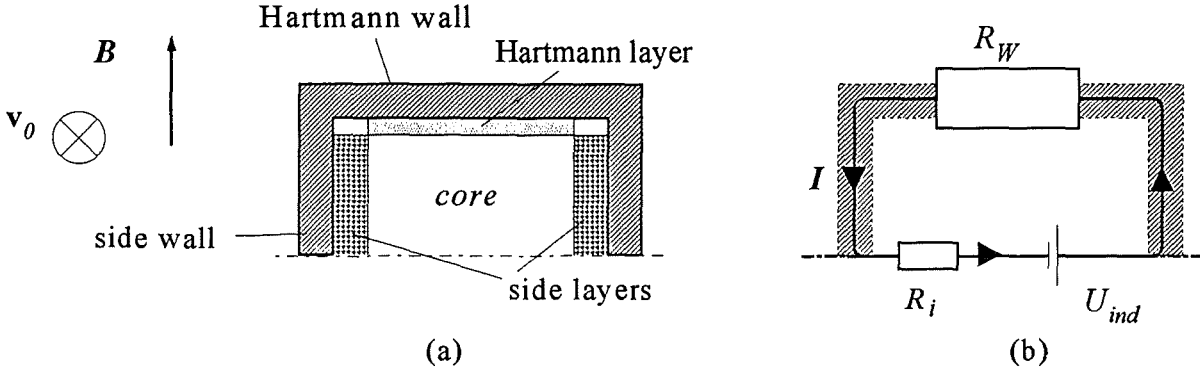


Figure 2.2: (a) boundary layers appearing in a MHD flow. (b) Simplified electrical circuit for a MHD flow in a duct with electrically conducting walls.

The relation 2.5 shows some characteristic features of MHD flows. The pressure drop in a duct is proportional to the square of the magnetic field strength. The pressure drop in a duct can be minimised by increasing the electric resistance of the wall etc..

Of course such a simple model is not able to describe the flow patterns appearing in a MHD flow especially in the boundary layers near the walls. But, it gives an insight in the mechanisms of MHD flows. The idea to reduce flow problems to electric networks has recently been used by Picologlou (1985) and Tillack (1990) and it will be also in the future used in the absence of MHD models especially for complex three-dimensional geometries.

2.2 Transport equations, characteristic numbers and boundary conditions

The flow of an electrically conducting fluid applied to a strong steady magnetic field can be described by the following non-dimensional equations accounting for the conservation of

$$\text{momentum} \quad \frac{1}{N} \left[\frac{\partial \vec{v}}{\partial t} + (\vec{v} \cdot \nabla) \vec{v} \right] = -\nabla p + \frac{1}{M^2} \Delta \vec{v} + \vec{j} \times \vec{B} \quad , \quad (2.7)$$

$$\text{energy} \quad Pe \left[\frac{\partial T}{\partial t} + (\vec{v} \cdot \nabla) T \right] = \Delta T + Q \quad , \quad (2.8)$$

$$\text{mass} \quad \nabla \cdot \vec{v} = 0 \quad , \quad (2.9)$$

$$\text{charge} \quad \nabla \cdot \vec{j} = 0 \quad , \quad (2.10)$$

and by

$$\text{Ohm's law} \quad \vec{j} = -\nabla \Phi + \vec{v} \times \vec{B} \quad . \quad (2.11)$$

The non-dimensional variables \mathbf{v} , \mathbf{B} , \mathbf{j} , p , and ϕ , denote velocity, magnetic induction, current density, pressure, and electric potential, scaled by the reference values v_0 , B_0 , $\sigma v_0 B_0$, $\sigma a v_0 B_0^2$, and $a v_0 B_0$. The fluid properties like the density ρ , the viscosity ν , and the electric conductivity σ are assumed to be constant. v_0 is the average velocity in a cross section where a is a characteristic length; B_0 is the magnitude of the applied magnetic field induction. Usually a is half of the duct width in magnetic field direction.

The term Q in the energy equation expresses the effect of volumetric heating by electric currents, nuclear heating or chemical reaction. In the energy equation the heating by viscous diffusion is neglected. The temperature T in the energy equation is a dimensionless temperature which is scaled by $T=(T^*-T_0)/\Delta T^*$ (the sign "*" denotes the physical property and the index "0" the reference temperature).

The flow is characterised by the Hartmann number M

$$M = a B_0 \sqrt{\frac{\sigma}{(\rho \nu)}} \quad , \quad (2.12)$$

and by the interaction parameter N

$$N = \frac{a \sigma B_0^2}{(\rho v_0)} \quad , \quad (2.13)$$

which describe the importance of electromagnetic effects with respect to viscous (2.12) and inertial effects (2.13), respectively. The hydraulic Reynolds number Re is then expressed by M and N in the form $Re=M^2/N$. The ratio of the induced magnetic field to the applied strong field is determined by the

$$\text{magnetic Reynolds number} \quad Re_m = \mu \sigma v_0 a \quad . \quad (2.14)$$

For fusion* applications the induced magnetic fields are usually small compared to the applied strong field (see e.g. Holroyd and Mitchell 1984; Hua & Walker 1990). Thus, the externally applied magnetic field remains unchanged by the magnetic field induced by the currents due to the fluid motion. This fact justifies the inductionless approximation of equations (2.7-2.11).

The last parameter appearing is the Peclet number Pe which expresses the ratio of the convective transport compared to the molecular heat conduction. The Peclet number is defined by

$$Pe = \frac{v_0 a}{\aleph} \quad , \quad (2.15)$$

where \aleph is calculated by $\lambda/(\rho c_p)$ and λ is the molecular thermal conductivity and c_p the heat

capacity of the fluid.

The boundary conditions for the flow variables at channel walls are the same as in hydrodynamics, namely the

$$\text{no-slip condition} \quad \vec{v} \big|_{\text{wall}} = 0 \quad . \quad (2.16)$$

At the entrance and exit of the fluid domain considered the flow is assumed to be either fully developed or exhibits a prescribed velocity distribution.

Also for heat transfer problems the boundary conditions remain unchanged. If a thin wall of the thickness t_w has a constant temperature at the outer surface of $T_{w,o}$ the temperature at the fluid-solid interface which determines the removable heat flux the related dimensionless boundary condition can be written as

$$\frac{\partial T}{\partial \vec{n}} = Bi (T_{w,o} - T) \vec{n} \quad . \quad (2.17)$$

\vec{n} is the inward normal unity vector on the heated/cooled plane. The Biot number Bi describes the relative thermal conductivity of the wall to that of the fluid and is defined by:

$$Bi = \frac{\lambda_w \alpha}{\lambda t_w} \quad . \quad (2.18)$$

A given surface heat flux \dot{q} leads to the dimensionless condition (2.19)

$$-\frac{\partial T}{\partial \vec{n}} = \dot{q} \quad . \quad (2.19)$$

For an isothermal fluid-solid interface the condition reads $T=T_w$.

Additionally to the already named conditions boundary conditions for the electric current or the electric wall potential have to be satisfied. Most often used is the thin-wall condition (see Walker 1981)

$$\vec{j} \cdot \vec{n} = c \nabla_{\perp}^2 \Phi_w \quad , \quad (2.20)$$

where \vec{n} is the inward unit normal to the wall, and ∇_{\perp} denotes the projection of the gradient on the wall surface. The thin-wall condition describes the balance of charge in the conducting duct walls. The currents $(-\vec{j} \cdot \vec{n})$ leaving the fluid to the wall enter this balance as a source term. If the fluid is in perfect electrical contact with the duct walls so that there is no contact resistance across the fluid-wall interface, the potential of the wall and that of the adjacent fluid are equal, i.e. $\Phi_w = \Phi$ at the interface. The condition (2.20) has to be modified at the interior

dividing walls common to channels i and $i+1$, if multi-channel problems are treated, see e.g. Hua& Picologlou (1991)

$$\left(\vec{j} \cdot \vec{n}\right)^{(i+1)} + \left(\vec{j} \cdot \vec{n}\right)^{(i)} = -c \Delta_t \Phi_w^{(i)} . \quad (2.21)$$

Conditions (2.20) and (2.21) mean that the net current input to the wall from the fluid is balanced by a tangential current flow in the wall, creating there a potential distribution Φ_w .

Finally the potential at the fluid-wall interface is continuous, if no electric contact resistance at the interface exists

$$\Phi_{Fluid}^{(i)} \Big|_w = \Phi_w^{(i)} \Big|_w . \quad (2.22)$$

Many structural materials, e.g. stainless steel, have a passivated surface in the form of oxides or alloys and therefore have an undefined electrical contact. The contact resistance is removed before the experiment by a wetting procedure. The effect of the contact resistance on the velocity profiles and the pressure drop may be dramatic (see Bühler&Molokov 1994). In case of a defined contact resistance the potential of the wall is related to the fluid potential by

$$\vec{j} \cdot \vec{n} = \frac{1}{\kappa} (\Phi_w - \Phi) . \quad (2.23)$$

where κ is the contact resistance or the resistance $\rho_i \delta_i$ of a thin insulating coating (resistivity ρ_i , thickness δ_i) scaled by a/σ . For a perfect contact between the fluid and the wall, $\kappa=0$, the fluid potential at the wall is equal to the wall potential, $\Phi_w=\Phi$, whereas for a perfect insulation, as $\kappa \rightarrow \infty$, the wall normal component of current vanishes.

A full description of the thermal and electrical boundary conditions appearing in blanket relevant MHD flows is given by Bühler (1993) and Bühler&Müller (1994).

2.3 Fully developed MHD duct flows

The design of an experimental facility to investigate fusion relevant magneto-hydrodynamic duct flows requires the knowledge about the pressure gradients appearing in characteristic duct geometries. Of course, the aim is to investigate the such flows and the appearing flow patterns. However, the pressure gradient appearing in fully developed flows (2D-flows) in electrically insulating ducts ($\kappa \rightarrow \infty$) as well as in electrically conducting ducts ($\kappa \rightarrow 0$) formulates the minimum conditions to be fulfilled by the experimental facility. Experiments of strongly three-dimensional MHD -flows performed by Barleon et al. 1992 and Stieglitz et al. 1995 reveal that the pressure drops obtained are significantly higher than those of fully developed MHD flows.

In order to give the reader a feeling about the pressure gradients and the velocity

distributions appearing in ducts of circular as well as rectangular cross-section the table 2.1 shows an overview and the relevant literature related to the different geometries.

The results of correlations for the pressure gradient ∇p expresses the dimensionless pressure gradient over one characteristic duct length a . The pressure in the dimension of *Pascal* is obtained by multiplying the dimensionless pressure gradient with the duct length l , the specific electric conductivity of the fluid σ , the mean velocity v_0 and the square of the magnetic of magnetic field strength B . The accuracy of the results which are all only valid for $M \gg 1$ is more than sufficient for engineering applications. The maximum error of the pressures calculated compared to the ones measured in experiments is about $\pm 10\%$.

In the second column of the rectangular duct geometries the case discussed in the introduction of this chapter (§2.1) appears. The pressure drop correlation 2.5 derived there corresponds to the case of a rectangular duct in which either the aspect ratio b/a or the conductance ratio of the side walls c_s are large. The additional terms arising in the table appear due to the treatment of the boundary layers neglected in chapter §2.1. The flow in which the pressure drop correlation 2.5 holds is known in magnetohydrodynamics as the "HARTMANN-FLOW" corresponding to the scientist who investigated magnetohydrodynamic flows for the first time systematically (see e.g. Hartmann 1937). By the way, the pressure drop obtained in a Hartmann flow represents the highest one of a 2D-MHD flow and is therefore most often used for engineering purposes, where a conservative assessment is required.

The sketch of velocity profiles shown in table 2.1 corresponds to the position $y=0$ in the cross section. Moreover, the velocity profiles depicted appear only if the Hartmann number $M \gg 1$. In such cases the velocity in magnetic field direction is constant except for the boundary layers at the wall. This region is called the "*core*". At walls which own a significant normal component of the magnetic field the core matches a rather thin viscous boundary layer in order to fulfil the non slip condition at the fluid-wall interface. This type of boundary layer is called Hartmann layer, the adjacent wall is called the Hartmann wall. The velocity in the Hartmann layer is characterised by a steep exponential decay according to the following equation :

$$\mathbf{v}(y) = \mathbf{v}_{core} \cdot (1 - \exp(-\eta)) \quad . \quad (2.24)$$

Here η represents the boundary layer coordinate along the inward wall-normal direction \vec{n} , stretched with $M(B \vec{n})$. At the wall where $\eta=0$ the velocity satisfies the no-slip condition and the tangential currents are given by Ohm's law for a media at rest ($\mathbf{v}=0$). Far from the walls as $\eta \rightarrow \infty$ all variables reach the core values. Equation 2.24 yields that the thickness of the Hartmann layers δ_H is proportional to M^{-1} .

The velocity profile in electrically insulating circular pipes takes an elliptic shape (see column 1 in table 2.1) while in conducting pipes ($c \gg M^{-1}$) the flow pattern is of the slug type.

The terminology "*slug flow*" characterises velocity profiles with a constant core velocity of one and a monotonous decrease of the velocity in the boundary layers towards the walls. In such slug type flows all flow rate is carried by the core.

Slug type velocity profiles are also obtained in the cores of rectangular ducts with electrically insulating walls (column 3 of table 2.1). Although the velocity distribution a rectangular duct looks similar to that of a circular pipe a second type of boundary layers appear at walls exactly parallel to the applied magnetic field. This viscous boundary layer is called the side layer and the wall adjacent to it is called side wall. The thickness of these side layers δ_s is of order $M^{-1/2}$ and the velocity profile establishing within these layers obeys a parabolic equation, see Molokov and Stieglitz 1995. In case of electrically insulating walls the flow rate carried by these layers is negligibly small and the core carries nearly the whole flow rate.

However, if the duct walls are conducting the core velocity is reduced to $v_{core} < 1$. The volume flux $4ab(1-v_{core})$ which is now not carried by the core is carried by high-velocity jets along the side wall. The flow carried by the core can get even zero in extreme cases, if Hartmann walls are conducting and the side walls are electrically insulating (see Hunt 1965). All flow rate in the duct is then carried by the side layers.

In practical applications of rectangular duct flow one will often find the more general case where the magnetic field is not aligned with any pair of walls. Results for such flows have been obtained by e.g. by Sterl 1990 on the basis of a DNS (Direct Numerical Simulation) or based on an AM (Asymptotic Model) by Morley 1991, Molokov & Shisko 1993, Bühler 1994. For inclination angles $\beta > 0$ the rectangular duct splits into an inner core C_i and two outer cores C_o as shown in figure 2.3. They are separated by two thin internal viscous layers which spread from the inner corner along field lines into the fluid. Internal layers or shear layers appear in MHD flows at locations, where the ducts cross-sections discontinuously changes with respect to the magnetic field lines. These internal layers obey the same laws as the side layers and therefore their thickness is of $O(M^{-1/2})$. The internal layers matches both cores. The inner core exhibits a flat velocity profile while in the outer cores the velocity distribution is linear in the field direction with the highest value at the inner corner. Results for pressure drop and velocity profiles for different inclination angles β and wall conductance ratios are shown in figure 2.3.

Another issue, which has to be addressed while designing an appropriate experimental facility is the developing length of the MHD-flow from the three-dimensional state into a two-dimensional state. For example, the flow comes from an area outside the magnet into the region of homogeneous magnetic field strength. The flow in the fringing field yields a three-dimensional velocity profile, which causes a higher pressure drop and a flow pattern different to that in a two-dimensional flow. The length in flow direction to establish a two-dimensional velocity profile is analogous to hydrodynamics called developing length.

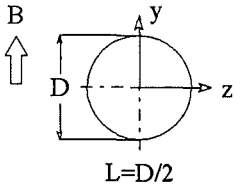
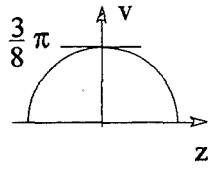
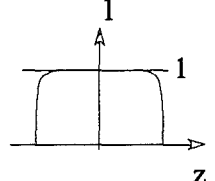
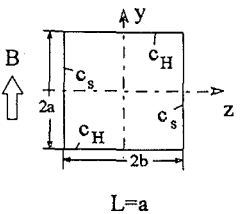
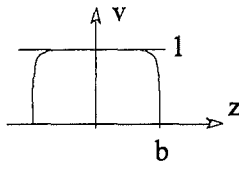
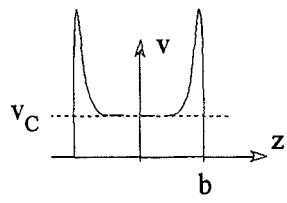
Geometry	conductivity	pressure gradient ∇p	experim. Reference	velocity
 <p>$L=D/2$</p>	insulating $\kappa \rightarrow \infty$	$\frac{3\pi}{8M}$ a)	e	$\frac{3}{8}\pi\sqrt{1-z^2}$ 
	conducting $\kappa=0$	$\frac{c}{1+c}$, $c \gg \frac{1}{M}$ b)	f	
 <p>$L=a$</p>	insulating $\kappa \rightarrow \infty$	$\frac{1}{M}$ c)	g	
	conducting $\kappa=0$	$\frac{\partial_x p_H}{1 + \frac{a}{3b} \frac{1}{c_s^*} \partial_x p_H}$ where $\partial_x p_H = \frac{c_H + \frac{1}{M}}{c_H + 1}$ $c_s^* = c_s + \frac{1}{\sqrt{M}}$	h	$v_C = \frac{\nabla p}{\partial_x p_H}$ 

Table 2.1: Pressure drop correlations for fully developed MHD channel flows. For details see a) Shercliff 1956, Gold 1962; b) Boyarevich 1990; c) Hunt&Stewartson 1965; d) Walker 1981, Tillack 1990 e) Miyazaki 1991; f) Barleon et al. 1991; g) Branover, H. 1986; h) Miyazaki et al. 1986.

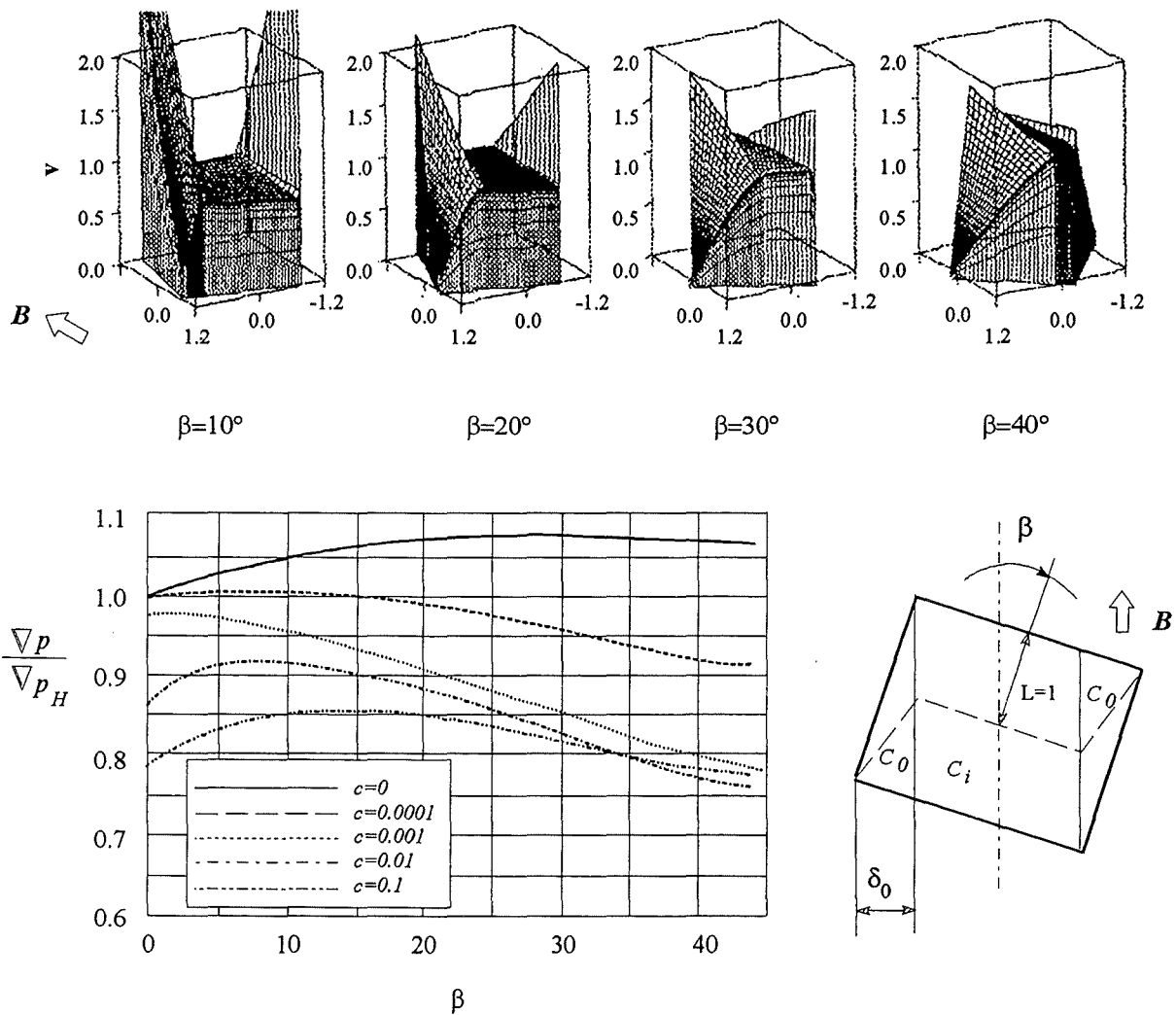


Figure 2.3: MHD flow in inclined rectangular ducts. The upper graph shows the numerical results for velocity profiles. The lower graph shows the pressure drop ∇p (compared to the analytically obtained pressure drop $\nabla p / \nabla p_H = \cos\beta / (1 - 1/3 \tan\beta)$ obtained by Molokov & Shishko 1993 for the case $c=0$).

Direct numerical simulations of three-dimensional MHD flows reveal that these developing length l_{dev} may reach significant values. In table 2.2 the developing length of circular and rectangular shaped ducts is depicted for the cases of electrically insulating and electrically conducting walls. The table shows that it is likely impossible to obtain in an experimental device a fully developed MHD flow in an insulating circular duct at high Hartmann numbers, because the developing length increases with the square root of the Hartmann number. A simple calculation demonstrates this.

Consider a duct with the characteristic length $a=40\text{mm}$ and a Hartmann number of

$M=10^4$, which is fusion typical. The length to obtain a 2D-flow would be 4 meters, which is considerably longer than any commercially available magnet. This length would be required only to get a fully developed two-dimensional flow.

wall property	insulating ($\kappa \rightarrow \infty$)		conducting	
geometry	rectangular	circular	rectangular	circular
l_{dev} in characteristic length a	$O(l)$	$O(\sqrt{M})$	$O(1/\sqrt{c})^{*a}$	$O(l)$

Table 2.2: Developing length l_{dev} of a MHD single duct flow for different geometries from Holroyd & Walker 1978 and ^{*a} Grinberg et al. 1985.

The necessity to obtain a two-dimensional flow in the experimental device can not be emphasised too much. Only the presence of a two-dimensional flow which can be measured is a healthy basis to investigate complex three-dimensional phenomena and flow configurations. The presence of a two-dimensional flow allows moreover the operator to check the experimental facility.

2.4 Three-dimensional MHD-Phenomena

The main physical effects described by equations (2.7-2.11) can be demonstrated in a steady fully developed two-dimensional duct flow. In a second step three-dimensional (3D) effects are discussed by heuristic arguments (see Bühler&Müller 1994).

At high values of the Hartmann number ($M \gg 1$) the flow exhibits an inviscid core surrounded by viscous boundary layers at the walls (see fig. 2.2a). In the core the interaction $\vec{v} \times \vec{B}$ of the moving fluid with the magnetic field drives the current of density \vec{j} perpendicular to the field and perpendicular to the fluid motion. The interaction of this current with the field causes the Lorentz force $\vec{j} \times \vec{B}$ opposing the fluid motion and thus creating the main part of the high MHD pressure drop. The induced currents complete their circuit in the layers where $\vec{v} \times \vec{B}$ is reduced due to viscous effects. Since these layers are very thin (Hartmann layers of thickness $\delta_H = O(M^{-1})$ at walls perpendicular to \vec{B} , or side layers with $\delta_S = O(M^{-1/2})$ at walls aligned with \vec{B}) it is obvious that they provide the main electric resistance in the current path and determine the pressure drop in insulating ducts. If the walls are in perfect contact with the fluid and better conducting than the viscous layers ($c \gg M^{1/2}$) the main electric resistance is not longer determined by the layers since almost all the returning current now is flowing inside the wall. The total current is much larger than for the insulating case and results in a pressure gradient of the order $O(c)$, but it is still small. In ducts with highly conducting walls, as $c \rightarrow \infty$, the resistance against currents is provided only by the core. This leads to highest currents and to a pressure gradient of the order $O(l)$.

Three-dimensional (3D) effects in MHD flows occur if the induced potential difference between the sides varies in axial direction. Such variations are possible because of a non-uniform magnetic field at the ends of the magnet, a reduced x -component of velocity observed in expansions or bends, or because of varying conductance properties of the channel walls (see figure 2.3). All these effects cause an axial potential gradient which drives additional currents j_{3D} inside the fluid. In one part of the duct the current density j_{3D} has the same direction as the 2D currents of the fully developed flow and gives additional contributions to the pressure gradient. Further down stream j_{3D} is in opposite direction as the 2D currents. Here it creates a Lorentz force acting in the flow direction. This leads to some pressure recovery. In the first part of the duct mechanical energy is transferred into electrical energy (generator effect). Since the transmission to the second part suffers from Ohm's dissipation only a part can be recovered downstream as mechanical energy (pump effect). Therefore, a pressure drop Δp_{3D} remains irreversibly lost. The axial components of j_{3D} cause Lorentz forces which displace the fluid towards the sides. Finally a flow pattern is established in the 3D region with a significantly reduced velocity in the centre and an increased velocity near the side walls. These simple considerations demonstrate that 3D effects can not be excluded by the use of poorly conducting or insulating channel walls because the currents j_{3D} take their path inside the fluid itself.

Methods to solve the equations 2.7-2.11 are described in the books of Moreau (1990) and more briefly in Bühler & Müller (1994).

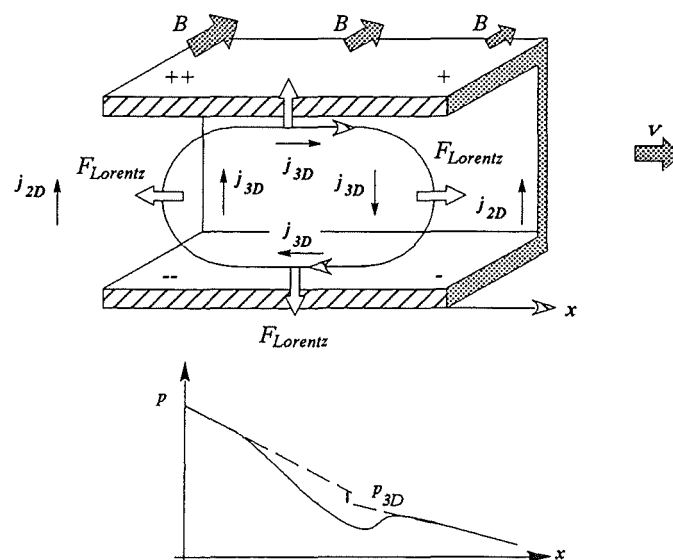


Figure 2.4: Sketch of currents and pressure distribution in three-dimensional MHD flows.

3 Fusion reactor blankets with liquid metal as coolant

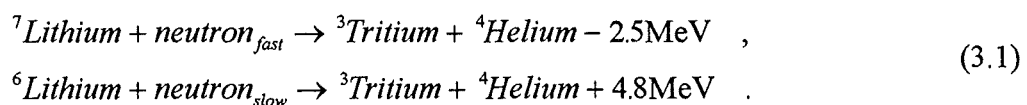
3.1 The principle of the fusion process

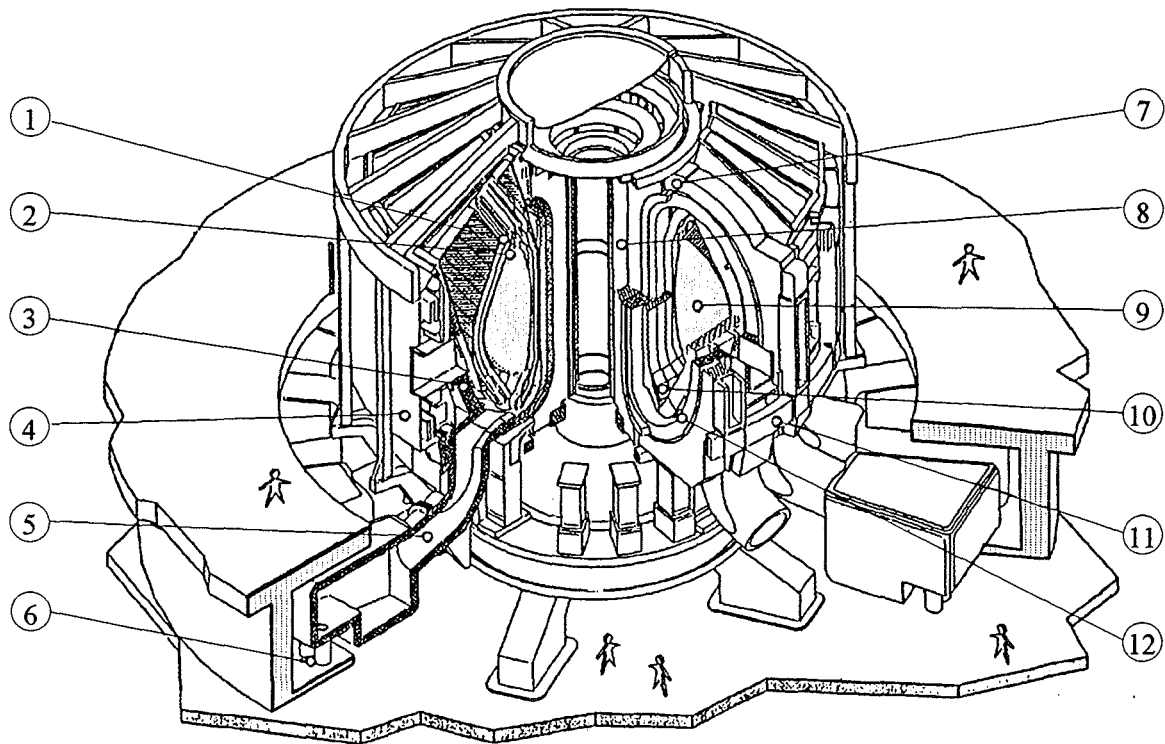
As already mentioned in the introduction of this report the MHD-research being performed in the experimental facility MEKKA has its origin in investigating fusion relevant MHD flows. The MHD flow phenomena has been outlined in the previous section. In order to link these rather general MHD duct flow phenomena with the problematics and key issues appearing in MHD flows of liquid metal cooled fusion reactor blankets a small excursion on fusion reactors is necessary. A detailed description of the fusion process, the technical and physical problems appearing are well described in Rebhahn 1992.

An alternative to fossil energy resources is the nuclear energy, which can be utilised using two different methods, nuclear fission or nuclear fusion. The fusion process is based on merging of two light nucleons to a single one. The basis of the released energy is the bonding energy related to the number of nucleons. One of the most promising fusion reactions is the fusion of deuterium and tritium shown in equation 3.1.

The energy necessary to fuse both atoms, the so-called activation energy is supplied by a plasma heating. At the temperatures required ($T=10^8$ Kelvin) the atoms are dissociated in their elements, electrons and nucleons. Such an ionised gas is electrically well conducting and is called a plasma. Due to the high plasma temperatures an effective thermal insulation of the "*combustion chamber*" to the blanket is necessary, which is realised by the contactless embedding of the plasma in a magnetic field, because the motion of charged particles can be controlled in magnetic fields. One of the possible technical configurations is the embedding in a toroidal magnetic field. This kind of configuration is called the TOKAMAK principle. A drawing of a such TOKAMAK reactor is depicted in figure 3.1. The TOKAMAK is actually the most favoured principle, however, several other configurations like the mirror machine or a stellarator are also under consideration. A description of the main features of the different operating principles, their advantages and disadvantages may be taken from Rebhahn 1992.

The fuel necessary for fusion is Tritium with a half time of 12.3 years. Tritium which appears hardly in nature it has to be breded continuously during the reactor operation. The only promising breeder medium is lithium, which releases tritium while exposed to the neutron flux from the plasma via the two following reactions.





- | | | | |
|----|-----------------|-----|------------------------------|
| 1. | Blanket | 7. | Toroidal main coils |
| 2. | "First wall" | 8. | Inner poloidal control coils |
| 3. | Shielding | 9. | Plasma chamber |
| 4. | Cryostat | 10. | Divertor |
| 5. | Exhaust channel | 11. | Outer poloidal control coils |
| 6. | Vacuum pumps | 12. | Active control coils |

Figure 3.1: Principal sketch of a TOKAMAK fusion reactors from Toschi et al. 1985.

The structure located between the plasma and the magnetic coils is the so-called blanket. It has to fulfil with regard to the technical utilisation of fusion process the following tasks.

- ◆ Breeding of Tritium.
- ◆ Shielding of the super-conducting magnets from the neutron flux released by the plasma.
- ◆ Cooling of the plasma facing wall, the so-called "first wall".
- ◆ Removal of the thermal reactor power. The thermal power consists of
 - a.) γ -radiation, which acts as internal heat source. The γ -radiation originates from the collision of the neutrons released by the plasma and the coolant.
 - b.) The heat radiation of the plasma ($T=10^8$ Kelvin), which contributes with 20% to the total thermal power to be removed.
- ◆ Removal of the breded Tritium.

In order to fulfil these conditions several blanket concepts are considered. Common to all concepts is only the use of Lithium in various forms, e.g. pure Lithium, Lithium alloys, Lithiums salts (silicates, oxides etc.).

The concept types which meet all named demands using only one coolant are the self-cooled liquid metal concepts. As mentioned pure lithium or lead-lithium alloys are attractive breeder materials in fusion power reactor blankets since they are immune to irradiation damage and additionally offer tritium self-sufficiency without any additional neutron multiplier. The high thermal conductivity of liquid metals facilitates robust and rather simple blanket designs, especially if the liquid metal serves both as breeder and coolant. The use of one coolant significantly reduces the amount of auxiliary systems, the maintenance and increases therefore the availability of the reactor. Moreover, pure lithium does not lead to a sudden blown down of the plasma in case of a blanket leak like it would happen in gas cooled blankets and consequently allows a controlled shut down of the reactor.

The problem which has to be considered using liquid metals as coolant in fusion blankets is the interaction of the circulating electrically conducting fluid with the strong plasma confining magnetic field. Due to this interaction of flow and magnetic field electrical currents are induced which create a body force opposing the fluid motion. As a result unusual velocity distributions and high pressure losses can occur, which may lead to unacceptable material stresses. The electromagnetic interaction of the flowing liquid with the external magnetic field forms the field of magnetohydrodynamics to be investigated in the MEKKA facility.

There are numerous ideas, concepts and research activities dealing with the above issues. During the past ten years a lot of work has been dedicated to investigate both experimentally and theoretically MHD-problems associated with the design of liquid metal fusion breeder blankets which will be shown in the following paragraph. The Forschungszentrum Karlsruhe (FZK) in collaboration with the Argonne National Laboratory (ANL) and the Institute of Physics of the Latvian Academy of Science in Riga (LAS) is actively taking part in the design of blankets and the related MHD-research.

3.2 Blanket concepts and design limitations

In order to the readers a feeling about the blanket dimension the figure 3.2 shows the drawing of one outboard blanket segment for a test reactor. In such a test fusion reactor 48 outboard and 32 inboard blankets would be built in the torus.

The design requirements which are set for one outboard blanket and which should be achieved in terms of characteristic numbers in an experimental facility are given in the report of Malang et al. 1995. The technical thermohydraulic data are:

- ◆ volumetric heating : first wall 23.4 Wcm^{-3} ,
first row 19.3 Wcm^{-3} ,
second row 0.61 Wcm^{-3} ,
- ◆ average surface heat flux at the first wall 50 Wcm^{-2} ,
- ◆ maximum material thickness of the foreseen reactor steel 6 mm (\rightarrow maximum tolerable pressure drop in the piping system 80 bars).
- ◆ average neutron flux of $5 \cdot 10^{14}$ neutrons/(s \cdot cm 2).

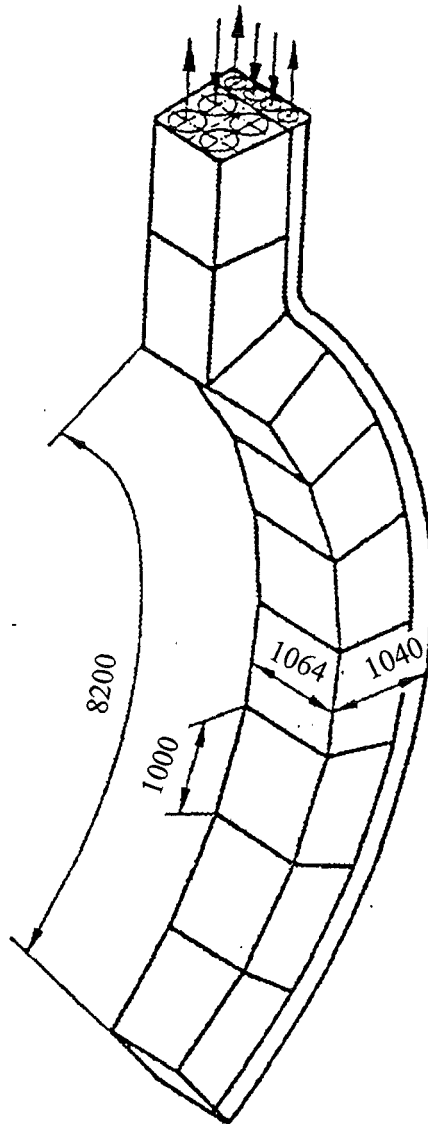


Figure 3.2: Sketch of the geometric dimensions of an outboard blanket foreseen in a fusion reactor.

The main issue of self-cooled blankets is the capability to cool the plasma facing first wall, in which heat fluxes up to 50 W/cm^2 are possible. Together with the volumetric heating by the neutrons a rather high thermal power has to be removed within a small region. In order to achieve a sufficiently effective electricity production the bulk temperature of the coolant at the

blanket outlet should be higher than 400°C.

It is obvious that material properties limits the desires formed by the thermohydraulic postulations. The developed rather sophisticated ferritic reactor steels borders the allowable temperature of the first wall to about 550°C. In case of using vanadium alloys temperatures of up to 750°C can be accepted. Nevertheless, in any design the maximum temperature at the wall/liquid interface has to be maintained approximately 100°C lower than the maximum allowed material temperatures in order to limit corrosion of the structure material by the liquid metal.

The coordination of these contrasting requirements form the actual design task. The design limitations can be expressed in terms of an upper and lower limit for the coolant channel pressure load to ensure structural integrity and sufficient flow rate for heat removal.

Similar to chapter §2.1 one can develop an expression for the upper and lower design limitations of the pressure load caused by a MHD flow heated from one side like shown n figure 3.3. Of course, while deriving such a correlation some simplifications has to be introduced. Let us assume the following conditions:

- Laminar slug flow with a constant velocity throughout the ducts cross section.
- A developing thermal boundary layer.
- Negligibly small electrical and heat contact resistances at the fluid-wall interface.
- A two-dimensional geometry of the length L .

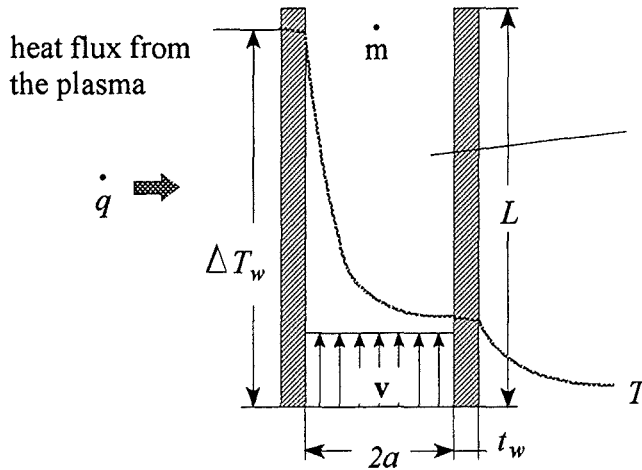


Figure 3.3: Sketch of a two-dimensional MHD-flow radiation heated from one side.

The named conditions yields the following correlation,

$$\frac{4q^2 L^2}{a \Delta T_w^2} \cdot \frac{\sigma_w t_w}{\pi \lambda \rho c_p} B^2 \leq \Delta p \leq \frac{t_w^2 S_{al}}{2a^2}. \quad (3.2)$$

Herein, Δp denotes the pressure drop in the duct, \dot{q} the first wall heat flux, ΔT_w temperature rise along the cooling channel, σ_w the electrical conductivity of the duct wall, λ the heat conductivity of the fluid, ρ the density, c_p the specific heat, S_{al} the maximum tolerable material wall stress, a the half duct width, t_w the wall thickness and B the magnetic field strength. It is obvious that any design should follow the aims of the minimising the coolant pressure drop and achieving the largest possible rise in the bulk temperature at the same time. Guidelines for this procedure can easily be derived from relation (3.2).

There are two crucial consequences of this relation: As the pressure drop increases linearly with the wall thickness for a constant magnetic field strength the mechanical stresses in the wall can not be reduced by increasing the wall thickness, because this would increase the pressure drop and thus the overall pressure load in the same way. The minimum required pressure drop to ensure a sufficient coolant flow rate in the first wall coolant channel is controlled by the surface heat flux, the channel length and the increase in the coolant temperature. Taking into account the limiting conditions of a fusion power blanket, relation (3.2) shows clearly that liquid metal cooling of the first wall by simple poloidal conduits without any electrical insulation or heat transfer enhancement e.g. by turbulence promotion would either lead to unacceptable high temperatures or to mechanical stresses beyond tolerable limits.

Another hydraulic issue of major importance is the flow partitioning into a number of parallel channels. Unequal flow rates in the different channels may lead to local hot spots either caused by the heat flux to the first wall or by the volumetric heat generation in the liquid breeder itself. In principle two MHD methods can be used to divide the flow into equal parts:

- proper adjustment of the geometric channel dimensions,
- electromagnetic control by the means of properly chosen duct wall-thicknesses and/or duct wall conductivities. (Walls with high conductivities causes high pressure drops; for a given pressure drop in this ducts the volumetric flow rate is decreased !).

Besides the MHD issues just outlined, there may be other decisive design aspects directed towards safety and operation performance. Some general guidelines should be mentioned:

- The mechanical stresses at the first wall should be as low as possible.
- The number of welds should be minimised particularly in and in the vicinity of the first wall.
- A double containment should be used in order to reduce the risk of liquid metal spills.

Estimates have shown, that long term stable MHD-flows at reactor conditions are hardly or even not feasible without any electrical decoupling of the electric load carrying walls. Many investigations of electrically insulating materials have shown, that these materials turn at

the neutron fluxes present in a reactor from an electrically insulating into an electrically conducting state. This behaviour would cause global current flows throughout the blanket leading to a drastic pressure drop increase in the coolant ducts and therefore to a higher pressure load if the structural material is coupled to the fluid globally. In any case a direct electrical contact between the rather thick blanket structure supporting walls and the liquid metal should be avoided. This represents for two reason an essential requirement. First an electrical decoupling reduces pressure drop significantly and second it allows to control each duct individually. The pressure drop may be reduced essentially if the wall conductance ratio c becomes very small or even becomes zero (electrically insulating duct). This opens the gate to generally two kinds of an insulation, which are both under development.

The first kind of technical solution is provided by the so-called **Flow Channel Inserts** (FCI) consisting of rather thin electrically conducting walls. Since such walls would be extremely thin they could stand the mechanical stresses caused by the liquid metal pressure. A FCI consists of an insulating ceramic layer sandwiched between two thin steel sheets (see figure 3.4b). These sheets are welded together at all edges, so that a direct contact between liquid metal and the ceramic is avoided. In contrast to direct insulating coatings the selection of the insulation material does not cause any compatibility problems with the liquid metal. FCIs are fitted loosely into the duct. Mechanical stresses are negligible because pressure equalisation is possible by providing slots between the stagnant fluid in the gap and the flowing liquid metal. The pressure drop in channels equipped with FCIs is considerably reduced (Barleon 1989) and determined by the electric resistance of the inner liner wall. Therefore, this wall should be made as thin as possible. A thickness of 0.5 mm seems sufficient for fabrication and corrosion reasons and is thin enough to reduce MHD - pressure drop to an acceptable value. The reduction of pressure drop can reach values up to 95%. The remaining pressure drop is determined by the ratio if the thickness of the inner conducting sheet and the thickness of the wall.

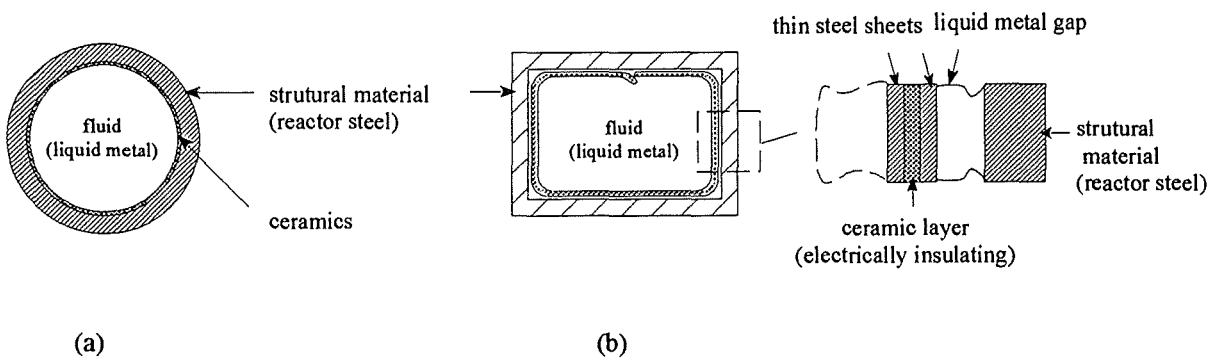


Figure 3.4: a.) Example of a duct with a direct electrically insulated coating. b.) Example of a duct with a "**Flow Channel Insert**" (FCI). In a FCI the electrically insulating ceramic layer is protected from the liquid metal by a steel sheet. The pressure drop in these duct corresponds to the thickness of the steel sheet adjacent to the wall.

The other kind of insulation is based on a direct coating of the duct surface with insulating ceramic materials which are in contact with the liquid metal, as shown in figure 3.4a. It is considered while using that method that the insulating material layer thickness is steadily refreshed by mixing an appropriate oxidising gas into the coolant.

The development of both kinds of insulation is an ongoing task. It may turn out that insulation may not be feasible at the first wall itself, because of the irradiation of the ceramics due to the high neutron fluxes present there. Therefore other methods are required to ensure acceptable limits of temperature and stresses.

The following general ideas are being pursued in blanket design work. A graphics is shown in figure 3.5:

- a) The first wall is cooled by liquid metal flow in parallel toroidal channels (in magnetic field direction). This concept has been proposed originally by ANL (Smith et al. 1985) and was adopted by the Forschungszentrum Karlsruhe for a DEMO-reactor, see fig. 3.5a (Malang et al. 1988). This basic idea is to divert the coolant from large diameter poloidal ducts to small, short channels at the first wall arranged in toroidal direction in order to generate high coolant velocity without extreme MHD-pressure losses.
- b) The first wall is cooled separately by helium gas while liquid metal cooling is used for heat removal from the breeding zone. The incentive to elaborate such a dual coolant concept is the requirement for the plant safety and high availability of the blankets (Malang et al. 1994). Several MHD related problems are avoided at all with this concept, the others are covered by the more severe issues being present in the concept named in A.. The general structure of this concept is shown in Fig. 3.5b.
- c) A principle sketch of a purely liquid metal cooled poloidal flow concept is shown in fig. 3.5c. Similar designs are being discussed for application in ITER (Hua&Gohar 1994), where extreme testing conditions require a high flexibility (softness) of the overall structure. Due to the high magnetic field strength discussed for ITER a concept like this demands an excellent electrical insulation of the duct walls and is feasible with lithium only. The heat transfer from the first wall is enhanced by stimulating turbulent motion perpendicular to the flow direction by mechanical or electrical means. The potential of this procedure is being explored with the aim of demonstrating first wall cooling by a simple assembly of poloidal ducts only.

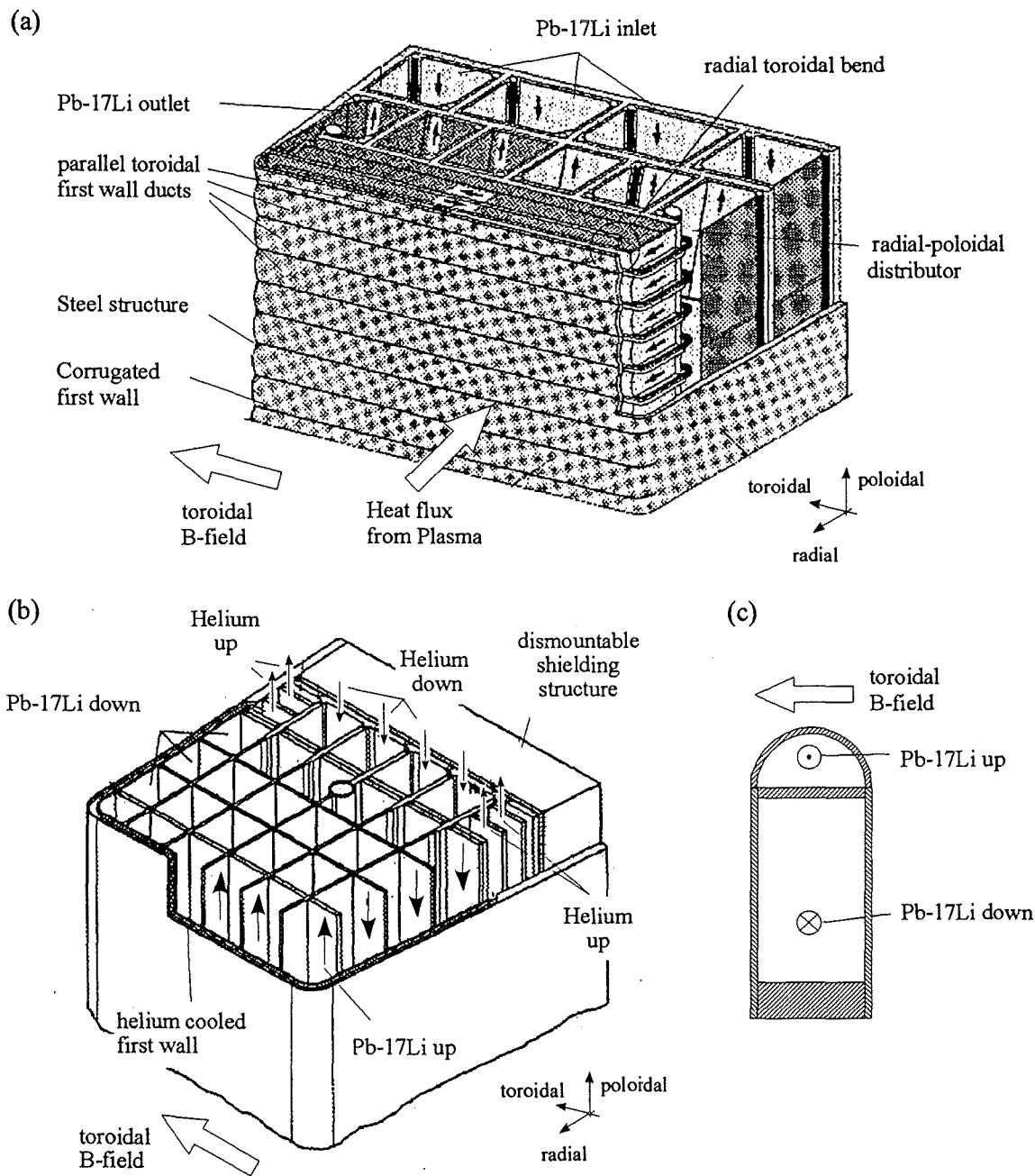


Figure 3.5: a) Poloidal- radial-toroidal flow concept for a self-cooled blanket proposed by Malang et al. 1988. b.) Dual-Coolant-Concept mainly based on poloidal flow from Malang et al. 1994. c.) pure poloidal concept proposed by Hua et al. 1994.

3.3 Flow configurations and flow geometries appearing in blankets

The previously shown designs of the blanket use nearly the same geometric flow configurations. A list of the flow geometries, their location in the blanket and the orientation of the flow with respect to the magnetic field is given in figure 3.6. An MHD-facility should be capable to measure the geometries appearing in a blanket within the relevant parameters.

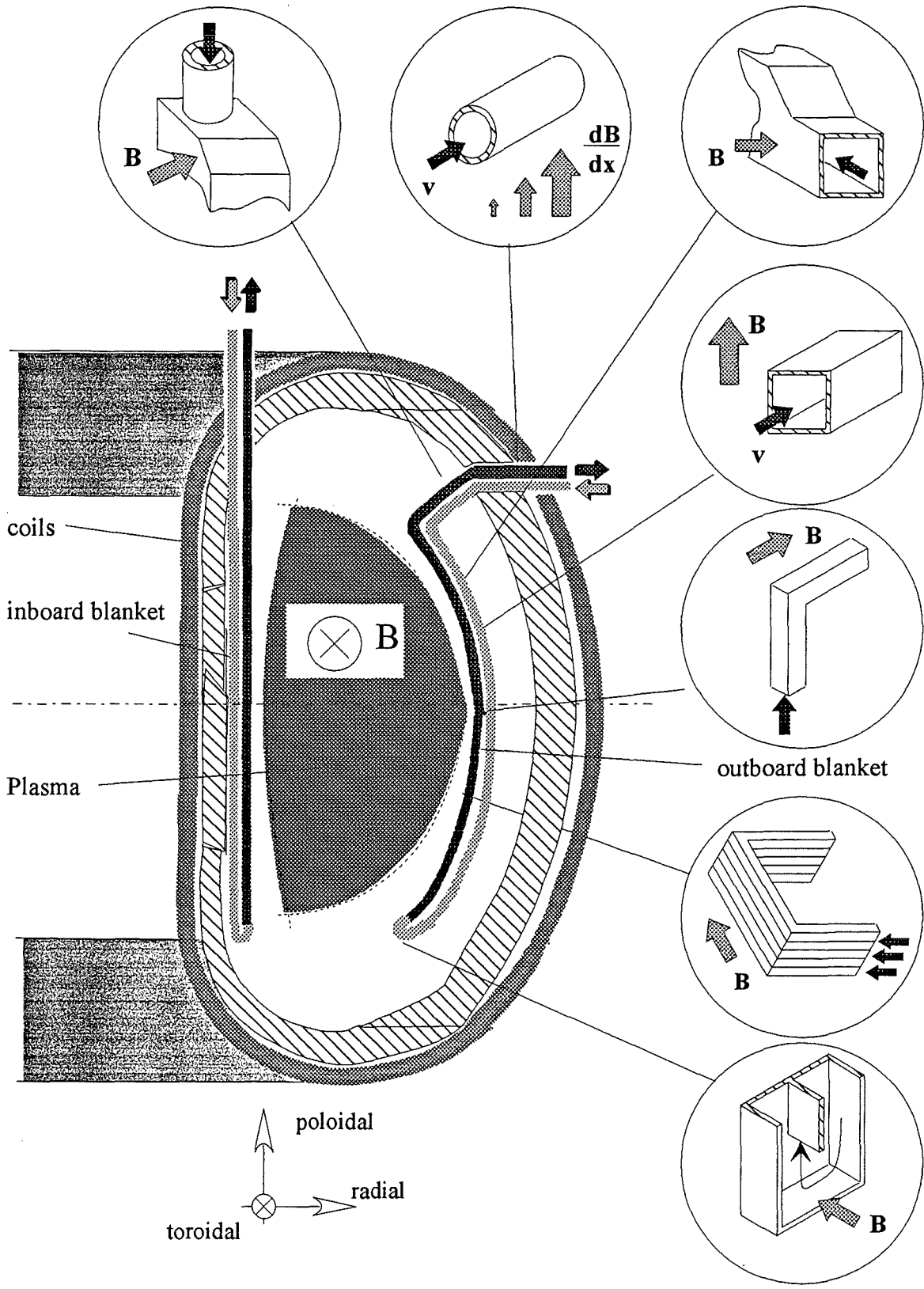


Figure 3.6: Typical flow geometries appearing in self-cooled liquid metal blanket concepts and their location in the blanket.

4 The MEKKA-program and the design formulation

In chapter 2 the main characteristics and the special features of MHD flows have been described. The chapter 3 dealt with the principle features of fusion blankets and the flow geometries to be investigated in order to design a thermohydraulically operable liquid metal cooled fusion reactor blanket.

The design specifications set for the fusion reactor yield for the two coolants considered in the application, namely lithium or the eutectic lead lithium alloy $\text{Pb}^{83}\text{Li}^{17}$, the thermohydraulic characteristic numbers shown in table 4.1.

Parameter	Li	$\text{Pb}^{83}\text{Li}^{17}$
M	$10^4 - 10^5$	$10^3 - 10^4$
N	$10^4 - 10^6$	$10^2 - 10^4$
Pe	$10^0 - 10^4$	$10^0 - 10^4$
Re	$10^2 - 10^6$	$10^2 - 10^6$
c	$10^{-3} - 10^{-1}$	$10^{-4} - 10^{-2}$

Table 4.1 The parameter range of the thermohydraulically relevant characteristic numbers of an MHD flow in the different blanket concepts.

It is clear that an experimental facility is not able to cover the whole parameter range of all characteristic number at the same time. However, the aim is cover as much as possible to enable the transfer to reactor conditions. For this specific reason the MEKKA-program (Magnetohydrodynamische Experimente in Natrium Kalium Karlsruhe) and the equally named facility has been started in the late eighties. The following mentioned topics are set in descending order of importance.

◆

The proper design of an experimental facility begins with the choice of the coolant, which is capable to cover the named parameter range without excessive costs for the necessary auxiliary systems like magnets and liquid metal pumps. This choice is of major importance since all relevant characteristic numbers contain the fluid properties. Moreover, the chosen coolant should allow to investigate all specific flow features appearing in reactor MHD flows. These topics will be discussed in section 5.

◆

In order to obtain sufficiently high Hartmann numbers and interaction parameters magnets of sufficiently high magnetic field strength should be used. The experimental

volume required should be large enough to reach defined flow conditions as discussed in section 2.3. The figure 3.4 shows that in a reactor blanket mainly two magnetic magnetic field orientations with respect to the duct appear. Therefore, an experimental device should own two magnets, one with a toroidal field and one with a poloidal magnetic field direction. The technical data the operation and the properties of the magnets used in the MEKKA facility will be discussed in section 6.



The sections 7 and 8 describe the design and the main components of the two liquid metal loops installed in the MEKKA-laboratory.

5 Coolant/operating liquid

5.1 Commonly available liquids and formulation of requirements

Most often experimental facilities are significantly smaller than the later technical solution. In order to get the same characteristic numbers like M , N , Re etc., which is determined to the main order by the physical properties of the liquid often model liquid are used. But not only the physical properties of the liquids should be closely considered but also the chemical behaviour of them. Some liquids which may be used reveal chemical reactions or behaviours, which exclude the investigation of flow problems relevant for the blanket research. And finally also operational and safety aspects restrict the choice of the liquid metal to be used in an experimental device. Summarising the criteria for the determination of the liquid metal in descending order of importance the following subsections deal with:

1. Transferability of the experimental results to fusion blanket relevant conditions in the main characteristic numbers.
2. Pressure drop and velocity distribution.
3. Operation process.
4. Environmental aspects and containment.

The liquid metals being compared in the following subsections for the use in a loop system are:

1. mercury (Hg),
2. eutectic gallium-indium-tin alloy ($\text{Ga}^{68}\text{In}^{20}\text{Sn}^{12}$),
3. eutectic sodium-potassium alloy ($\text{Na}^{22}\text{K}^{78}$),
4. sodium (Na),
5. lithium (Li),
6. eutectic lead-lithium alloy ($\text{Pb}^{83}\text{Li}^{17}$).

The survey, in which the weighting factors and the importance of the specific aspects for the user are depicted is shown in table 5.4 of section §5.5. The choice of the operating liquids for the built up facility is a immediate result of this table.

5.2 Transferability of experimental results

Of main importance for the transferability of the experimental results to fusion blanket relevant conditions are comparable Hartmann numbers and interaction parameters. In all blanket concepts discussed in section §3 either lithium or the eutectic lead-lithium alloy ($\text{Pb}^{83}\text{Li}^{17}$) are foreseen as operating liquids. Using these fluids the range of the Hartmann number M and interaction parameters N , which are the leading parameters in MHD flows,

varies in liquid metal cooled fusion blankets as shown in table 4.1. Both parameters M and N depend on the magnetic field strength and the aim is to reach these ones as close as possible.

In order to get a feeling for the Hartmann numbers feasible in an experimental facility let us consider an commercially available magnet. The gap size of those magnets is mostly of the order of 80mm which yields a characteristic length a of 40mm and the highest field strength amounts at maximum to 4 Tesla. With a conventional liquid pump velocity variations of the velocity from $v=0.01\text{ms}^{-1}$ to $v=2\text{ms}^{-1}$ are possible. Assuming these boundary conditions the values shown in table 4.2 are obtained for the different liquid metals.

Parameter	Hg	Ga ⁶⁸ In ²⁰ Sn ¹²	Na ²² K ⁷⁸	Na	Li	Pb ⁸³ Li ¹⁷
M	6880	4765	11150	20300	14125	4000
$N_{\text{max.}}$	5	35	200	340	400	6
$N_{\text{min.}}$	0.025	0.2	1	2	2	0.03

Table 5.1: Hartmann numbers and interaction parameters obtained for different metals at a liquid metal temperature of 400°C.

It can be seen easily from table 5.1 that the alkali metals sodium, lithium and the sodium-potassium alloy NaK are suitable to meet blanket relevant M , since they own a high specific electric conductivity and a low density. Similar arguments can be applied for the interaction parameter N as well. The eutectic lead-lithium alloy and mercury show much lower parameters due to their high density and low conductivity and can therefore be excluded from this contest.

An overview of the thermophysical data of the different liquid metals including the temperature dependence of the specific properties may be taken from table 5.2.

Metal	Hg	Ga ⁶⁸ In ²⁰ Sn ¹²	Na ²² K ⁷⁸	Na	Li	PbLi ¹⁷
Melting point [°C]	-38.87	10.5	-11	97.82	179.1	234.85
Volume change on fusion of solid volume in [%]	3.6	-3.5	2.48	2.5	1.5	3.5
Density ρ [kg/m ³]	20°C 13546.0	20°C 6363.2	20°C 868.2	150°C 915.3	300°C 504.9	300°C 9491.7
A ₀	13595.4	6372	873.55	950.46	535.2	9993.3
A ₁	-2.455	-0.44	-0.258	-0.2307	-0.101	-1.672
A ₂	2.472E-7	0	0	-1.8017E-5	0	0
valid temperature range [°C]	-20°-300°	25°-200°	0°-204°	98°-1370°	200°-600°	235°-400°
Heat capacity c_p [J/(kg K)]	20°C 139.068	20°C 365.813	20°C 982.1	150°C 1425.65	300°C 4278.7	300°C 189.78
A ₀	139.6	368.01	990.7	1437.08	4530.2	192.51
A ₁	-0.0275	-0.11	-0.5133	-0.5806	0.8382	-9.116E-3
A ₂	4.5E-5	6.67E-6	5.37E-4	4.624E-4	0	0
valid temperature range [°C]	0°-300°	25°-200°	0°-450°	100°-600°	180°-420°	235°-530°
Kinematic viscosity ν [m ² /s 10 ⁶]	20°C 0.1148	20°C 0.34809	20°C 1.05	150°C 0.5916	300°C 0.8911	300°C 0.2209
A ₀	0.1245	0.3853	1.278	0.936775	1.6925	0.6525
A ₁	-4.633E-4	-0.001926	-0.0134	-0.0025806	-0.003515	-0.001943
A ₂	1.136E-6	3.2686E-6	0.0001	2.571E-6	2.9E-6	1.7324E-6
valid temperature range [°C]	-20°-200°	25°-200°	0°-80°	100°-300°	180°-550°	235°-660°

Table 5.2: Continued next page

Metal	Hg	Ga ⁶⁸ In ²⁰ Sn ¹²	Na ²² K ⁷⁸	Na	Li	PbLi ¹⁷
Electric conductivity σ [A/(V m) 10 ⁻⁶]	20°C 1.04452	20°C 3.30737	20°C 2.878	150°C 8.6356	300°C 3.3434	300°C 0.78917
A ₀	1.0635	3.4882	2.976	13.1155	4.458	0.876
A ₁	-9.502E-4	-0.00932	-5.05E-3	-0.03344	-0.00438	-3.13562E-3
A ₂	5.95E-8	1.3933E-5	7.188E-6	2.9028485E-5	2.248E-6	8.09524E-8
valid temperature range [°C]	20°-350°	20°-200°	0°-80°	100°-400°	200°-1200°	235°-720°
Thermal conductivity λ [W/(m K)]	20°C 8.7169		20°C 21.8	150°C 84.4	300°C 40.64	300°C 13.184
A ₀	8.214	39	21.38	91.752	34.9275	7.30374
A ₁	0.0257	only available	0.0208	-0.048688	1.903E-2	1.96E-2
A ₂	-2.784E-5	for 100°C	-2.207E-5	-3.03E-7	0	0
valid temperature range [°C]	0°-220°		0°-400°	100°-550°	200°-1100°	235°-400°

Table 5.2: Thermophysical values for different liquid metals. *¹ The temperature dependent values are fitted by polynomial regressions in the form $A_0 + A_1 T + A_2 T^2$ with T in °C. The fit formulas for all values have in their range an error of less than 0.5%. The thermophysical data have been taken from: **Lyon, R.N. (1952)** Liquid metals handbook; Navexos P-733; Second edition. **Foust, O.J; (1972)**, Sodium-NaK engineering Handbook; Vol.1; Sodium chemistry and physical properties; Gordon and Breach SCIENCE Publishers; ISBN0677030204. **Addison, C.C. (1984)**; The chemistry of the liquid alkali metals; John Wiley&Sons Ltd; ISBN0471905089. **Smith, D.L. et al. (1984)** Blanket comparison and selection study; Final report; ANL/FPP-84-1;Volume 2, Chapter 6. **Schulz, B. (1986)** Thermophysical properties in the system LiPb; KfK-4144.

5.2 Velocity distribution and pressure drop

The pressure drop in a duct as well as the velocity distribution in the ducts cross-section are essentially influenced by the electric resistance between the liquid metal coolant and the structural material. The electric resistance between the structural material and the fluid is called the contact resistance κ according to equation 2.23. This contact resistance may be:

- $\kappa=0$, which means no electric resistance (or perfect electric contact) at the fluid-solid interface.
- $\kappa \rightarrow \infty$, with an infinitely high resistance (e.g. an electrically insulating layer between fluid and wall).
- $\kappa = \text{const.}$, which describes a electric resistance between fluid and wall (e.g. an electrically conducting oxide layer between the fluid and the structural material).

The last state is hardly viable in laboratory especially with the highly aggressive alkali metals. A state in which no contact resistance is present at the fluid-wall interface is only achievable if the wall surface is completely "*wetted*". It should be clearly said in this context that the terminological expression "*wetted*" means not the physical wetting due to adhesion forces, which are determined by the surface tension. Wetting here means a state in which a direct electrical contact without any resistance between the fluid and the structural material exists. The difference between physical and electrical wetting can be easily explained by an example. The eutectic Gallium-Indium-Tin alloy wets nearly every surface because of its surface tension ($\alpha=0.353\text{Ncm}^{-1}$) physically. However, an electrical contact resistance remains. In the further report the terminology wetting means electrical wetting.

Most used structural material in laboratory but also in the blanket like steel, copper, etc. owns a passivated surface caused by the manufacturing process. This surface consists mainly of oxides, impurities and/or alloy components; it is usually electrically insulating and prevents a wetting of the wall. Thus, a contact resistance appears.

There are different possibilities to wet a surface. The easiest way is the direct wetting without the use of third materials or covered/plated surfaces. The method of a direct wetting procedure is only possible for liquid metals which has a higher affinity to oxygen than the alloy components and the structural material itself. These metals are via a reduction reaction able to solute the oxygen from the surface layer. The developing "clean" surface can then be wetted easily by the liquid. The reaction rate for the reduction increases with decreasing nobleness of the liquid metal compared to the structure material. The nobleness of the metals within the reduction row of the metals is documented in Rademacher et al. 1976. Resulting from this alkali and earth-alkali metals wet due to their disnoblness e.g. stainless steel. Since the

reduction process at the surface of the wall is diffusion controlled, the reaction rate increases with increasing temperature level.

The method of a direct wetting shown in a row of descending wetting capability is possible for the following metals:

lithium, sodium, sodium-potassium, lead-lithium

Another possibility to wet a surface is to plate the clean surface, which is intended to be wetted, with third materials. The plated material dissolves in the liquid and enables a direct contact of fluid and wall. Problematic in this context is, that during the solution process chemical reactions of the liquid with the plating material are possible, which can lead in an extreme case to a change of the thermophysical properties of the fluid. The described type of wetting procedure is oftenly used for GaInSn, where the structural material is plated with tin, which dissolves in the alloy during the wetting process. However, a wetting of electrically conducting walls for GaInSn is also possible with the liquid metal itself. Before filling the duct a few GaInSn droplets can be poured on the surface which should be wetted. By rubbing the droplets on the surface a black film develops. After filling the duct with GaInSn the pressure measurement in a 2D-MHD duct flows reveals a pressure drop, which is only achievable if there exists no contact resistance between wall and fluid. It is unclear what happens due to the rubbing. Possible is the formation of an intermetallic compound due to friction rubbing processes. Nevertheless, this rather empirical methods ensures rather long an electrical wetting of the surface.

Mercury is a rather inactive material and shows a very small solubility against other metals, except silver and gold. Up to now no technically reliable method has been invented to ensure a steady wetting of copper or stainless steel.

In the fusion process neutron flux densities of up to $5 \cdot 10^{14}$ neutrons per square centimeter and seconds (see e.g. Malang, Tillack et al. 1995) are produced, which is three to four orders of magnitudes higher than in nuclear fission reactors. This neutron flux causes a material damage of approximately 70 (!) displacements per atom in steel. Up to now no electrically insulating material has been found, which could withstand such a high neutron load. Moreover, these electric insulators turn at a certain amount of dpa's from an electrically insulating state into an electrically conducting state. This transition would lead in the coolant ducts to a drastically different flow distribution with a different heat transfer characteristics and what is more dangerous to an considerably increased magnetohydrodynamic pressure drop in the duct.

Since the appearance of electrically conducting ducts can not be excluded in a fusion relevant blanket design and MHD flows in electrically conducting ducts reveal other

characteristics and scaling laws than flows in electrically insulating ducts the fluid in an experimental facility should offer to investigate both cases. This necessity excludes the fluid mercury from the operation in a demorelevant laboratory.

5.3 Operation procedures

This section treats mainly two aspects, which can be assigned to the issues operation techniques and security aspects. Both expressions contain a large amount of subtopics, which are considered in their importance from the operators differently. The following judgement of the metals is only made under fusion relevant MHD aspects.

5.3.1 Operation technology

For simple laboratory operation the following issues are of importance:

1. The metal should be liquid at room temperature, so that no heating equipment is necessary.
2. The liquid should offer a high compatibility with commonly used laboratory materials like glass, Plexiglas, ceramics, stainless steel, etc.
3. It should be suitable to handle it at open atmosphere.
4. A simple purification method should be available to remove oxides and impurities, to ensure long term constant thermophysical data.
5. The liquid metal should be easily available and not too expensive.

Topic 1:

The table 4.3 shows the melting points of the different metals. Referring to topic 1 only mercury, GaInSn and NaK are liquid at room temperature and therefore can be operated in a loop without additionally heating elements, which reduces the costs and the technical expenses drastically.

Topic 2:

Another important issue is the compatibility of the liquid metal with commonly used laboratory materials. Due to the high affinity of alkali, earth-alkali metals and their alloys to halogens, oxygen and sulphur the variety of laboratory materials is strongly reduced. The use of PVC, Teflon and also solutants containing halogens is strongly forbidden. A good compatibility of alkali metals exists for pure carbon-hydrogens like polyethylen, perbunan and others, see e.g. Lyon et al. 1952. Their temperature range, however, is restricted to somewhere in the region of 150°C.

GaInSn is at room temperature compatible with nearly every laboratory material, except for aluminum and lead. In russia it is forbidden to transport Ga or Ga-alloys in planes, which mainly consists of aluminum. Known in this temperature range is only a high reactivity with chlorides and bromides as well as potassium hydroxid, see Lyon et al. 1952. At higher

temperatures, however, the reactivity drastically increases and the GaInSn is like pure Gallium able to solute nearly every metal in an infinite amount. The only exception known is the rather inactive behaviour to tungsten and tungsten alloys. Gallium reacts hardly in air and burns not even at temperatures of 600°C-800°C.

In the operation mercury loops only the use of sulphur containing compounds should be avoided. Due to the high solution capability of lead in mercury lead should not be taken as structural or component material.

Topic 3:

Due to the high affinity of alkali metals to oxygen they can not be handled open in atmosphere. They react vehemently with air, especially if the air is humid and then burn. Alkalis react furiously, partially in explosions with water. Due to this incompatibility water-cooled heat transfer units should not be taken into account in a loop design. All liquid metal loops using alkali/earth-alkali metals has to be contained permanently in an inertgas atmosphere. Possible inertgases are nitrogen, argon or helium.

The inactiveness of mercury in air would allow an open operation. However, due to the high vapour pressure of mercury at room temperature the laboratory air would be rather fast saturated with mercury vapour. Soon the limit of dangers for health, which is set in germany to a concentration of 0.01mgm⁻³, would be exceeded. The toxic behaviour is amplified by carbon dioxide and the always in laboratory air resident humidity by orders of magnitude, so that also for the use of mercury as a liquid metal in loops an inertgas containment has to be foreseen.

GaInSn underlies up to now no restrictions regarding an operation at open atmosphere.

Topic 4:

The purification of lithium is conducted by a distillation in glass columns and need a high standard technical equipment if a satisfactory purity shall be obtained. In case of sodium and sodium-potassium a recycling using the higher solubility of the oxide and the impurities at higher temperatures is performed. This kind of purification can be easily implemented in a loop (e.g. by a purification loop in bypass to the main loop). In the recycling unit the liquid is gradually cooled and guided in a oversaturated state through a filter, consisting of steel wires. At these wires the impurities separates from the liquid. This unit is called cold trap and the achievable purification is high.

The purification of mercury is carried out via a condensation at low pressures in an inertgas environment at temperatures of approximately 250°C.

GaInSn is purified by heating up. At higher temperatures the oxides and impurities are swimming on the surface due to their lower density. However, its not known what degree of purity can be achieved with this method.

Topic 5:

The availability of all considered laboratory metals on the world market is quite good. The only smaller exception is GaInSn which has cost in 1992 of 6500DM per litre. However, the break down of the iron curtain decreased the price for this material by a factor of four(!). Nevertheless, for a loop usual in reactor studies (inventory about 200 litres) the costs are still high and only small horse track loops or experiments can be realised with this metal as described in section 8.

5.3.2 Safety aspects

A part of the safety aspects has been already illuminated in the previous section. Nevertheless, four major issues should be discussed.

1. environmental impact,
2. storage,
3. toxic effects,
4. operation security.

Since alkali metals own a high reactivity to oxygen and halogens after leak in the loop mostly salts in form of oxides or cooking salt appear at the leaks. These reaction products can be soluted easily in water and poured in the normal waste water. After reactions with water, which can be of explosion type depending on the boundary conditions, mostly strong lys, e.g sodiumhydroxyd or potassiumhydroxyd, are produced, which can be neutralised with acids. Impure metals can be send back to the manufacturer. Piping or structural materials having contact with the fluid can be cleaned after a certain reaction time with alcohol and later with water. The wastage of this cleaning process has to be deposited in chemistry wastage.

Mercury can diffuse in air as vapour, which is highly toxic. Mercury pouring on the ground disperses in a tremendous amount of drops. All structural materials being in contact with mercury has to be heated before using again so that all mercury is evaporated from the surface. The disposal of mercury underlies special laws and permissions in germany.

Surfaces wetted with GaInSn can be cleaned using petroleum. A toxic behaviour of this metal is not known up to now. However, as a heavy metal the deposit of this fluid is governed by the laws valid for heavy metals. GaInSn has a vapour pressure which is 10^{-30} lower than that of mercury. So danger due to inhaled metallic vapour is rather small. Also the data sheet of the "State Research and Design Institute of Rare Metals Industry" (GIREDMENT) of russia (see Bochkarev, E.P. 1977) contains no information about a toxic behaviour of this alloy or of diseases originating from a long term operation with such an alloy.

The reactivity of the alkali metals, which require a permanent containment in inertgas, has already been mentioned. It should be explicitly noted in this context that during any

opening of such a loop type the operating personal should wear security clothing, because in case of a contact of the liquid with the skin the liquid continues burning on the skin due to the humidity of the skin. In order to extinguish small fires dry sand or graphite dust can be used. Moreover, the security laws of the working unions and the chemical industry are valid for operating such a loop.

The toxic effect of mercury has been noticed several times. In order to protect the operation personal for a too high mercury vapour concentration in the air, vapour detectors should be placed in the laboratory facility.

5.4 Determination of the coolant material

As previously mentioned the choice of the liquid metal for the loop system has to obey the requirements of the fusion blanket relevant research. Each of named sections got an importance scaling factor from 1 to 5, and within the subsections points from one to five (one≈worse; five≈excellent) are given. The result of one issue is obtained as a multiplication of the points with the weighting importance factor. This procedure has been carried out for all issues and the obtained result is displayed in table 5.3.

The sum of all aspects lead to the choice of the eutectic-sodium potassium alloy for a large loop and to the choice of GaInSn for a small horse track like loop. One aspect for the decision of sodium potassium for a large loop has been made because of the price of GaInSn at the time when the MEKKA facility has been started to built up in 1985.

The thermophysical data of both liquid metals and their dependence on the temperature are shown in table 5.2.

Description	Importance factor	Hg	Ga ⁶⁸ In ²⁰ Sn ¹²	Na ²² K ⁷⁸	Na	Li	Pb ⁸³ Li ¹⁷
transferability of experimental results	5	5(1)	15(3)	20(4)	25(5)	20(4)	5(1)
wetting behaviour	5	0	20(4)	25(5)	20(4)	20(4)	15(3)
laboratory operation fluid at room temperature	3	15(5)	12(4)	15(5)	6(2)	3(1)	0
compatibility	2	8(4)	10(5)	4(2)	4(2)	4(2)	4(2)
open handling	2	6(3)	10(5)	2(1)	2(1)	2(1)	2(1)
purification/ recycling	2	2(1)	6(3)	10(5)	8(4)	2(1)	2(1)
availability/ price	1	5(5)	0	5(5)	5(5)	2(2)	2(2)
security/ environment	2	2(1)	6(3)	6(3)	6(3)	6(3)	2(1)
working security	2	4(2)	10(5)	6(3)	8(4)	8(4)	6(3)
TOTAL SUM	24	47	89	93	84	67	38

Table 5.3: Determination of a liquid metal for fusion-relevant MHD-research.

6 The magnets

6.1 General

As the figure 3.4 has shown mainly two magnetic field orientations are relevant for fusion blanket MHD research, namely a poloidal and a toroidal magnetic field. Therefore, in the experimental facility MEKKA two magnets with different magnetic field orientations are installed.

The first one is a normal-conducting dipole magnet (name: MA-magnet) which has a maximum magnetic field strength (often called induction) of 2.1 Tesla. The other one is a super-conducting helium-cooled solenoidal magnet (name: CELLO) which is capable attaining field strengths up to 3.6 Tesla for long term operation. For measurement campaigns less than one hour a magnetic field strength of 4.1 Tesla is possible.

6.2 The MA-magnet

The MA-magnet is an electromagnet which induces by applying electric currents a magnetic field in the copper-coils. The pole shoes are made of iron. It is a dipole magnet, in which the magnetic field is directed perpendicular to the long axis in direction of the gravity vector. The cross section of the experimental volume is of rectangular shape.

The technical data and the geometrical dimensions of the MA-magnet may be taken from table 6.1 and the drawings in figure 6.1 .

data sheet	dimension [/]	
Magnet gap height (pole shoe gap)	mm	168
Magnet gap width	mm	483
axial extension of homogenous magnetic induction	mm	800
vertical length of homogenous magnetic induction	mm	165
maximum electric current	A	1500
maximum power	kW	450
time constant L/R (for 50°C)	s	1.35
number of coils	-	4
total number of windings	-	192
average winding length	mm	5000
cross-section of a winding	mm ²	144
cooling loops per coil	-	8
total ohmic resistance of a coil	Ω	0.16
total weight of the magnet	kg	20800
required cooling water at maximum power	l/s	2.33
therefore required min. pressure difference	MPa	0.45

Table 6.1: Technical data of the MA-magnet in the MEKKA-facility

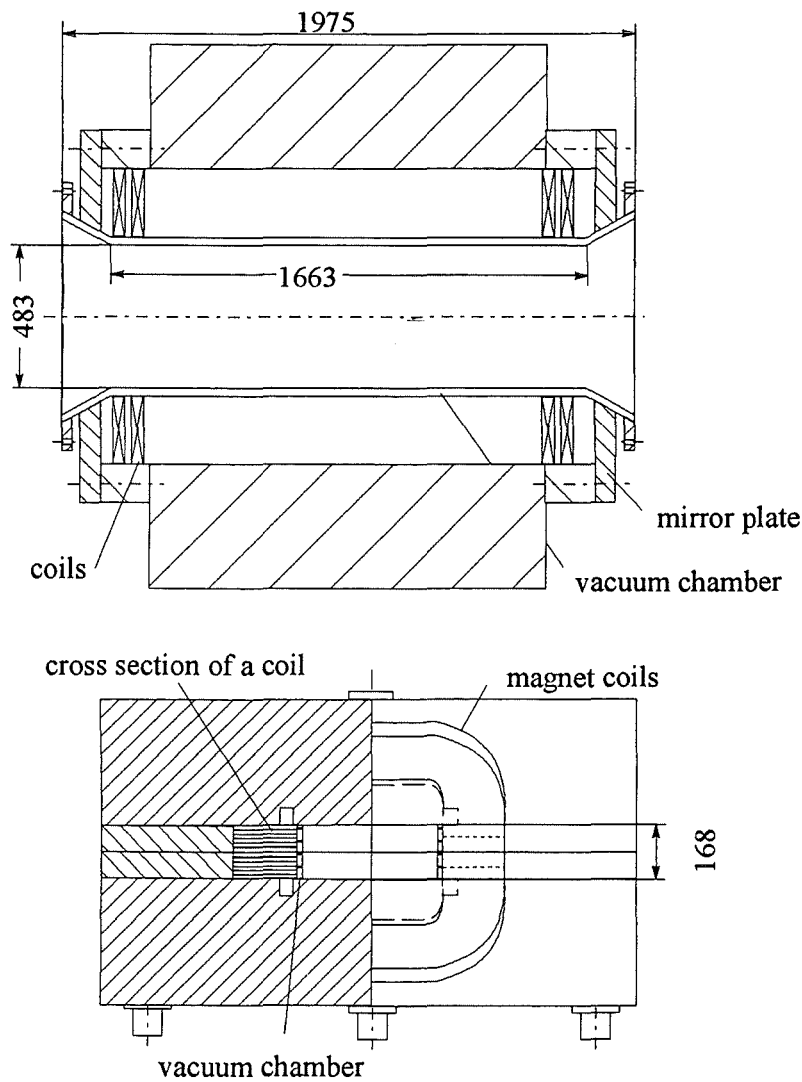


Figure 6.1: Technical drawing of the MA-magnet. Upper graph shows a cut along the long axis. The lower picture shows a cross-sectional cut.

6.2.1 The power supply

The operation of the magnet requires an infinitely variable DC power supply of 300 Volts and 1500 Ampère. Therefore, a transductor is used, which is three phase fed from the general power supply and which serves 0-300 Volts at the output. The three-phase output voltage of the transductor is rectified by a high voltage thyristor, which operates using a Graetz-switching. In order to obtain a rest undulation of the current of less than 1% a sieve unit consisting of a condensator and an inductance coil is used behind the rectifier. The electric system is shown in figure 6.2.

Due to the induction law a large potential can develop in case of a sudden shut down of the power supply, which may destroy the magnet. The induced voltage U_{ind} can be calculated with equation 6.1.

$$U_{ind} = L_{COIL} \frac{\partial I}{\partial t} , \quad (6.1)$$

where L_{COIL} is the inductivity of the magnet coils.

In order to protect the magnet and to release controllably the stored energy in the magnet a spark gap and additionally a discharge switching consisting of a resistor and an air-cooled power thyristor is used.

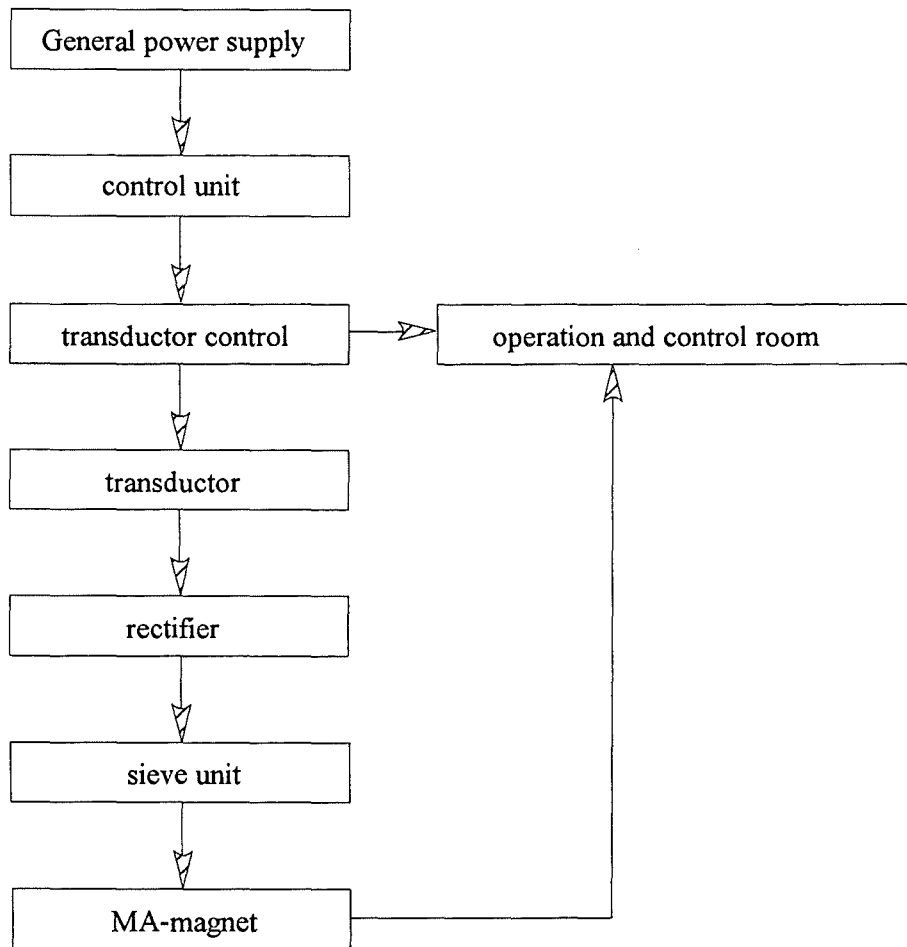


Figure 6.2: Schematics of the power supply of the MA-magnet.

6.2.2 The water-cooling system

The ohmic heat produced by the current flowing in the coils is removed via a closed water cooling system. The heat removal within the magnet is realised by a water flow over the surface and in the inner hollow core of the coils (the coils are of rectangular shape with a centred rectangular hole). The cooling loop consists of a water container, a water pump, a controlling valve and a heat exchanger. The heat exchanger transfers the heat to a secondary loop which is directly connected with an external cooling tower.

The maximum heating rate allowed for the water in the magnet is $\Delta T=40^{\circ}\text{C}$. The

maximum coil temperature during operation should not exceed 75°C, because of the rubber sealings used. Thus, at maximum magnet power a water flow rate of 8.4m³/h is required. For this flow rate the pressure drop in the coolant ducts is about 4.5bars. The maximum tolerable water pressure in the coolant ducts is limited to 9 bars. A schematics of the magnet cooling system is shown in figure 6.3.

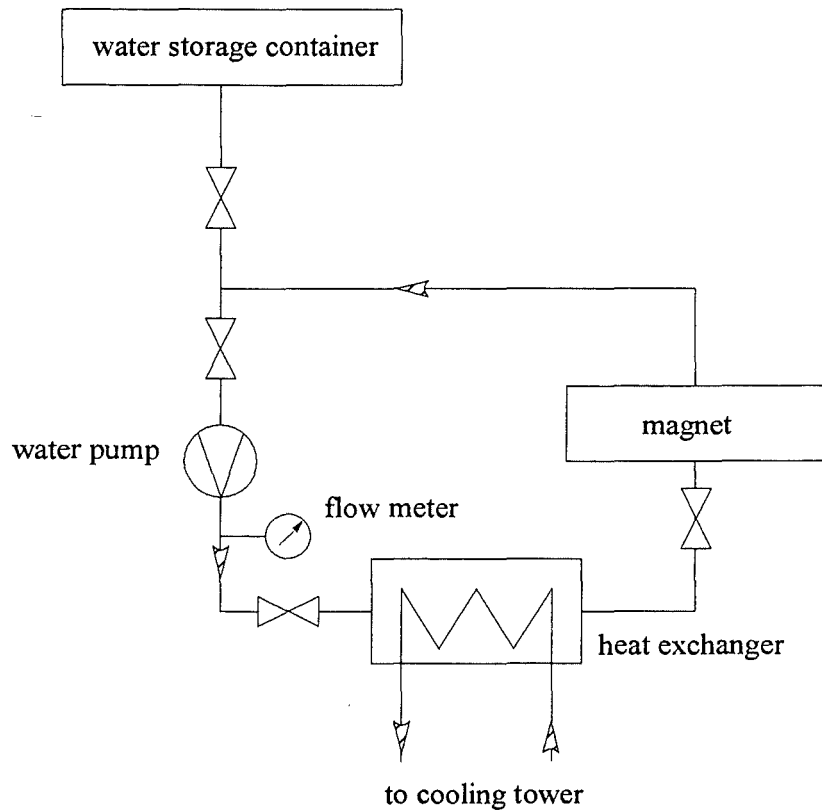


Figure 6.3: Water cooling system of the MA-magnet of the MEKKA-facility.

6.2.3 Magnetic field strength and field distribution of the MA-magnet

The detailed knowledge of the spatial distribution of the magnetic induction is extremely essential for the performance and the interpretation of experiments, since nearly all quantities depend on the value of the magnetic field strength.

In figure 6.4 the magnetic induction along the coil axis is shown for different height coordinates z on the symmetry axis. The graph demonstrates that the volume of constant magnetic induction has the dimensions 800mm × 480mm × 165mm. As homogeneous is the region considered in which the magnetic field relative to the core value deviates less than ±1%.

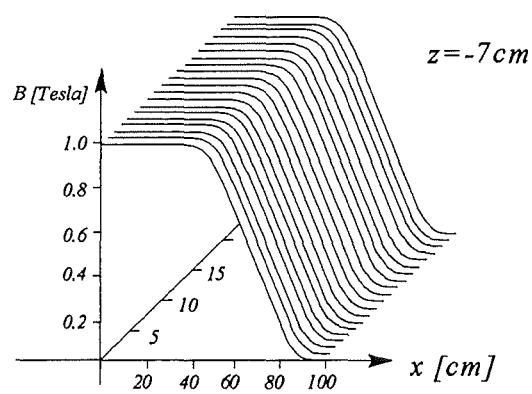
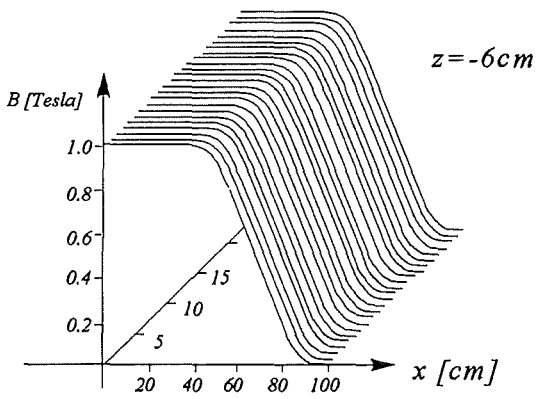
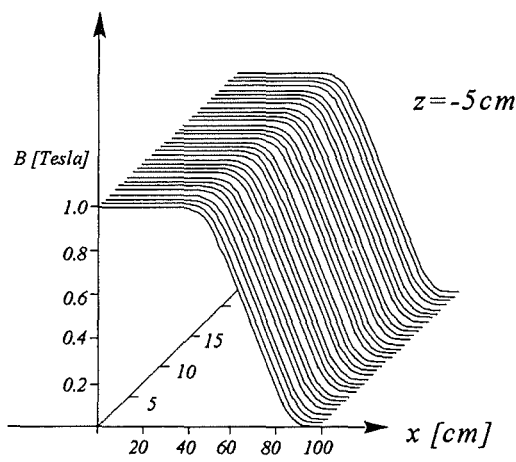
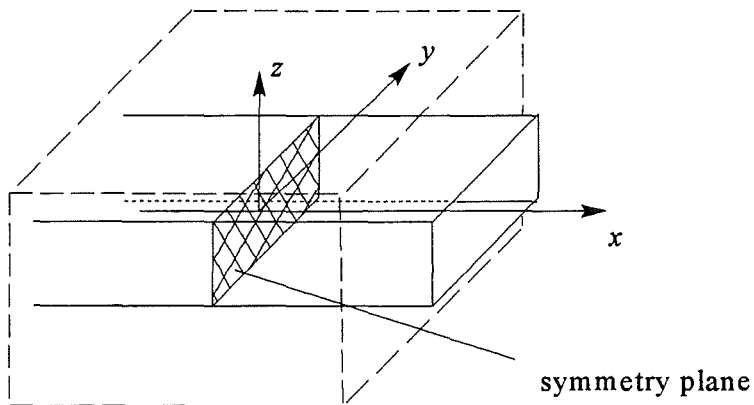


Figure 6.4: Spatial magnetic field strength distribution $B=B(x,y,z)$ in poloidal direction.

The MA-magnet shows nearly throughout the whole operation range a linear proportionality of applied electric current and produced magnetic induction, which is shown in figure 6.5. Only if the maximum limiting operation point of 1700 Ampère is exceeded deviations to the linear behaviour appear, which originate from the saturation of the pole shoes, which are made of iron .

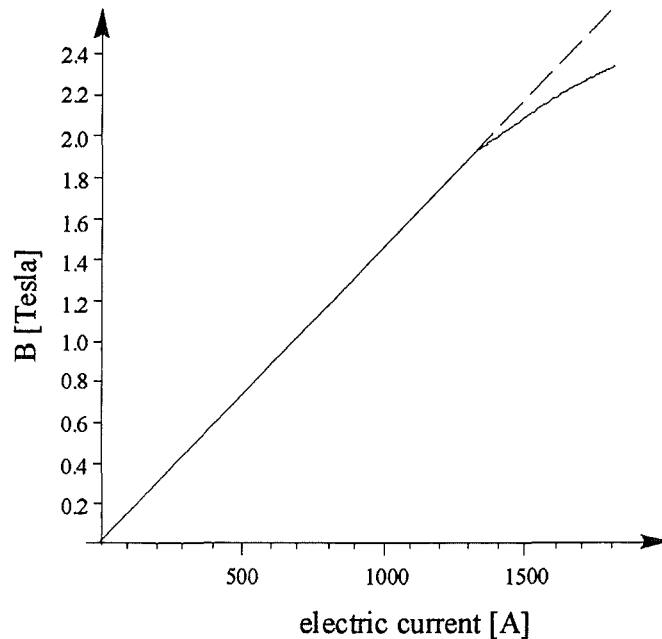


Figure 6.5: Average magnetic field strength of the MA-magnet in Tesla as a function of the applied electric current measured in Ampere.

6.3 The super-conducting CELLO-magnet

The CELLO-magnet is a super-conducting solenoid magnet, in which the magnetic field is oriented in direction of its long axis. The super-conducting windings which are fabricated of copper-mantled niob-titanium wires are located in a helium-cooled cryostat.

Supplying a DC-current of 1050 Ampères the coils provide a axial magnetic induction of 3.6 Tesla. The other relevant technical data may be taken from table 6.2. For short time operations maximum magnetic induction up to 4.1 Tesla are achievable.

For the operation of this magnet the following components are required:

1. liquid helium supply /backgas system,
2. vacuum system,
3. controlling systems,
4. security systems.

super-conducting material		niob-titanium
cross section of wires	mm ²	6.4
max. operation current	A	1150
critical current at $B=3.6T$ and 4.2Kelvin	A	2400
inductivity	Henry	1.6
solenoidal field	Tesla	3.7
max. induction at the wires	Tesla	4.0
max. stored energy	J · 10 ⁶	1.1
coil gap	mm	400
homogeneous magnetic field extension (maximum 10% deviation)	mm	450
magnet length	mm	1100
windings per coil	-	2680
number of winding columns	-	10
volume of cryostat	<i>litres</i>	26
max. pressure in cryo-chamber	MPa	1.0

Table 6.2: Technical data sheet of the super-conducting CELLO-magnet

6.3.1 The liquid helium supply

Because a niob-titanium alloy is used as super-conducting material, the super-conduction starts relatively late. The experiments in the magnet shows that super-conduction is reached at about 15-17 Kelvin, see figure 6.6. The liquid helium used for the coil cooling has at atmosphere pressure at temperature of 4.2 Kelvin, which is satisfactory for this purpose.

The helium supply to the cryostat is done via cans. In order to feed helium in the cryochamber a small overpressure of approximately 150 mbars is set on top of the liquid helium surface in the cans. Opening the motor supplying valve (see schematic graph of helium system figure 6.9) the liquid helium flows through vacuum insulated pipes in the cryo-chamber.

The piping network of the cryopipes has been designed so that the pressure losses in the pipings are rather small, since the temperature of the liquid helium depends strongly on the pressure level. The helium exhaust gas also flows via vacuum insulated pipings out of the magnet. Then it is heated up in a water bath and flows back to a refrigerator station.

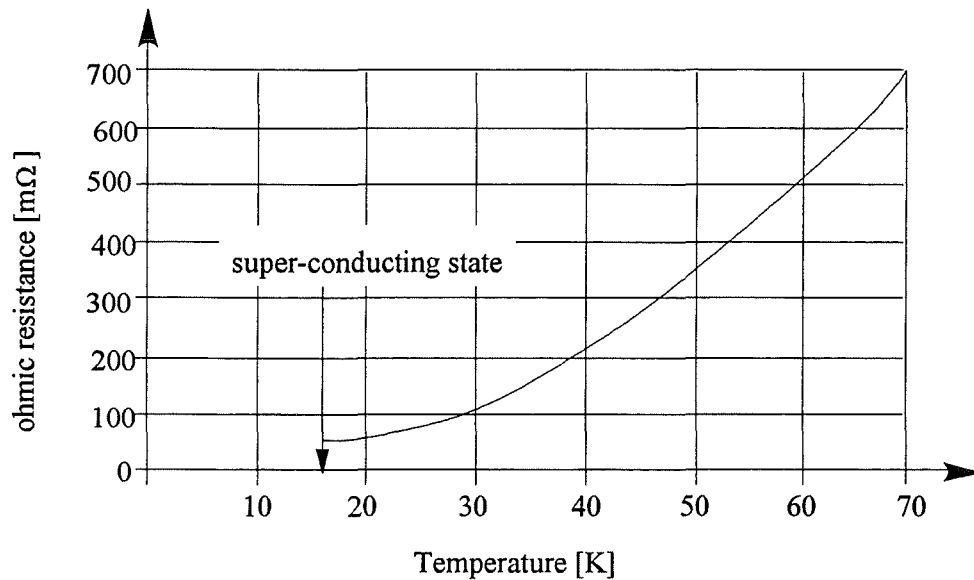


Figure 6.6: Ohmic resistance of the super-conducting coils as a function of the temperature in the cryo-chamber.

The operation of the super-conducting magnet demands due to the sensitivity of the super-conducting material to temperature gradients and super-normal-conducting transition a detailed control of the temperature in the cryochamber, see Lehmann et al. 1979. In order to control the temperature in the magnet in the range of 3.5° to 400° Kelvin three different kinds of temperature detectors based on an electric resistance principle are used. The range from 70° to 400° Kelvin is covered by platinum elements, so-called PT100, which are fed by a constant current of 100μA. The range from 6°-80° Kelvin is measured with carbon resistors (C100), which require a constant current supply of 10μA. Finally, the range 3° to 30° Kelvin is controlled by carbon-glass-resistors (CGR), also fed by a constant current of 10μA. The dependence of the electric resistance of the specific elements on the temperature may be taken from the figures 6.7a and 6.7b.

The figure 6.8 shows the location of the temperature detectors within the CELLO magnet. A homogeneous temperature distribution over the coils which allows a secure magnet operation exists, if a certain liquid helium level on the coils is reached. The measurement of the liquid helium level is performed using a super-conducting wire. The detectable accuracy of liquid helium level obtained with this method is ±1mm.

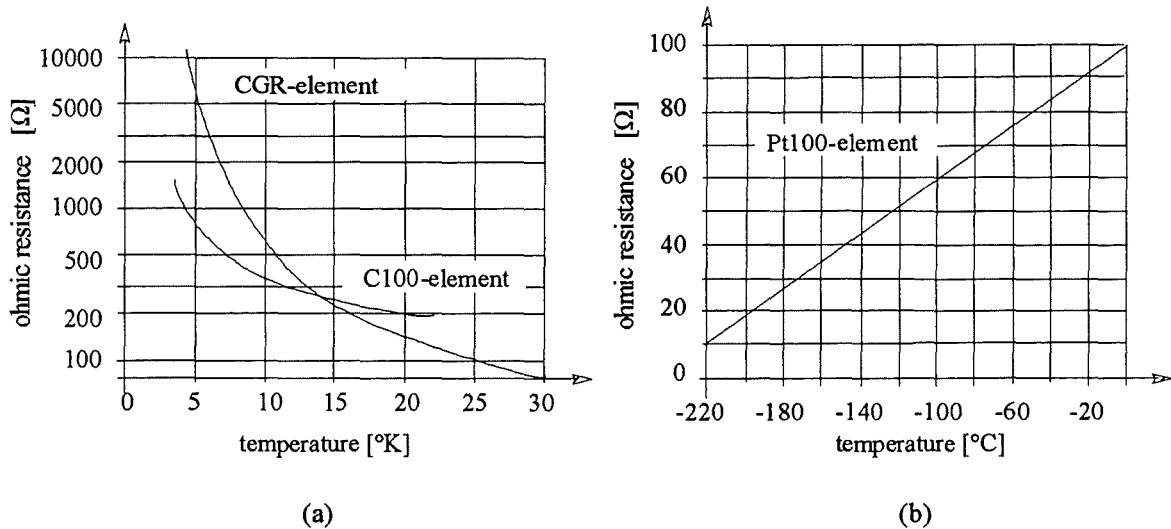


Figure 6.7: Ohmic resistance of the temperature detectors used in the CELLO-Magnet as a function of the temperature. a.) CGR and C100 elements; b) PT100 element.

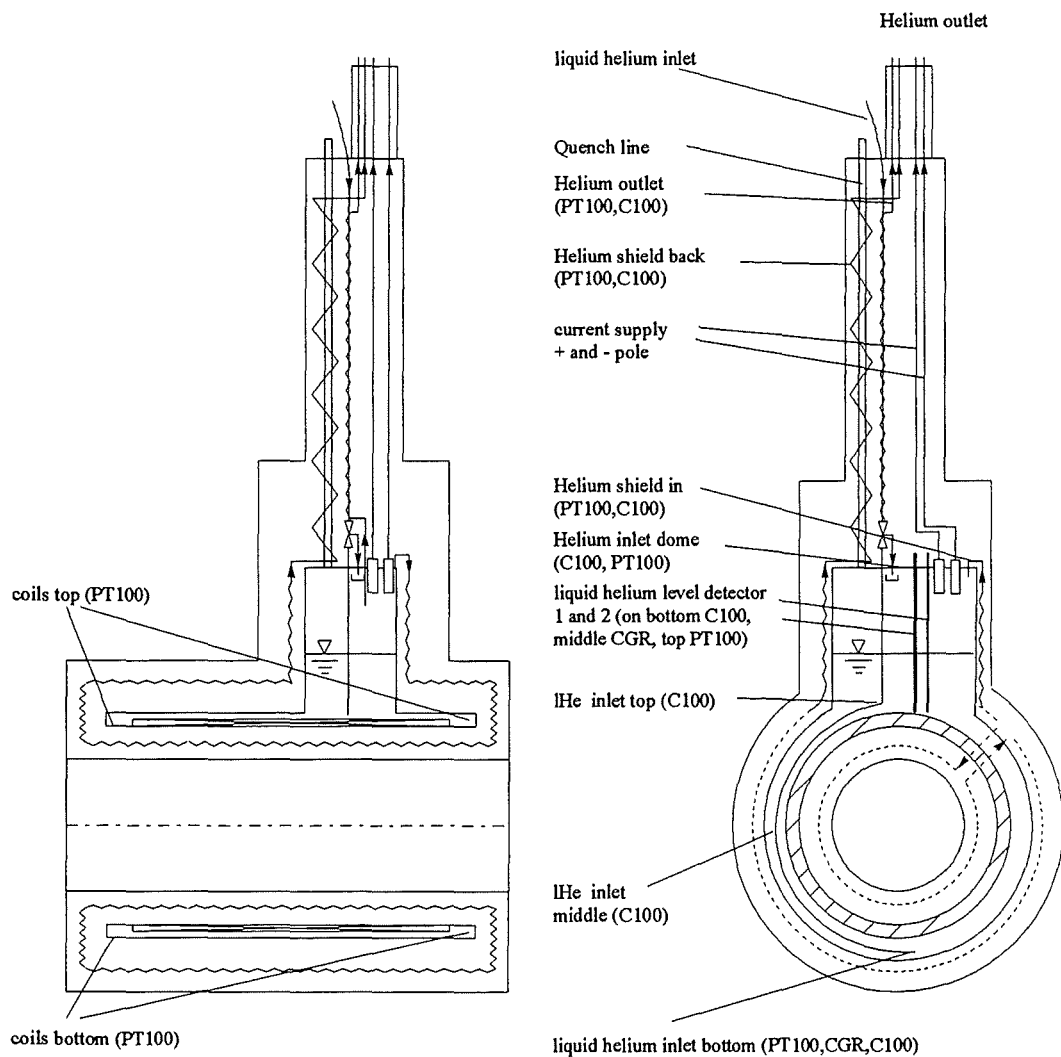


Figure 6.8: Location of the temperature detectors in the CELLO magnet.

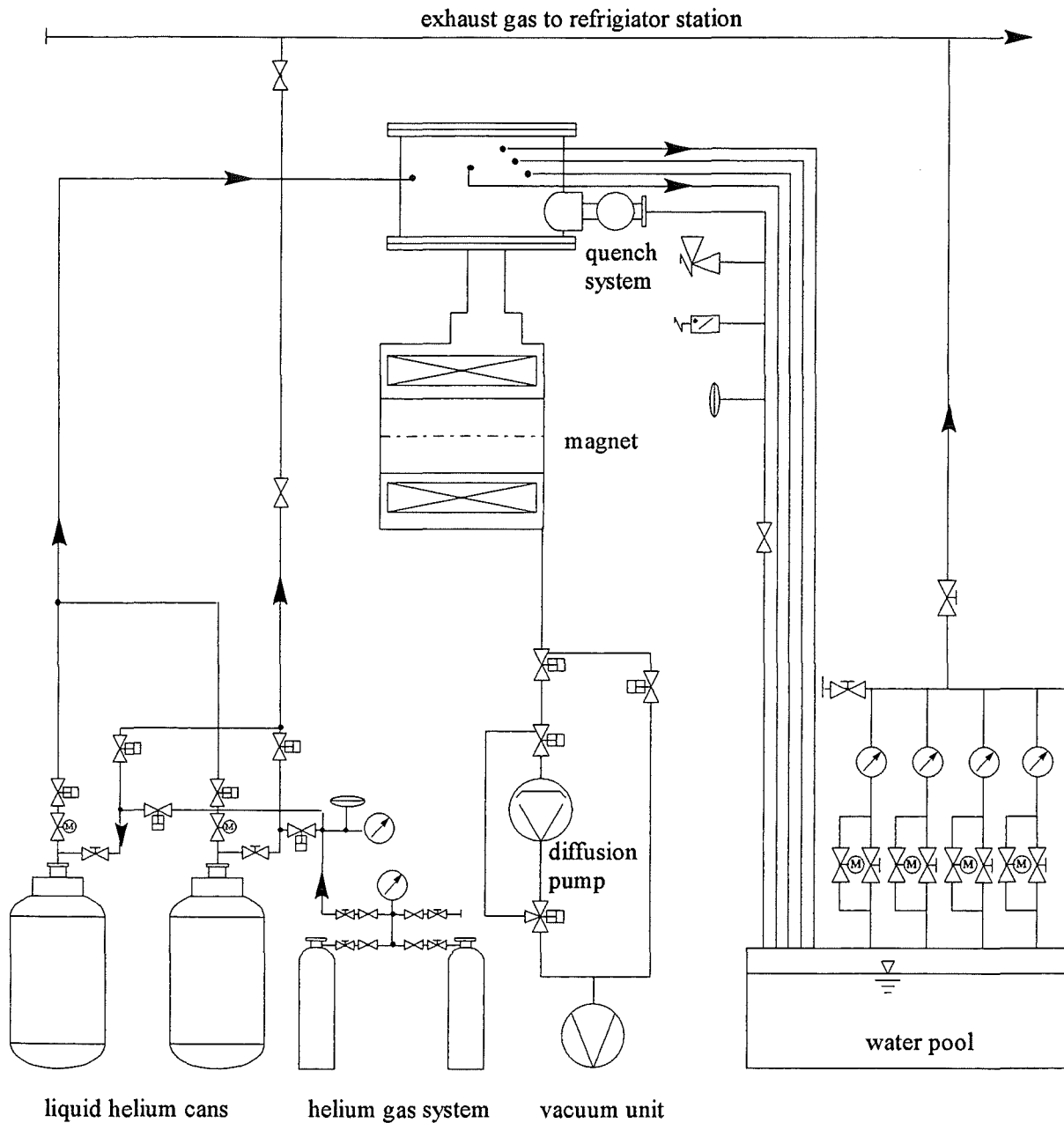


Figure 6.9: Loop scheme of the helium gas system of the CELLO magnet.

6.3.2 The vacuum system

In order to keep the heat transfer from the environment into the cryochamber as small as possible the cryoroom is protected from the environment by a evacuated room. The vacuum prevents a convective and conductive heat transfer. The remaining heat input via radiation can be minimised by highly reflecting multi-layer foil insulation to values of some miliwatts.

During operation the vacuum has a value of $2 \cdot 10^{-7}$ mbars. The vacuum system is steadily controlled by the measuring system shown in figure 6.10.

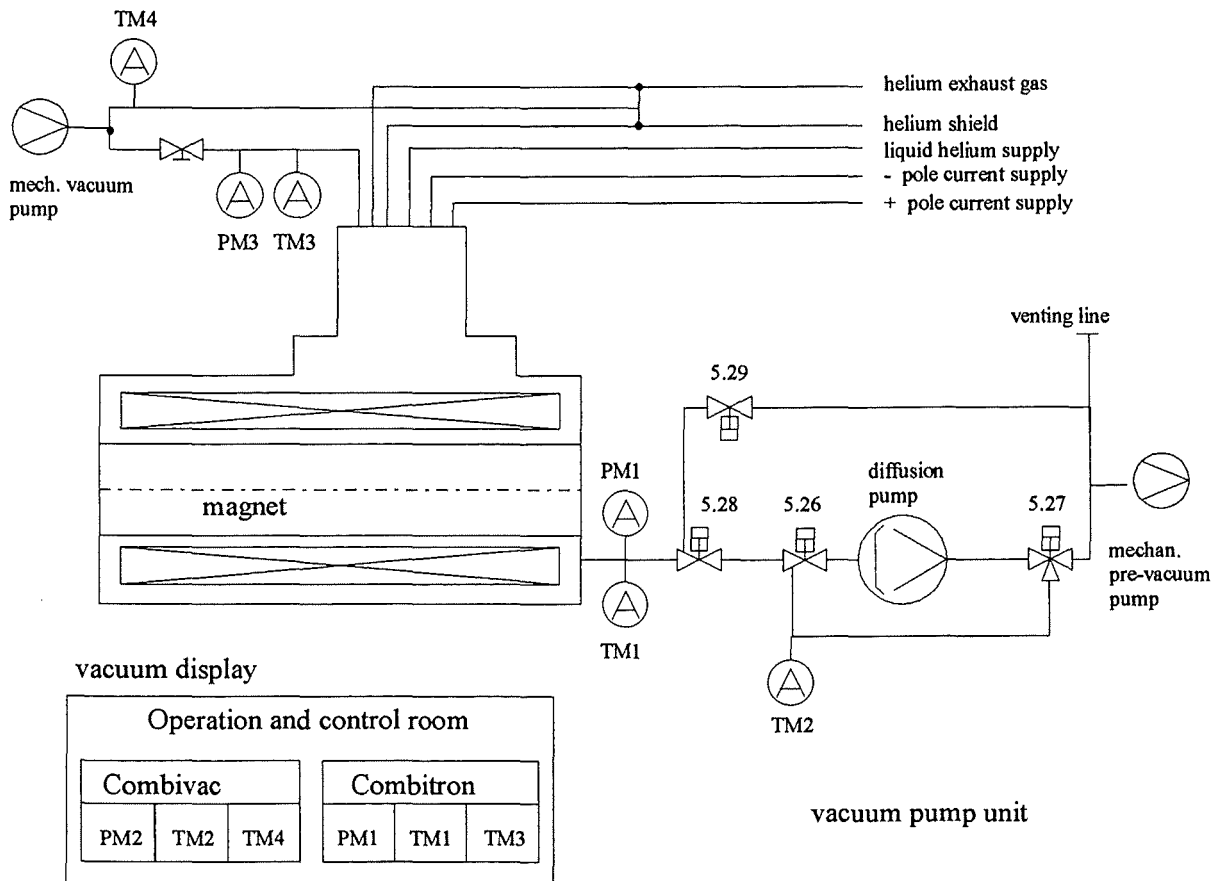


Figure 6.10: Vacuum measuring system of the CELLO-magnet.

Two different types of vacuum measurement elements are used in the CELLO magnet, Thermovac elements (TM) operating in a range from 10^{-3} -1000mbars and Penning tubes for the range 10^{-9} - 10^{-2} mbars, respectively.

The Thermovac probes work use the Pirani-principle and consist of a measurement pole and measurement cell. The pole, which is an extremely thin tungsten wire is located in the measurement cell. The wire is heated with a constant voltage and forms one branch of a Wheatstone bridge, which is compensated at extremely low pressures. If the gas pressure in the measurement tube increases, the temperature of the wire decreases due to the heat conduction and as a consequence the Wheatstone bridge is detuned.

Penning probes operate using the Penning principle of a self reliant gas discharging in a measurement tube with a cold cathode. The self-reliant gas dischargement is maintained up to low pressures by means of an electric field and a magnetic field connected in parallel to the cathode.

The vacuum in the cryochamber is achieved via two different pumps. As a prime for pressure down to 10^{-3} mbars acts a rotary slide pump. In order to obtain a vacuum of $2 \cdot 10^{-7}$ mbars a diffusion pump is used. One reason for using a diffusion pump instead of a turbo-

molecular pump is that the CELLO magnet owns a quite large scattering magnetic field. The operation of pumps with rotation mechanical parts consisting of electrically conducting materials in the scattering field of the magnet should be avoided, because electric currents could be induced in the rotors leading to a destruction of the pump.

6.3.3 Operation/control/security systems

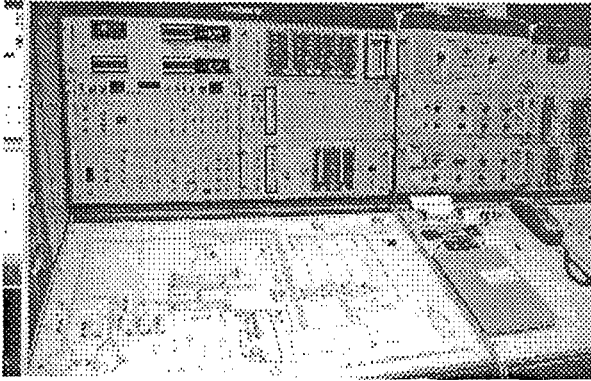
As already mentioned the liquid helium supply of the magnet is done with cans. A change of the cans in the region of the scattering field of the magnet is not allowed during magnet operation, because the strength of this field in the region of the cans is higher than permitted by the working security. Therefore, the switching from one can to the other is performed automatically. For this purpose in the cans a liquid helium level meter has been built in. If the liquid helium level in the cans falls below a critical value a programmable logic controller switches from one can to the other and simultaneously opens/closes the relevant supply/exhaust valves.

In order to prevent a serious damage of the magnet by turning on the power supply of the magnet, a turn on is only enabled if a certain liquid helium level on top of the coils is reached. The correct operation of the magnet in the power mode is controlled by a quench detector. This detector compare the ohmic resistance of one half of the coils with the other half. If a limiting value is exceeded a signal is send to the programmable logic controller which turns off the power supply.

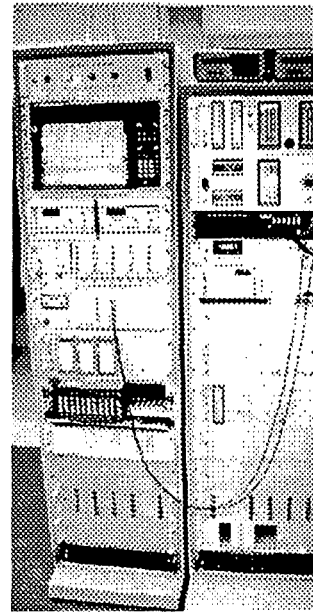
The control of the power supply is carried out by a digital sweep from the operating room. The digital sweep offers to adjust the current strength as well as to adjust a time dependent de- and increase of the current. The start up and the shut-down of the magnet is immediately interrupted by the programmable logic controller if the operator tries to turn off/on a too fast current change. In this case the logic controller turns off the power supply of the magnet and sends a signal to the power supply. Within the power supply the automatic shut down of the power supply is then activated and can not be interrupted by the user.

The maximum induction voltage allowed on the coils is limited to 400mV. This results in a maximum slope of the current of 900 Ampères per hour. As a consequence of the limited induction voltage the start-up to the maximum magnetic field strength requires a time of approximately 80 minutes and vice versa the same for the total shut-down. The used power supply is capable to remove the energy stored in the magnet by water-cooled thyristors in case of a general power loss.

The control and operating system of the CELLO magnet is located in the operation room, which is shown in the two photographs of figure 6.11.



(a)



(b)

Figure 6.11: Control panels (a) and towers (b) for the operation of the CELLO magnet.

6.3.4 Magnetic field strength and field distribution of the CELLO magnet

The CELLO magnet shows a linear dependence of the produced magnetic field on the supplied electric current throughout its whole operation range, see figure 6.12.

The magnetic field distribution of the CELLO magnet is cylinder symmetric in circumferential direction. The isolines of the total magnetic induction are shown in figure 6.13. Overlaid to this plot is a vector plot of the magnetic field vector. The vector plot reveals that near the coils a radial magnetic field component appears, which may be of influence for specific experiments. The radial magnetic field strength increases in direction of the coils, which is design related for this magnet type. The maximum radial field strength appearing directly at the wall near the coils in the cylindrical bore has a value of 0.26 Tesla. The magnetic field strength measured in a test of the magnet agrees with the calculated magnetic field strength by Maurer 1989. The deviations are in the range of $\pm 0.6\%$ which is within the measurement accuracy.

A region in which the relative deviation of the magnetic field is less than 10%, referring to $(B(r, \varphi, z) - B_{\max})/B_{\max}$, is defined as a volume of homogeneous field strength. According to this definition the experimental volume of homogeneous induction has a diameter of $\varnothing = 380\text{mm}$ and extends from $-225\text{mm} \leq z \leq 225\text{mm}$.

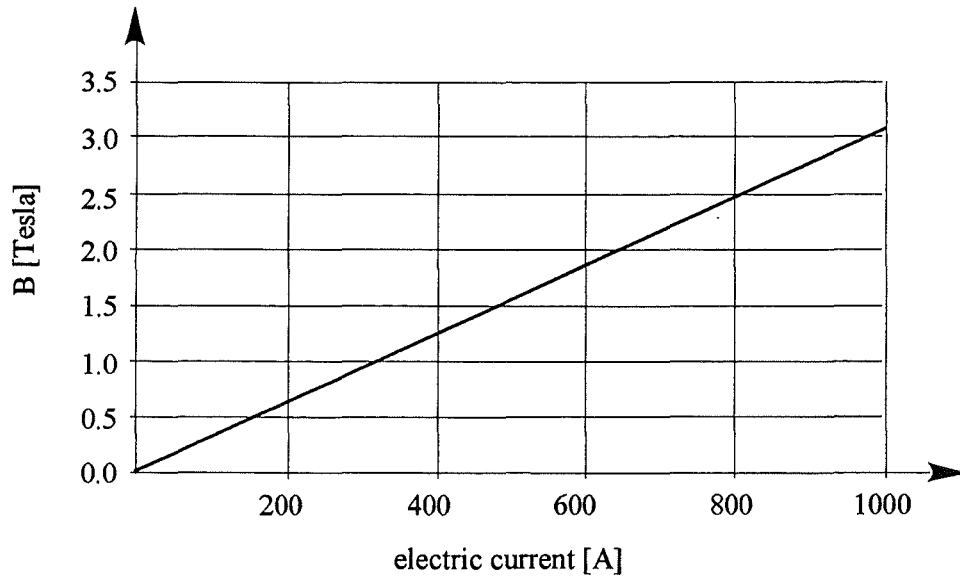


Figure 6.12: Produced magnetic field strength as a function of the applied current (CELLO).

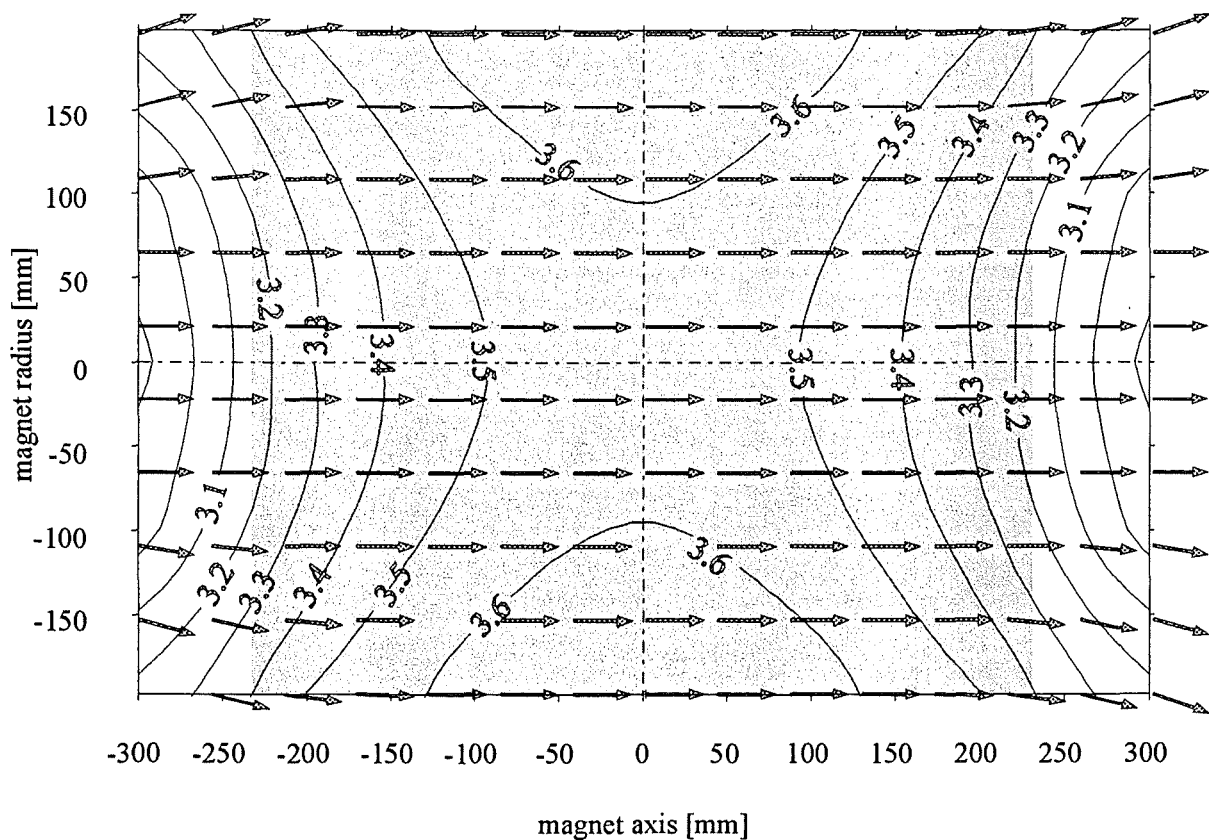


Figure 6.13: Isoline plot of the total magnetic induction appearing in the CELLO magnet. Overlaid is a vector plot of the magnetic induction. The region of homogeneous field strength is marked by dot bitmap.

The CELLO magnet has a large scattering magnetic field, which has even in a distance of 0.5m away from the magnet a strength of more than 0.5 Tesla. Therefore, the mounting of

measurement probes, which operate not on the basis of a currentless method, or the installation of controllers or regulators in the scattering field area is problematic. This means, that all sensors or controllers has to be magnetically guarded or be placed in a sufficient distance from the magnet, otherwise considerable measurement errors occur or a reliable controlling is not ensured.

The shielding against a steady magnetic field is not problematic at all. In case of such a field type the magnetic shield must not mantle the complete instrument, but it has to be placed in the direction of the magnet inbetween the instrument and the magnetic field lines. As protection ferritic steel of a high magnetic permeability can be used, in which the magnetic field lines are focused. The shielding is especially important for instruments working on the induction principle see section §8.

In case of the CELLO magnet all valves operating in the vicinity of the magnet are pneumatic controlled. The scattering field of the CELLO magnet is displayed in figure 6.14.

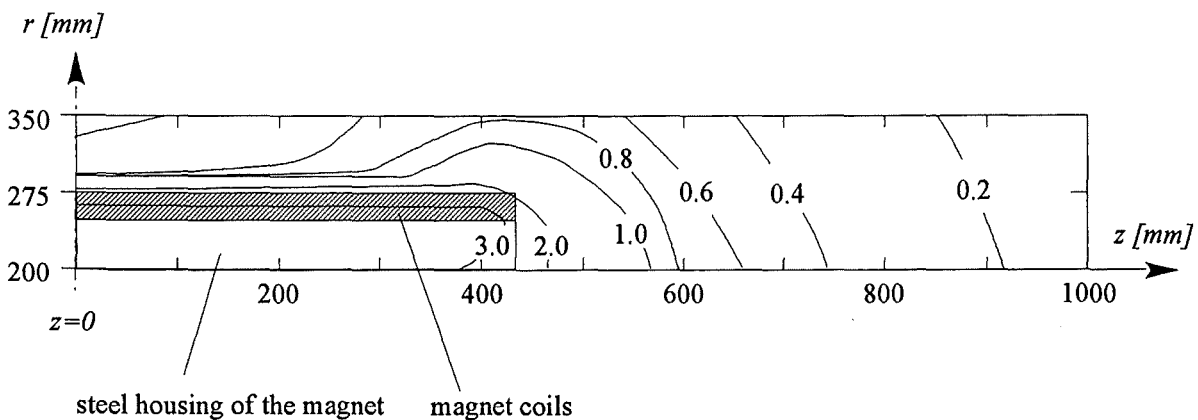


Figure 6.14: Scattering magnetic field strength distribution of the CELLO magnet in radial and in axial direction.

7 The sodium-potassium loop

7.1 Mechanical setup

The whole liquid metal loop with pumps, sump volume, expansion tank, heat exchanger, cold trap, pressure transducers, controlling valves etc. is mounted in a rack, which is beared on six rolls. The rolls are guided in rails, which are arranged in parallel to the long axis of both magnets installed in the MEKKA-facility. The setup is shown in figure 7.1.

All measurement, control and supply lines are flexible connected to the loop. The test sections to be measured including their piping are also on rails which are arranged in parallel to the axis of both magnets. They can be flexibly connected to the loop.

Between the loop and the test section pipings a valve station is interconnected which enables a reversal of the flow direction. This valve station is also beared on rolls and thus moveable. A possibility of a flow reversal is an important feature, since different flow directions especially in three-dimensional geometries leads for low interaction parameters (high flow velocities) to different experimental results.

The arrangement of a movable loop with connected test section enables the operator to drive the loop in any desired position relatively to the fixed magnets. Thus, special measurement positions of the test section within the magnetic field can be realised.

A hydraulic piston with a stroke of 2500mm drives the loop including the test section.

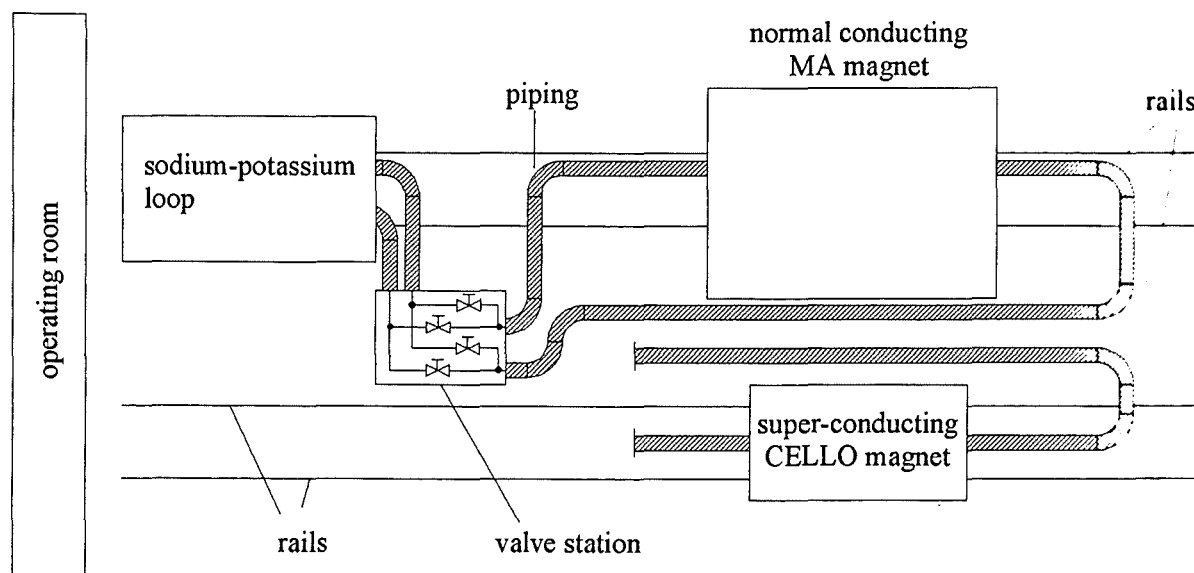


Figure 7.1: Geometrical arrangement of the sodium-potassium loop and the magnets in the MEKKA facility.

The hydraulic system has an adjustable velocity in the range from 0.1mm/s to 10mm/s and has a positioning accuracy of ± 0.1 mm. The position of the loop is measured with an ultrasonic measurement instrument. The hydraulic piston can be operated by a personal computer which is located in the operation room. The communication between the hydraulic system and the computer is performed by a serial RS232 interface.

The rack of the loop is manufactured of aluminium profiles and has on bottom a stainless steel tube. In case of a leak the liquid metal is caught in this tube, in order to guarantee a secure protection (alkali metal react rather aggressive with concrete which is usually used for laboratory floors). The complete liquid metal containing rack is air tight protected against the environment by stainless steel doors, which are tightened by rubber sealings. In case of an accident the closed volume can be flooded with nitrogen.

During the high temperature wetting procedure the closed volume can be cooled by a water-cooled circulation fan. The circulation fan has a cooling power of 4.5kW at 40°C, which is sufficient to keep the temperature below 50°C. Eventual liquid metal leaks are detected by short-cut electrodes, which are placed on the stainless steel tube on the bottom of the rack. In case of a leak the detectors send a signal to a programmable logic controller which itself then organises automatically the shut down of the loop operation and starts the security tasks.

7.2 The loop scheme

The loop scheme of the sodium-potassium loop called NaK1 is shown in figure 7.2. All components are remote controllable by the operator from the operation room. The loop consists mainly of three separate components fulfilling different tasks.

1. Operational loop:

- pumping of liquid metal during the experiments;
- controlling and adjusting the loop to ensure defined experimental conditions;
- data acquisition of important loop data during operation.

Components

- mechanical pump and electromagnetic (EM) pump;
- mass flow meter and EM flow meters;
- expansion tank;
- heat exchanger;
- sump volume.

2. Purification loop

- purification of the sodium-potassium alloy during the wetting procedure to ensure constant thermophysical data.

Components:

- cold trap;
- heat exchanger;
- EM flow meter.

3. Inertgas system

- protection of the liquid metal against oxygen;
- producing a pressure difference between loop and sump volume in order to fill the loop or to degas the loop.

Components:

- gas valves
- sodium-potassium separators.

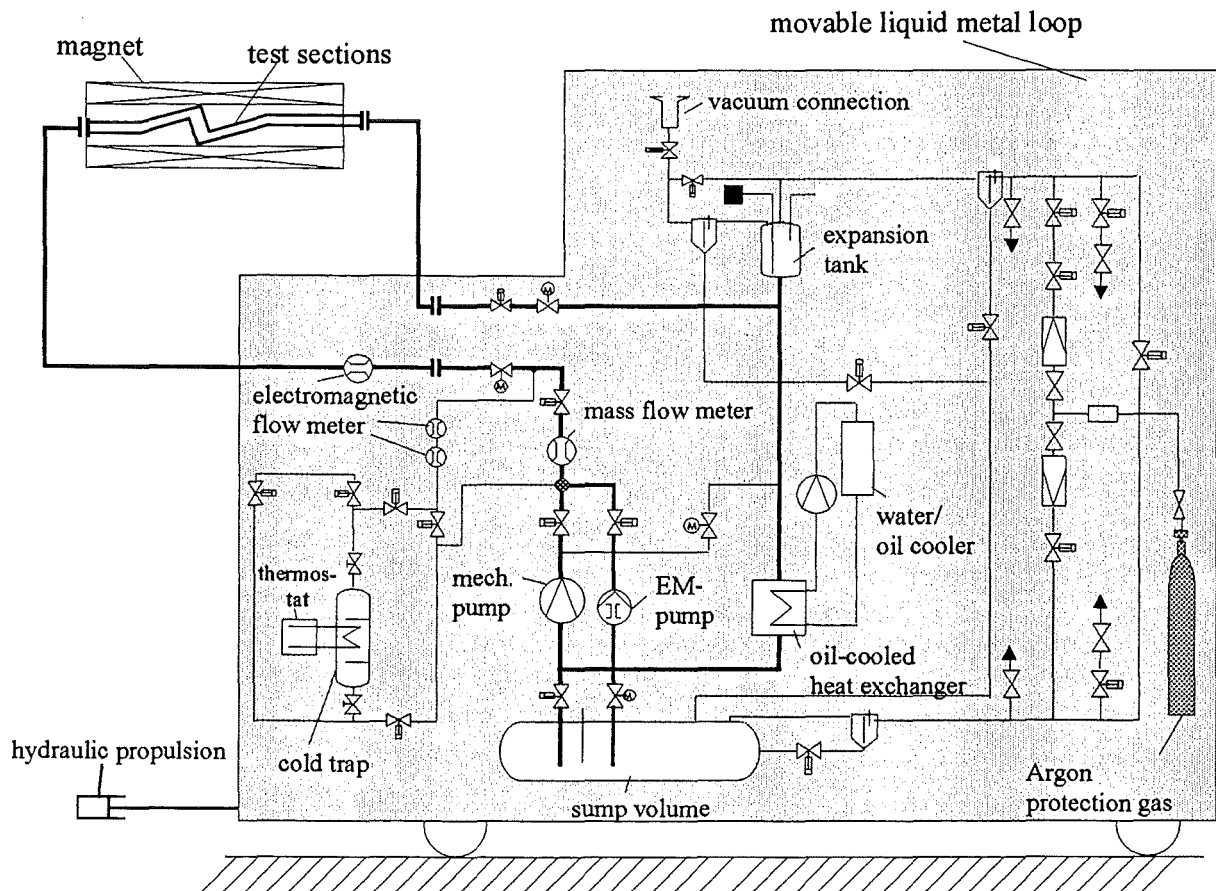


Figure 7.2: The sodium-potassium loop NaK1 of the MEKKA-facility.

In order to ensure a safe operation all systems have to be helium leak tight to get no alkali-oxide reactions. In the following subsections all main components of each system are described in detail.

The measurement components which acquire the MHD research relevant data (temperature, flow rate, pressure etc.) and which are incorporated in the loop are described with respect to their measurement principle and their accuracy in detail in section §9 (measurement techniques in MHD).

7.2.1 The operational loop

A schematic drawing of the operational loop is shown in figure 7.3.

Sump volume

The sump volume is fabricated of stainless steel and has a volume of 280 *litres*. It is filled with 200 *liters* of sodium-potassium. The prove pressure has been 15 bars which is considerably higher than the maximum pressure head producable by the pumps. It is foreseen to contain the whole liquid volume in non-operation times. The actual size has been chosen considering a maximum fluid inventory of the test sections including the piping of approximately 100 *litres*, which was sufficient up to now.

In case of a leak in the loop system the pneumatic valve 1.01 opens and the liquid flows in the storage tank. Level detector control the maximum and the minimum level in the sump volume.

In order to fill the loop and the test section the gas pressure in the sump volume is increased whereas the loop and the test section are evacuated. By a slight opening of the motor valve 2.01 the pressure difference between loop and sump fills gradually the loop. The evacuation of the loop with the test section has the advantage that even complex geometries can be filled and less effort has to be spent to degas the loop. However, a filling procedure by means of evacuation demands a fully gas leak tightness of all systems.

NaK1-pump

The NaK1-pump is a mechanical centrifugal pump. The lubricant and the pumped fluid are identical. Thus, eventual incompatibilities between lubricants and NaK are avoided. Problematic for a self-lubricating pump is the choice of the material for the bearing. In a test series with different materials at a temperature of 350°C and a time of 170 hours silicium carbide demonstrated the highest compatibility. Another problem arising is the flow past the annular gap and the bearings with liquid metal. A minimum flow rate has to be ensured in order to cool the pump satisfactory. This has been calculated and later realised by a hole drilled in the second compression step of the pump. Using liquid metal as coolant in the area of the electromotor MHD effects appear due to the rotating electric field in the rotor of the electromotor. These MHD effects produces pressure drop and therefore reduce the flow rate necessary for

cooling. However, by adjusting the size of the hole in an appropriate way this condition can be met.

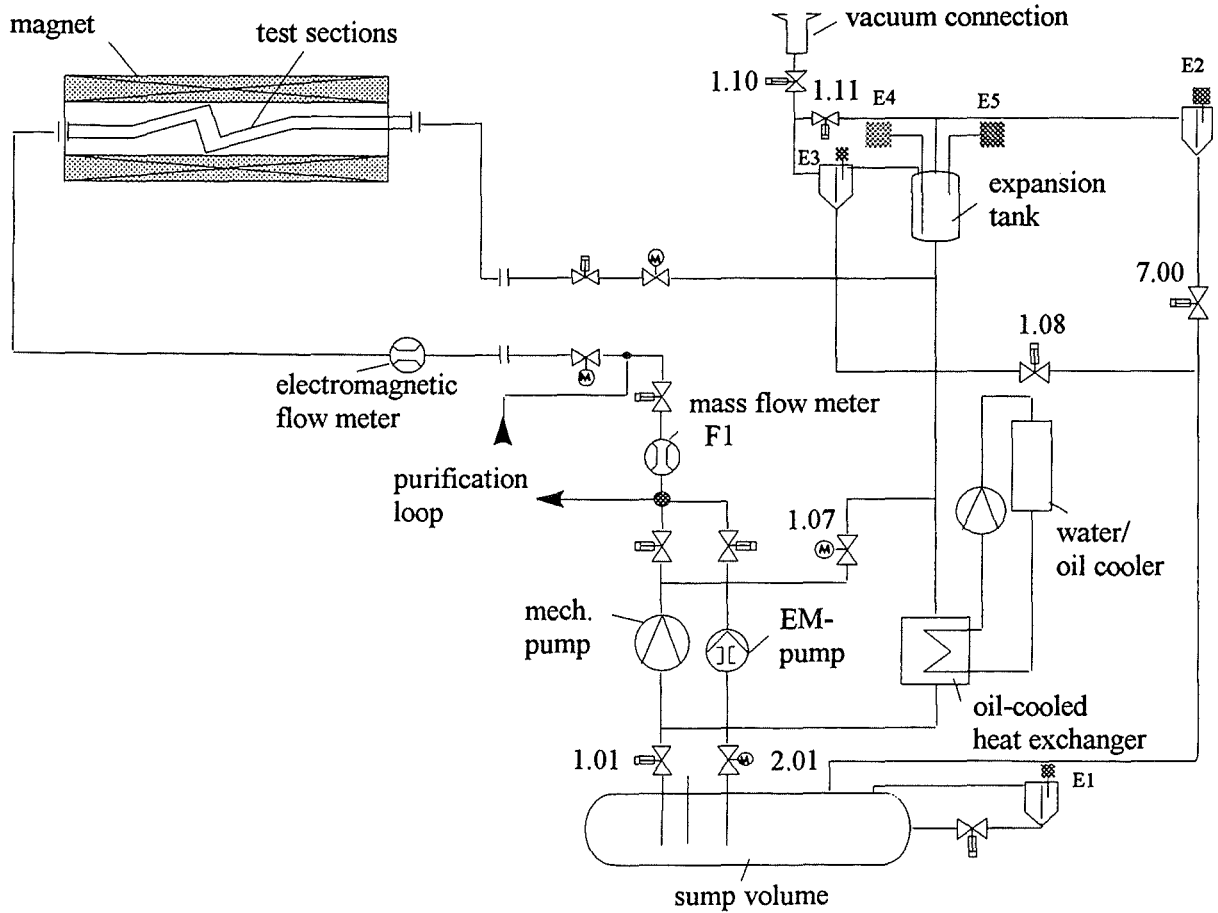


Figure 7.3: Operational loop of the MEKKA-facility (NaK1).

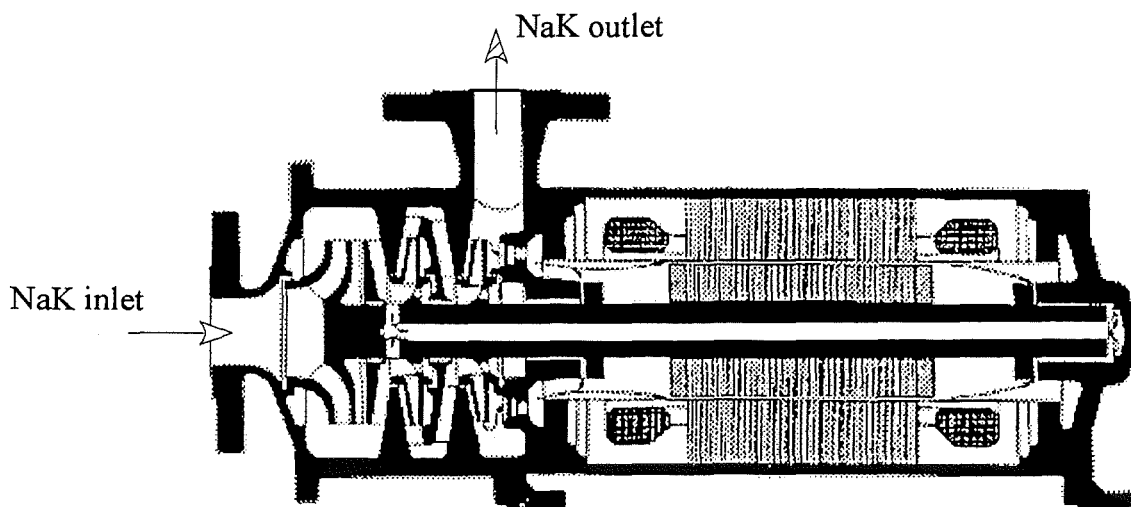


Figure 7.4: Schematical drawing of the pump (CAM3 from HERMETIC).

The electrical net power of the pump is 17 kW at 380 Volts. At maximum power the pump produces a pressure head of 9.5bars at a flow rate of 25m³/h. The maximum allowable temperature is limited to 170°C. In figure 7.4 a schematical drawing of the pump is shown. The characteristics of the pump as well as the effectivity are depicted in figure 7.5.

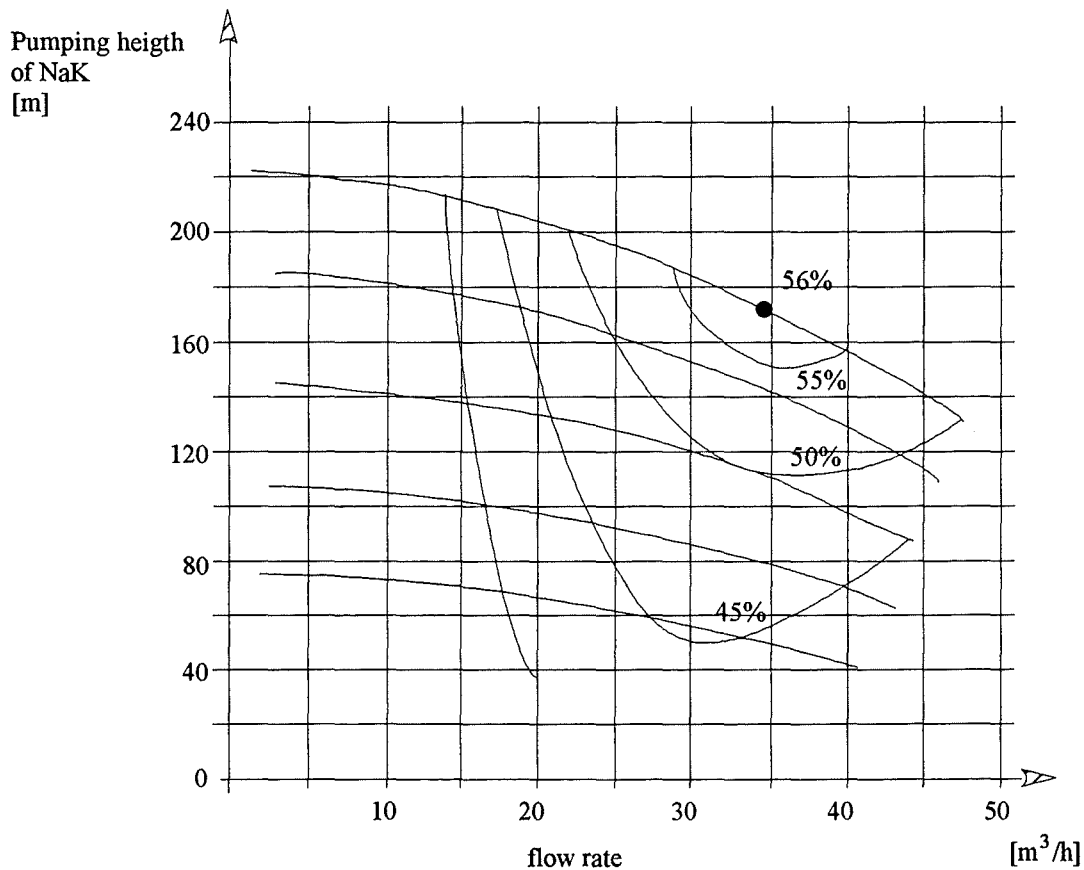


Figure 7.5: Efficiency and pumping height of the used mechanical centrifugal pump in the NaK1-loop as a function of the flowrate.

Electromagnetic pump

In the electromagnetic (EM) pump an AC magnetic field produces Lorentz forces within the fluid, which pushes the medium. The pump can be operated independently from the mechanical pump. The EM-pump is used for high temperature wetting runs up to 350°C. The usability at high temperatures is a general advantage of EM pumps since only the pumping channel is exposed to the high temperatures. Besides they offer the possibility for an extreme exact adjustable flow rate also at rather small flow rates. Therefore, this pump is used in the experiments for realising flow rates below 50g/s. The pump characteristics of the used pump is shown in figure 7.6.

With the motor valve 1.07 the flow through the test section can be additionally minimised, so that for a complete open valve 1.07 flow rates down to 25g/s can be achieved which is necessary to obtain the high interaction parameters appearing in some fusion blanket designs.

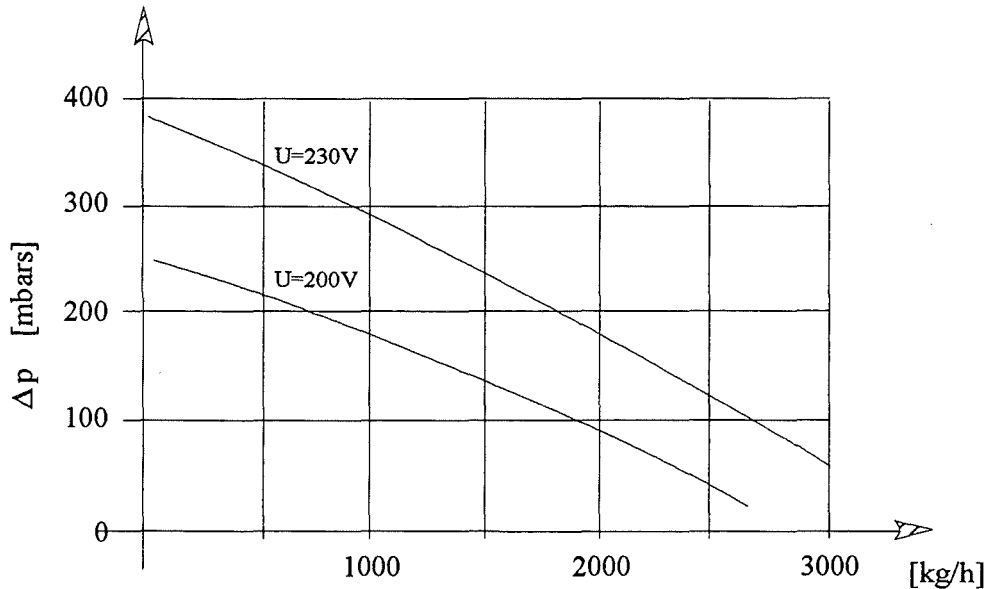


Figure 7.6: Pumping height of the EM-pump in the MEKKA-facility as a function of the mass flow for two different voltages at the coils..

Heat exchanger

The heat exchanger removes the heat produced by the pumps, the hydraulic and the magnetohydrodynamic pressure drop. In heat transfer experiments it additionally removes the heat from the heater elements. Its task is to ensure a constant temperature throughout a measurement campaign.

For this purpose a helix type double-tube heat exchanger has been chosen. Due to safety aspects a specific heat transfer oil is used as coolant on the secondary side. During the wetting procedure the heat exchanger can be used as a heater. For this purpose the heating elements of the oil loop system can be used. The design of the heat exchanger and all its related components was made so that it could stand long term the maximum loop temperature of 350°C.

The technical drawing of the heat exchanger is shown in figure 7.7. The thermophysical data of the heat exchanger oil "Marlotherm" which is toxic is given in table 7.1.

fluid	c_p [J/(kgK)]	ρ [kg/m ³]	$\nu \cdot 10^{-6}$ [m ² /s]	λ [W/(mK)]
Na ²² K ⁷⁸	953	847	0.468	23.200
oil "Marlotherm"	2260	805	2.000	0.128

Table 7.1: Thermophysical data of the heat exchanger oil Marlotherm compared to the liquid metal Na²²K⁷⁸.

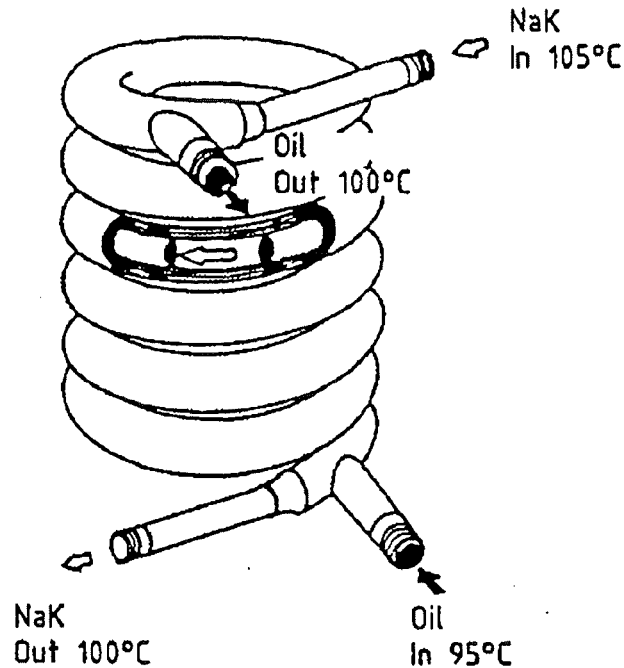


Figure 7.7: Technical drawing of the double tube heat exchanger unit.

Operation and controlling valves

All valves used in the sodium potassium loop are metal bellow sealed valves made of stainless steel. Also the valve seat is made of stainless steel.

The valves are operated externally from the operation room. The current position of the valves is visualised on a panel in the operation room by red (\approx valve closed) and green (\approx valve opened) lights. The signal of the current position is carried out in case of the pneumatic valves by end detectors. In case of the electrically driven motor valves the positioning is assigned by potentiometers which also shows the opened percentage of the cross section.

Extremely high requirements regarding the leak tightness are necessary for the following valves.

1. The fast draining valve 1.01 and the filling valve 2.01

- reason:
- during operation no liquid is allowed to get in the sump volume;
 - by opening the loop for e.g. repairing works the sump volume has to be protected from oxygen input;
 - during the filling procedure the pressure in the sump volume is higher than in the loop. In case of a leak a preliminary pressure equalisation would occur, which disables a filling of the loop.

2. The gas valve 1.08

- reason:
- during operation the fluid should not penetrate into the gas system, because at the next filling procedure while evacuating NaK would be sucked in the gas system and the vacuum pump.

The high leak tightness of the valves originates from the exact fabrication of the stainless steel bodies, which is realised by polishing. As an example of the used valve types a manually operated control valve is shown in figure 7.8.

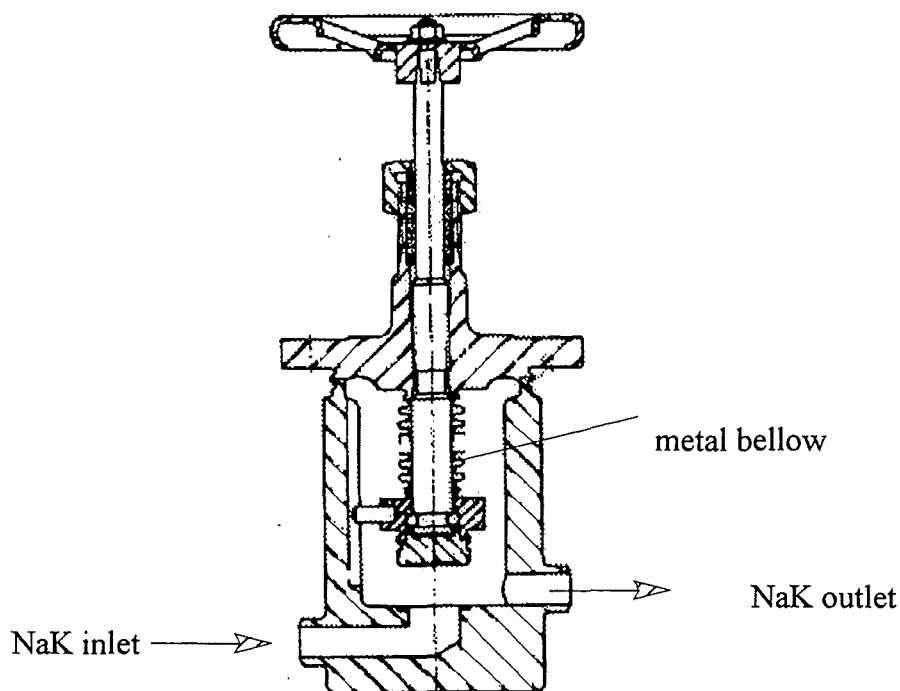


Figure 7.8: Metal bellow control valve manually operated. The valve is made of stainless steel and used in the MEKKA facility.

Expansion volume

One task of the expansion volume is to contain the differential volumina appearing by a temperature rise/fall of the fluid due to volumetric expansions. Another task of this volume is to collect gas bubbles from the loop. The function of gas collection is important, since in test

sections with a complex geometry during the filling procedure gas filled holes and pockets may develop. The degassing of the test section is performed by the following procedure. Running EM-pump and closed valve 1.5. The liquid metal is pumped over a degassing line directly in the expansion volume.

The expansion volume is the highest part of the loop. It has a volume of 100 *liters*. The maximum allowed pressure of this stainless steel container is 10bars at 250°C.

The height of the fluid level in the container is measured by a pressure difference measurement and a magneto-swimmer. The accuracy of the pressure measurement is $\pm 1\text{mm}$, whereas the magneto-swimmer has a poor accuracy of $\pm 5\text{mm}$. During loop operation a certain fluid level in the volume must exist. Therefore, two electrodes acting as end detectors are built into the expansion volume. One electrode is the minimum detector the other indicates the maximum allowable fluid level. If the fluid level during operation falls below the minimum level the pumps and coolers are shut down in order to prevent a serious damage of the loop. If during the filling procedure the maximum level detector is activated two simultaneous processes start. The gas pressure equalisation valve 7.01 (see figure 7.9 inertgas system) is opened and secondly the filling valve 2.01 is closed.

7.2.2 The inertgas system

The inertgas system is shown in figure 7.9. It has mainly two tasks.

1. Protection of the liquid metal from oxygen.
2. Production of a pressure difference for the filling of the loop with liquid.

Both tasks require a high level of leak tightness of the whole gas system against atmosphere. In contrary to the liquid metal loop here valves with a plastic valve seat are used. Their maximum allowable pressure is 10bars.

A twofold inertgas system is used. One gas supply line goes to the sump volume the other one to the loop via the expansion volume. A pressure equalisation of both systems can only be achieved if the valve 7.01 is opened.

In order to protect the gas system and all its components from NaK between the loop and the gas system NaK separators are interconnected. If NaK somehow gets in the separators it will flow back in the sump volume. The detection of a possible NaK content in the separators is performed by means of an electrode. If NaK is penetrating into the separator the electrode is activated and on the control panel in the operating room a yellow light turns on. The NaK separator E2 of the loop additionally owns an oil cooler, which in case of the appearance of sodium vapour allows to condense the vapour in the separator. All separators are made of stainless steel and have a volume of 0.25*litres*. The maximum pressure is limited to 10 bars.

The pressure level in both loop and sump volume can be adjusted via controlling valves to a certain value. During operation and shut down times usually a pressure level of 0.2bars is set. The pop-off valves (5.05, 6.05) of the gas system can be stepless adjusted from 0-4bars and prevent the gas system from a too high over pressure.

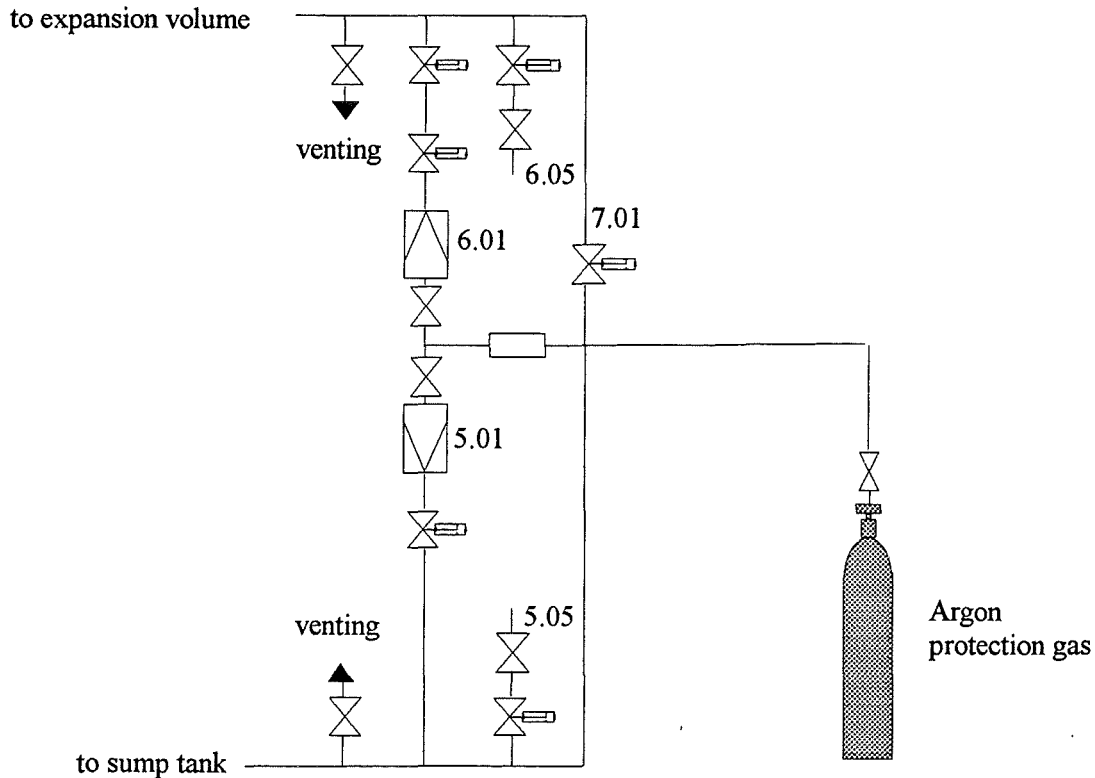


Figure 7.9: Inertgas system of the sodium-potassium loop in the MEKKA facility.

7.2.3 The purification loop

The purification loop consists mainly of the cold trap with thermostat and two electromagnetic flow meters. The purification loop is shown in figure 6.10.

By heating up during the wetting phase a large part of the oxygen removed by the NaK from the duct surfaces is solved in the liquid metal. In the cold trap the solved metal oxides are separated from the liquid. The separation process takes advantage of the weaker solvability of the metal oxides in pure NaK at lower temperatures. For this purpose the NaK is cooled by an oil-cooler embedded in the cold trap to temperature near the solidification temperature (solidification temperature -11°C). The oxides are separated in a dense sieve grid made of stainless steel wires. At operating temperatures of the cold trap between -4°C and -6°C at the inlet an extreme high purification ($>99.9\%$) is achieved. The purification effect of the cold trap rapidly decreases if a temperature of 40°C is exceeded. This may happen if the flow rate trough

the cold trap is too high. Hence, the flow rate is controlled by an electromagnetic flow meter F3.

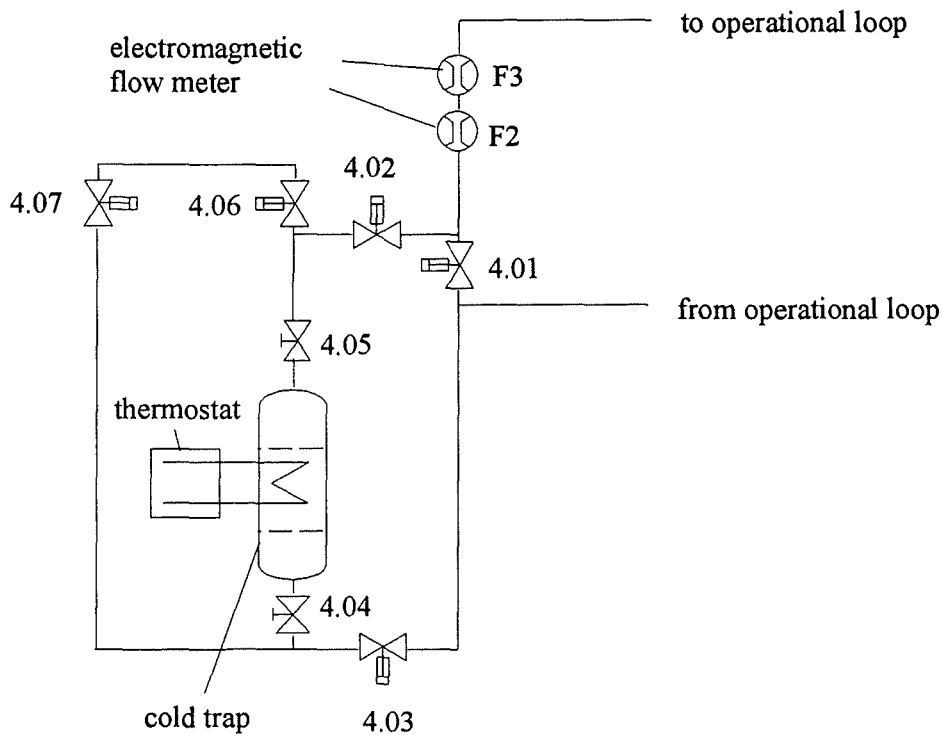


Figure 7.10: Purification loop of the sodium-potassium loop in the MEKKA-facility.

A technical drawing of the cold trap used in the sodium-potassium loop of the MEKKA facility is shown in figure 7.11.

At longer shut down periods of the loop and the test sections a wetting phase should be performed before operation even if the test section has been wetted. By opening/closing of the valves 4.02 and 4.03 the purification loop can be connected/disconnected from the operation loop. In order to cool the heat transfer oil of the cold trap a water-cooled thermostat is used. This thermostat has an effective cooling power of 3Kilowatts at -10°C .

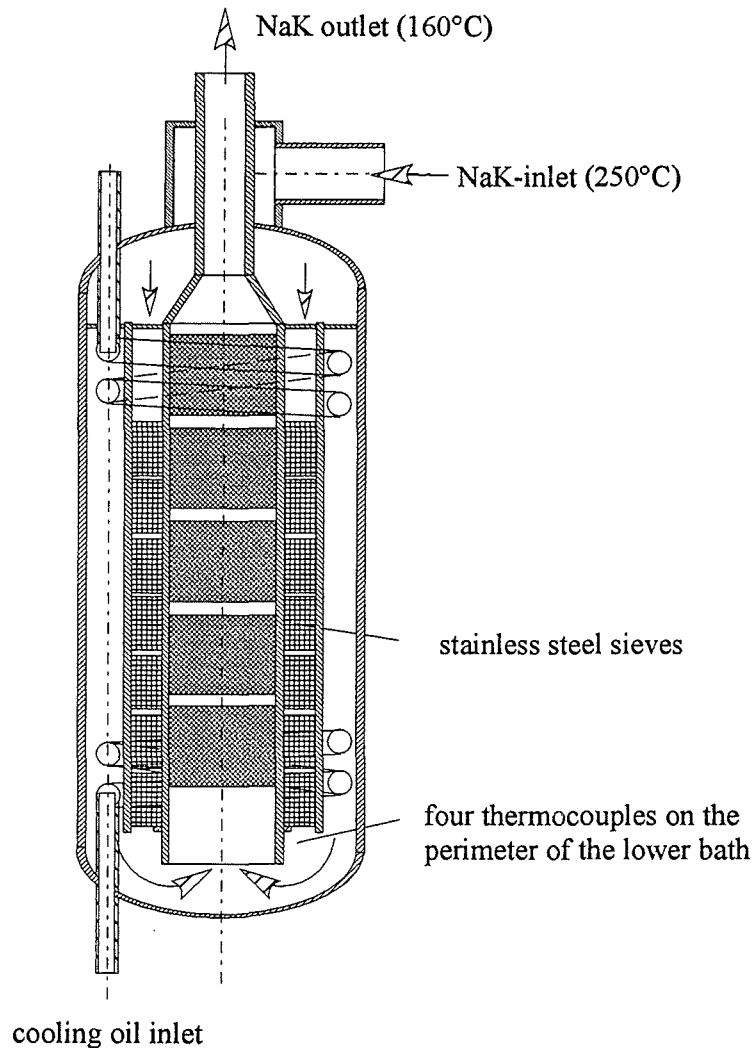


Figure 7.11: The cold trap used in the sodium potassium loop.

7.3 Control and operation of the sodium-potassium loop

The loop with all its systems is totally remote controlled from the operation room. Due to the large amount of components, alarm and level detectors a fully manual operation and a visual control only is hardly possible. Moreover, in case of an accident quite a lot of steps has to be made almost simultaneously or in defined time steps. All together this would require a large operation team. Therefore, all critical components are connected via alarm sensors to the input gates of a programmable logic controller.

Via logic coupling of input signals with output signals the correct control of the components is ensured. Due to the large amount of possible states of the liquid metal loop a large amount of programs is embedded in the logic controller, which in case of a specific input signal leads to an appropriate reaction. This method prevents the facility from a misoperation by a user.

Two different kinds of programs has to be distinguished:

1. Operational programs.
2. Security programs.

Both types of programs are steadily resident in the logic controller. The operational programs ensure a secure experimental operation, also if alarms of minor importance appear, which could not lead to a serious damage of the facility. In this case the logic controller shows optically or acoustically the alarm and reacts by its own to the signal. The operational program prevents the user from turning on/off certain components if a signal is present or not, e.g. it is impossible to switch on a fluid pump if there is not enough liquid in the expansion volume. A part of the operational program is displayed in Appendix A table A1.

If critical signals or signal combinations are present at the input of the logic controller, the logic controller immediately activates the security programs, which themselves react with a controlled shut down of the loop. A list of the security programs is shown in table A2 of appendix A.

Another part of the loop control is the control of the main loop data, which are written on a 32 channel printer. The paper feed can be flexible adjusted in order to resolve time relevant steps. With the printer a long term control of the loop during shut down times is enabled. Also heating or cooling procedures of the loop can be followed.

The printer is also connected to the programmable logic controller. In the printer alarm and security values can be set to each channel. If the alarm or security values are exceeded the signals are displayed by a light and sent to the logic controller.

Finally on the main control panel all valves, pumps alarm signals are displayed. The operator can open/close valves, drive pumps etc. by pressing the switches on the control panel. The control panel, the programmable logic controller and the printer are located in the operation room. The photo in the figures 7.12 shows the control panel in the operation room.

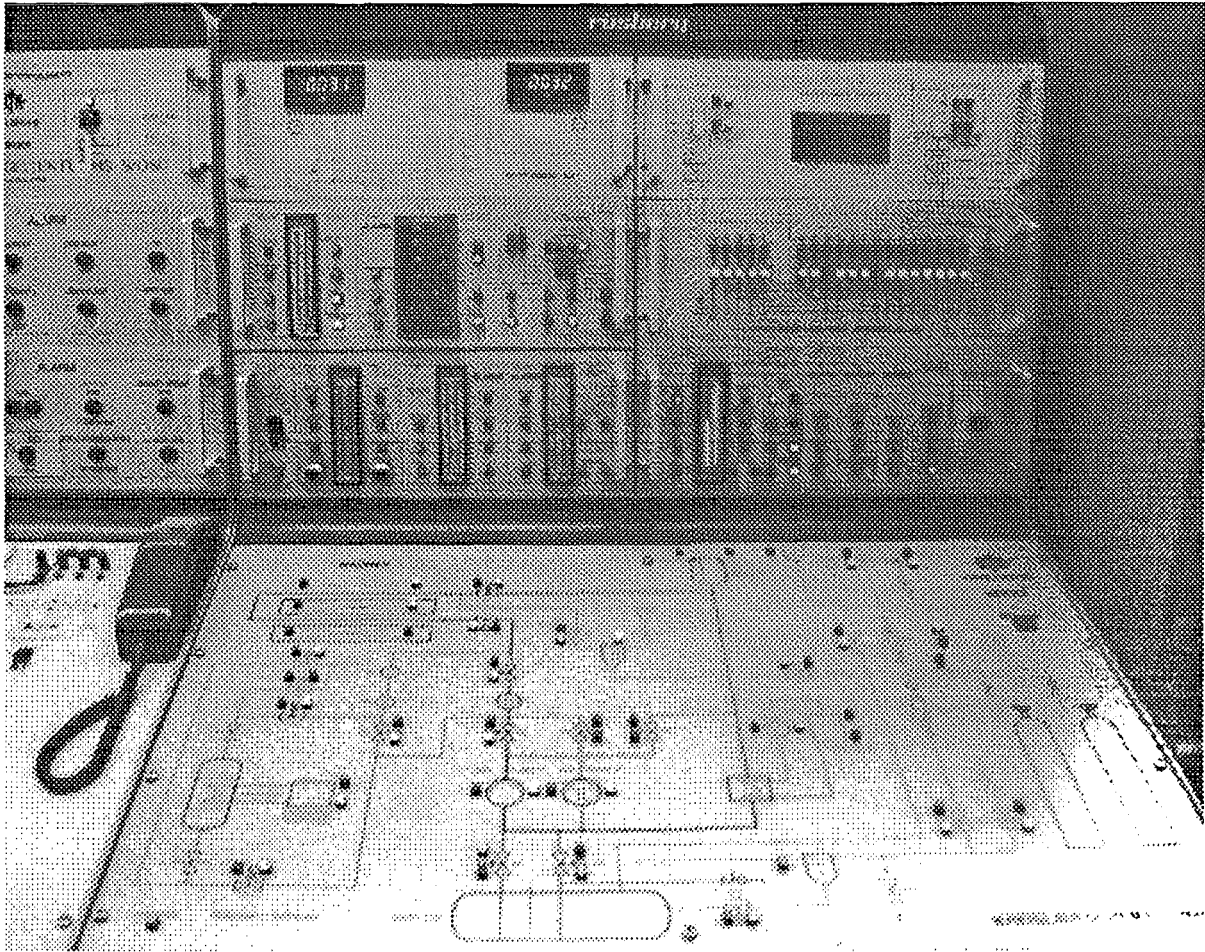


Figure 7.12: Control panel of the liquid metal loop (NaK1) in the operation room of the MEKKA-facility.

8 The gallium-indium-tin loop (GALINKA)

8.1 The design features of the gallium-indium-tin loop

As already described in section §5 the relatively high price of the GaInSn alloy allows not to built a large loop with a large fluid inventory. But by using a horse track design the fluid volume can be drastically reduced.

All components of the loop, namely pump, flowmeter, heat exchanger and test section are placed within the magnet. A schematic drawing of such a loop type is shown in figure 8.1. The whole loop is connected with flexible pipings and flexible supply and acquisition lines mainly to the environment. The flexible pipings are mainly rubber hoses. The complete loop is beared on rails in a closed rack, which can be manually moved within the magnet.

The loop itself is fabricated of a carbon glass structure which is glued in its single duct parts. The duct parts, 180° bends, pump branch and the test section are afterwards screwed together. The sealings between the individual parts are made of rubber. The test section is connected via a draining line with the storage tank.

In order to fill the test section the loop is evacuated via a pressure measurement pipe. In the line between loop and storage tank, in which a gas over pressure is set, a valve is interconnected. By opening a filling valve fluid is sucked into the loop. The rest of the procedure is similar to the one of the sodium-potassium loop previously discussed.

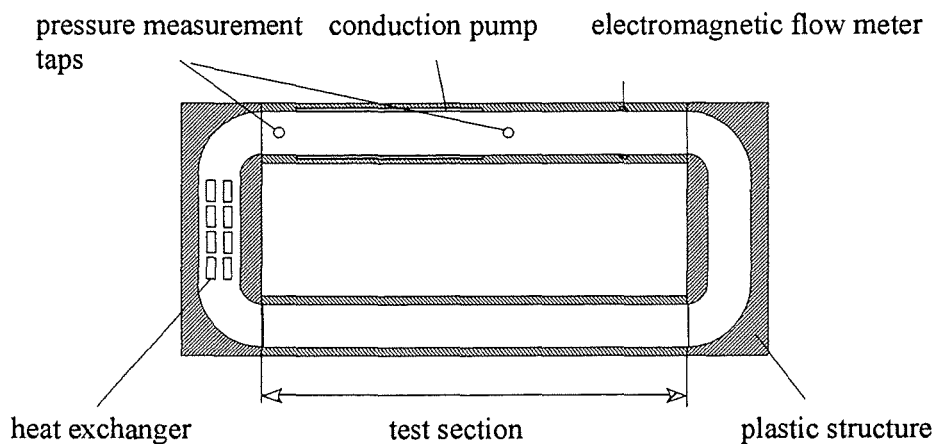


Figure 8.1: Schematical drawing of the GALINKA loop used in the MEKKA facility.

In order to protect the liquid metal from oxygen the same inertgas as in the other loop type, namely argon, is used. So the same valve types and equipment can be used.

The whole loop shown in figure 8.1 is placed in the homogeneous part of the magnetic

field of the normal-conducting MA-magnet of the MEKKA-laboratory. Due to the geometric extension of the homogeneous magnetic field strength the maximum loop dimensions are restricted to 800mm×485mm×168mm. A photograph of the loop is shown in figure 8.2.

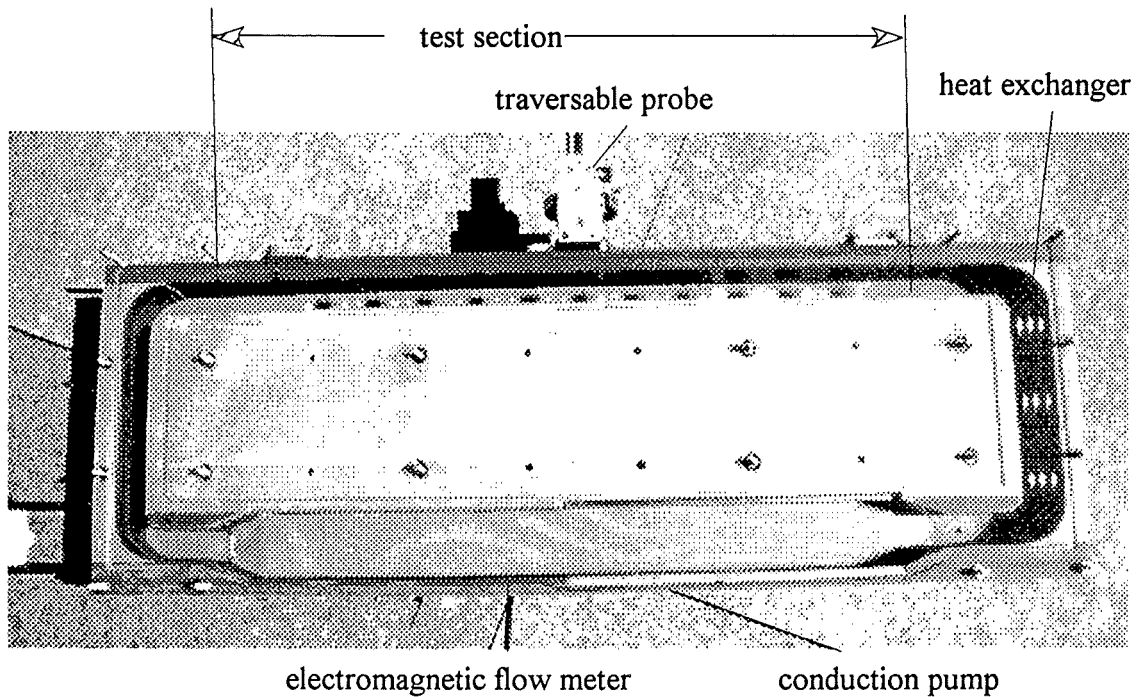


Figure 8.2: Photograph of the GaInSn-loop used in the MEKKA-facility.

Although the operation and security requirements by using GaInSn are not as restrictive as for sodium-potassium a similar profile of the security and operational programs is required. In order to save time and money the electrical connections of this horse track loop are made identical to the sodium-potassium loop. By switching the connectors from the NaK loop to the GaInSn track the same operation and security programs with the same programmable logic controller run also for the GaInSn loop.

The GaInSn loop is also completely remote controlled and operated from the operation room. A scheme of the operation panel is shown in figure 8.3.

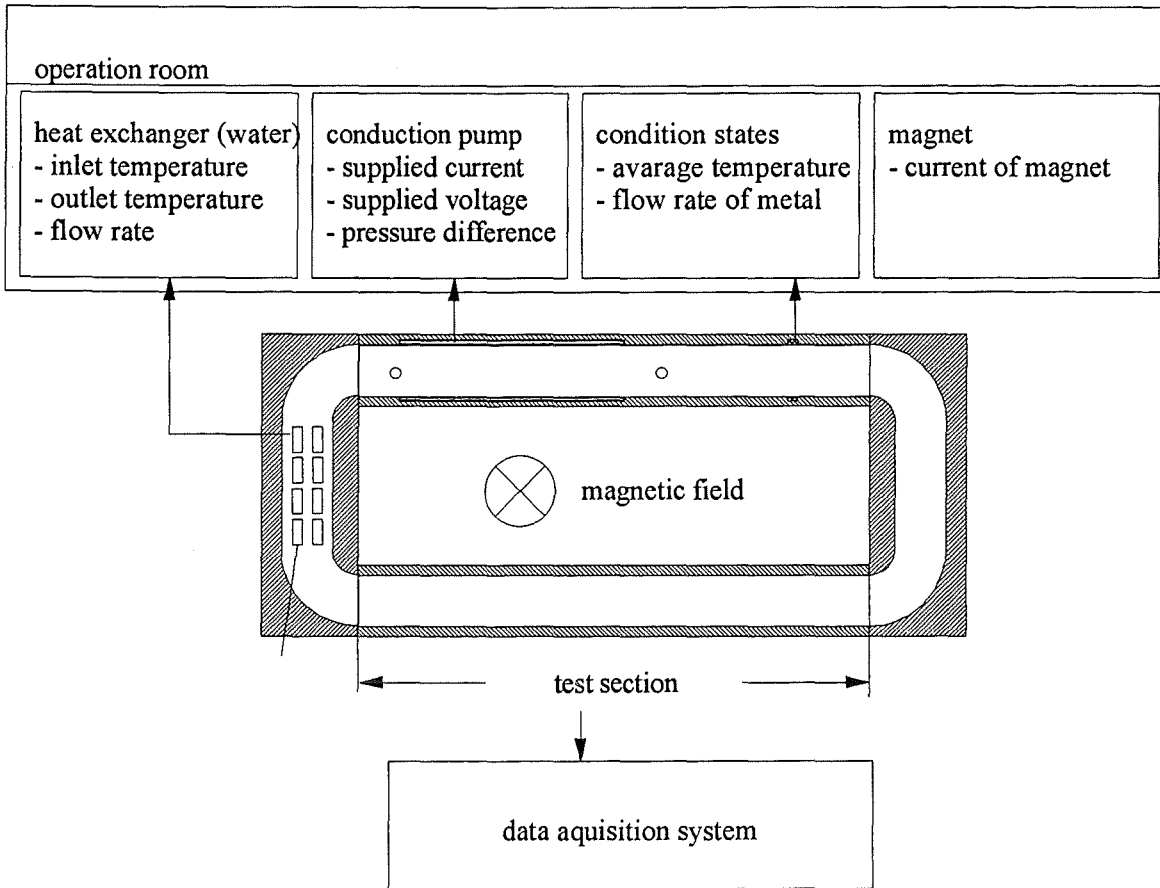


Figure 8.3: Schematical graph of the operation panel of the GaInSn-loop.

8.2 The pump design

In order to circulate the liquid metal in the loop an electromagnetic pump based on the electromagnetic conduction principle is used. This operation principle, shown in figure 8.4 is explicitly described in Foust 1972 or Birzvalks 1986, the side walls are made as electrodes supplied with a voltage. This voltage drives an electric current I in the liquid metal.

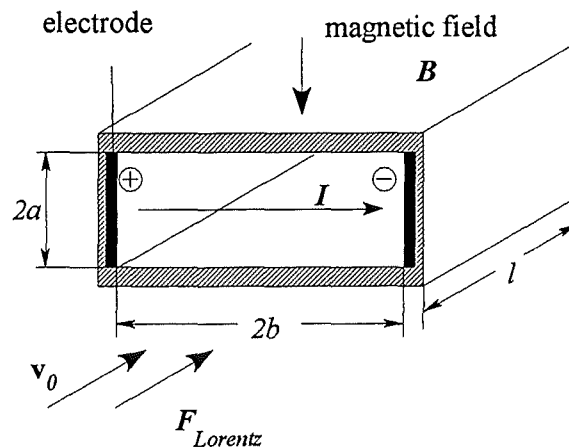


Figure 8.4: Operation principle of an electromagnetic conduction pump.

The interaction of the externally applied perpendicular magnetic field B with the current I leads to a Lorentz force $F_{Lorentz}$, which drives the liquid metal according to equation 8.1.

$$F_{Lorentz} = I B 2 b \quad (8.1)$$

The resulting pumping height Δp of the conduction pump can then be calculated with relation 8.2;

$$\Delta p = \frac{F_{Lorentz}}{A} = \frac{I B}{2 a}, \quad (8.2)$$

where A is the cross section of the duct. Even from this simple relation two criteria for conduction pumps can be deduced.

1. At a given current I the pumping height increases with decreasing a .
2. For a constant cross section of the duct A a stretching of the width b increases the achievable pressure difference Δp .

The resulting electric potential between the two electrodes of the pump U is the difference between the potential served by the power supply U_0 and the potential induced by the flow U_{ind} and can be calculated by equation 8.3.

$$U = U_0 - U_{ind} = U_0 - 2b v_0 B \quad [V]. \quad (8.3)$$

The ohmic resistance of the liquid metal between the two electrodes R_i is

$$R_i = \frac{2 b}{2 a l \sigma}, \quad (8.4)$$

where σ is the specific electric conductivity of the liquid. Thus, using Ohms law the electric current I flowing between the electrodes is determined by equation 8.5.

$$I = U R_i = 2 a l \sigma B v_0 \left[\frac{U_0}{2b B v_0} - 1 \right] \quad [A]. \quad (8.5)$$

Introducing relationship 8.5 in equation 8.2 yields for the achievable pressure difference Δp

$$\Delta p = l \sigma B^2 v_0 \left[\frac{U_0}{2b B v_0} - 1 \right] \quad [Pascal]. \quad (8.6)$$

The mechanical hydraulic power P_{mech} of the pump can then be calculated to

$$P_{mech} = \Delta p \dot{V} = v_0 I B 2 b = 4 a b l \sigma B^2 v_0^2 \left[\frac{U_0}{2b B v_0} - 1 \right] \quad [W]. \quad (8.7)$$

Herein, \dot{V} is the volumetric flow rate in the cross-section and v_0 is the average flow velocity.

The relation 8.7 shows that the mechanical power of the pump is highest for small flow velocities and the power decreases monotonously with the average flow velocity.

In the next step the efficiency η of the pump is evaluated. The efficiency of any device is defined by the ratio of the utilisable power versus the lost power, which reads in the treated problem

$$\eta_{Pump} = \frac{P_{mech}}{P_{mech} + P_{Ohmic}} \quad [/\]. \quad (8.8)$$

The ohmic dissipation P_{Ohmic} between the pump electrodes is given by relationship 8.9.

$$P_{Ohmic} = I^2 R_i = \frac{I^2 b}{a l \sigma} \quad (8.9)$$

So finally the efficiency of the pump is given by

$$\eta_{Pump} = \frac{1}{1 + \left[\frac{U_0}{2b B v_0} - 1 \right]} \quad [/\]. \quad (8.10)$$

The formula for the efficiency reveals that the pump efficiency increases with the flow velocity. Nevertheless, it should be mentioned that the whole derivation of the pump design displayed here is based on rather idealised boundary conditions, which are not fully present in reality. The simplification made in this derivation are:

- The Joulian (Ohmic) dissipation in the boundary layers are neglected.
- The viscous dissipation in the duct is neglected.
- A perfect electrical contact between the fluid and the electrode without any ohmic contact resistances is assumed.
- The electric current density between the electrodes is assumed to be homogeneous and constant.

However, although these simplifications have been made the derived formulas give a rather good estimate about the achievable characteristics of the pump.

For the GaInSn-loop Galinka of the MEKKA facility the power supply of the superconducting CELLO magnet is used which is capable of attaining 2000 Amperes at 10 Volts. For a given maximum electric current of 2000 Amperes and a duct with the dimensions $a=0.03\text{m}$, $b=0.06\text{m}$ a maximum pressure difference of $\Delta p=1.33 \cdot 10^5$ Pascal is calculated. In the corresponding experimental device a pressure difference in the pump of $1.0 \cdot 10^5$ Pascal has been measured (!).

Of course, the achievable average velocity v_0 depends strongly on the type of test section being used. In case of a test section with well electrically conducting walls the pressure losses are higher and hence also the achievable velocity decreases.

4.3 The heat exchanger

In the heat exchanger the produced heat caused by pressure drop and ohmic dissipation should be completely removed in order to keep the thermophysical data throughout the experiment constant. The heat to be removed is produced by the electric power of the pump and the heat input of a considered heat transfer experiment. The heat produced by the pump is rather small and accounts for about 250Watts, dependent on the boundary conditions. For a heat transfer experiment in the available dimensions the following conditions are assumed $\alpha=0.03$; $l_{heated}=0.5\text{m}$ and a maximum heat flux of 10 Wcm^{-2} . Thus, the heat exchanger should be capable removing a heat of approximately 3.25kW.

The heat exchanger used consists of three parallel water-cooled pipes, which are directly in contact with the liquid metal. A schematical drawing of such a pipe is shown in figure 8.5. The flow rate of water necessary to cool the liquid metal is about 140kg/h, assuming a maximum heating rate of 20°C of the cooler. The heat exchanger is electrically insulated from the liquid metal via an insulating painting to keep the possible MHD-effects in the area of this device small.

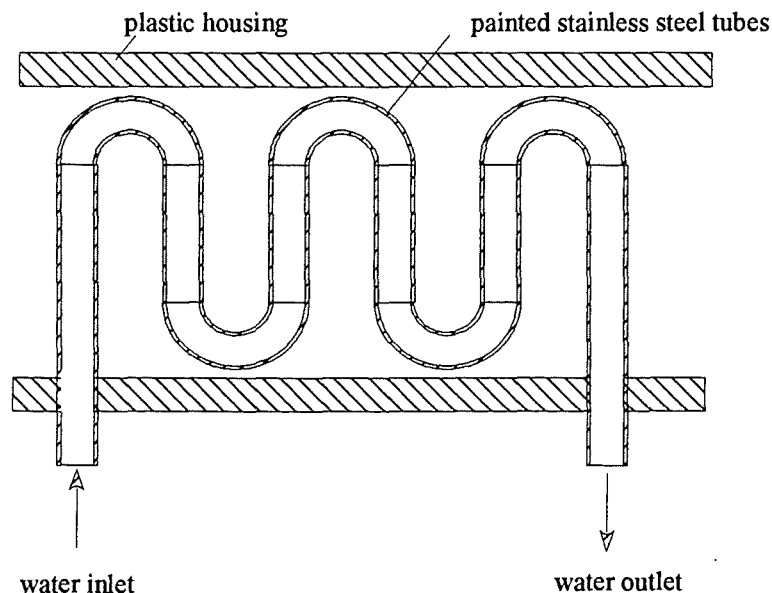


Figure 8.5: Schematical drawing of one cooling pipe in the GALINKA-loop.

9 Measurement techniques in liquid metal MHD

9.1 General remarks

This section treats the measurement techniques used in liquid metal MHD flows. The measurement elements including the measurement principle are described and an estimate about the achievable accuracy is given. Additionally the influence of measurement errors, which arise from the presence of the magnetic field, are discussed qualitatively and quantitatively in order to get an estimate about their size. If a correction of the measurement error is possible the relevant correction method is given.

9.2 Flow rate measurement devices

In order to calculate the characteristic numbers of a flow the detailed knowledge of the average flow velocity in the duct is of centered importance. Therefore, in the sodium-potassium loop two types of flow meters are installed in series. They are based on different operation principles. Hence, during operation a comparison of the readings of both flow meter types allows the detection of errors caused, e.g. by a shift of the instrument, gas bubbles in the system etc..

The flow meters used are a gyrostatic flow meter and an electromagnetic flow meter.

The gyrostatic flow meter measures directly the mass flow in a tube. The measurement principle used is the coriolis force. If a liquid flows through a U-tube oscillating on the axis A, see figure 9.1, in both branches of the U-tube coriolis forces of opposite direction appear. They lead to a oscillation around the axis B. The magnitude of the angle χ around axis B is directly proportional to the mass flow through the U-tube.

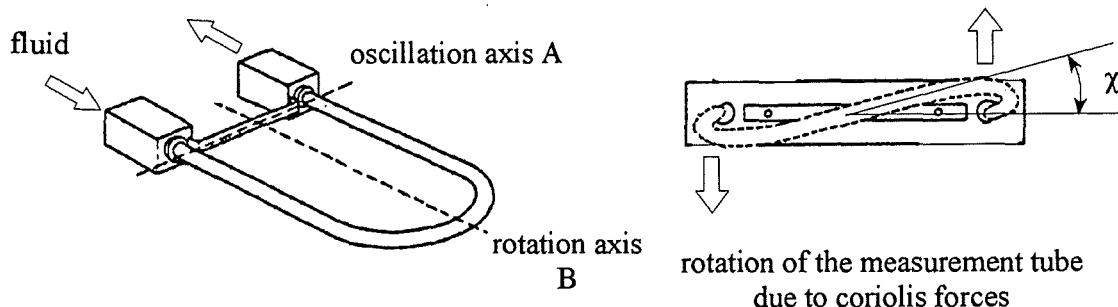


Figure 9.1: Measurement principle of a gyrostatic mass flow meter.

This measurement method is independent of the kinematic viscosity, the temperature,

the flow profile and the gas content in the fluid. The used mass flow meter can be adjusted stepless in its measurement range from 0-3840kg/h to 0-76000kg/h via a remote control from the operation room. Moreover, the instruments offers the possibility to a self-calibration. For the calibration the fluid in the measurement tube has to be at rest. This is performed via two valves interconnected in the line at inlet and outlet of the mass flow meter. The accuracy of the mass flow meter is $\pm 1\%$ or 1/100 of the chosen scale. The temperature operation range of the instrument is limited from -240°C to 204°C at a maximum pressure of 40bars. This component should not be installed close to magnetic fields due to the electronics in the instrument in order to avoid disturbances in the electronics.

The second type of flow meters used are electromagnetic flow meters, which are mostly used if the installation volume is rather small or low flow rates has to be resolved. The measurement principle is based on the measurement of an electric voltage, which is induced if an electrically conducting fluid flows through an externally applied steady magnetic field, see figure 9.2. The induced potential U_{ind} can be calculated by

$$U_{ind} = v_0 B d \quad [\text{Volts}], \quad (4.1)$$

where v_0 is the average velocity in the duct, B the magnetic field strength and d the tube diameter.

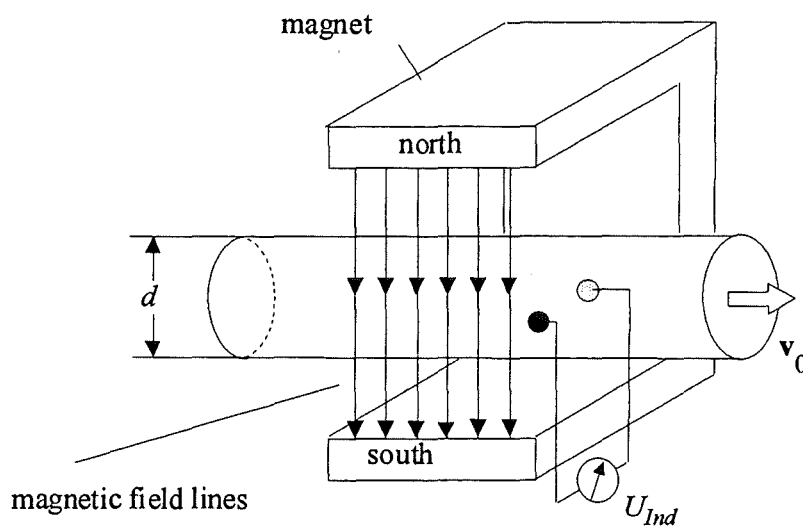


Figure 9.2: Measurement principle of an electromagnetic flow meter.

If the applied magnetic field is disturbed by another steady magnetic field the magnetic field lines are bended, see figure 9.3a. As a result the flow rate measured is not correct any more. However, if a magnetic shield in form of a ferromagnetic plate (with a high magnetic permeability $\mu_r \gg 1$) is placed between the flow meter and the scattering field the field lines of

the scattering field are focused in the plate and hence the measurement field remains unchanged, see figure 9.3b. The thickness of the plate can be calculated using the magnetic potential equation. In general a few millimetres are enough to compensate field of nearly one Tesla. The shown method of magnetic shielding works only for DC magnetic fields. In case of AC fields the flow meter has to be fully capsuled with ferro-magnetic materials.

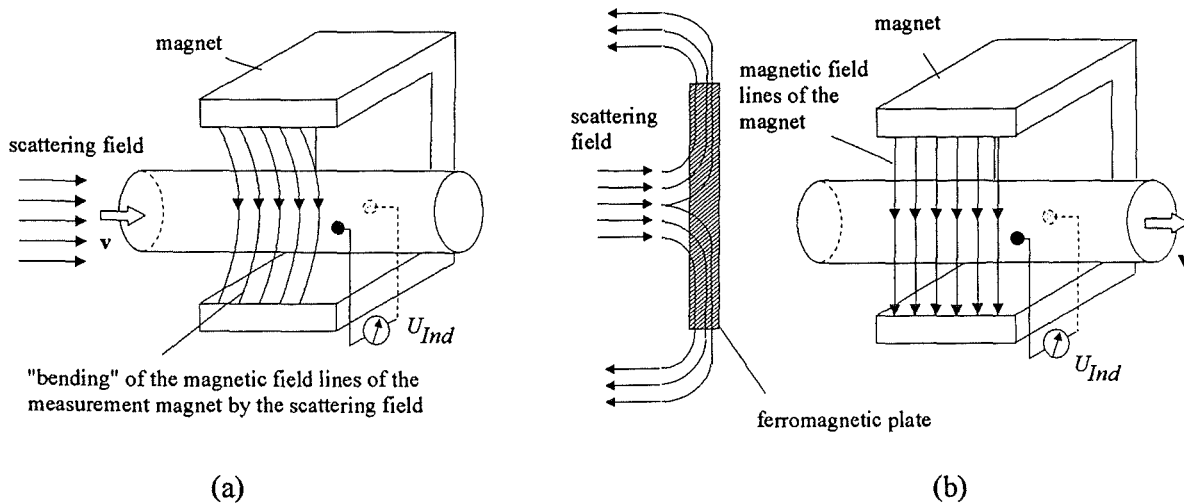


Figure 9.3: a) Influence of a scattering magnetic field on the magnetic field of an electromagnetic flow meter. b.) protection of the electromagnetic flow meter from a DC magnetic scattering field using a ferromagnetic shielding.

9.3 Pressure difference measurement method

The pressure difference measurements are performed in case of the sodium potassium loop via two independently operating line systems. In each line system four respectively two unipolar, capacitive pressure transducers are installed. They are adjustable flexible in their range and are arranged in parallel. The measurement ranges displayed in figure 9.4 can be adjusted to another value desired by a remote control. Since the pressure transducers are unipolar, the pressure measurement lines consists of a line for low pressure, abbreviated with "L" and another one for high pressure, abbreviated with "H", respectively. In order to avoid measurement errors due to nonlinearities near the end of the measurement ranges the measurement range should be chosen overlapping.

The pressure measurement in case of the GaInSn loop is carried out using the same principle as described, but there only one line exists, in which three pressure transducers of different ranges are arranged in parallel.

The measurement principle of a capacitive pressure transducer is shown in figure 9.5. If between the two measurement membranes a pressure difference exist the membranes are bended which leads to a change in the capacity. This capacity change is transformed in a current (4 - 20mA) and can be measured by a datalogger. The accuracy of the pressure transducers used is 0.5% of the maximum value of the chosen measurement range. An eventual shift of the measurement instrument by temperature changes is compensated by electronics. The operation temperature is limited to 120°C and the maximum pressure allowed at the membrane is restricted to 140bars.

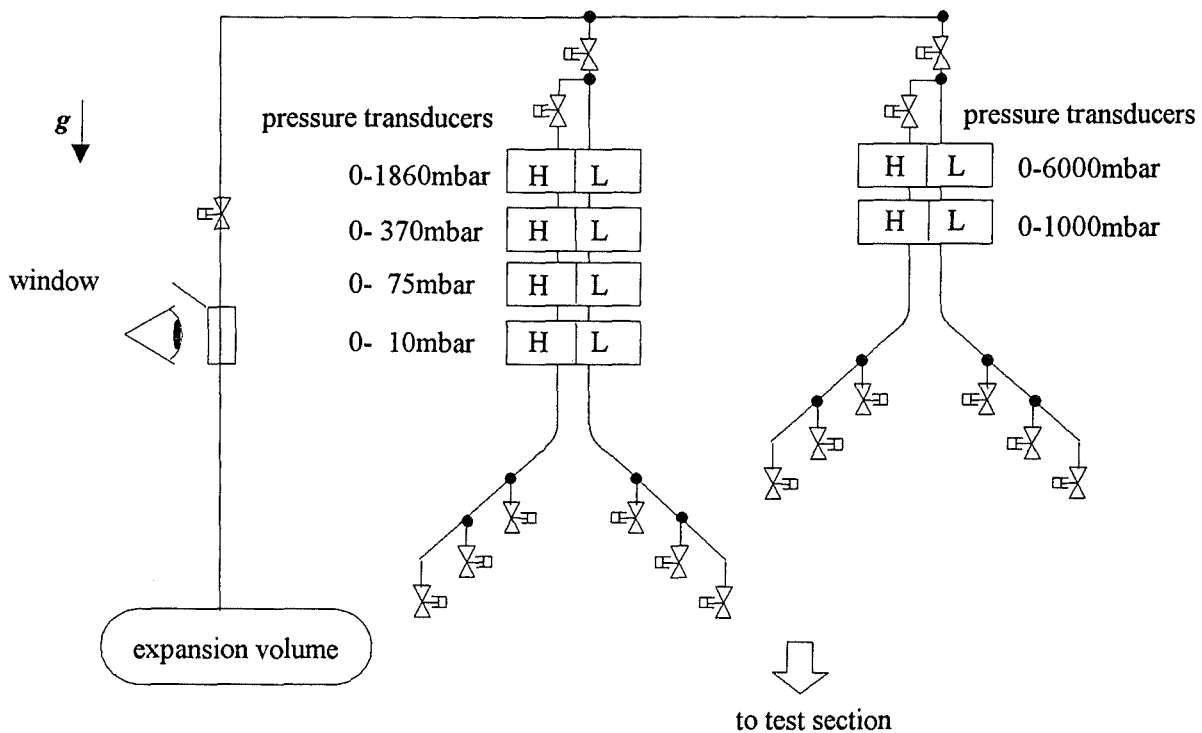


Figure 9.4: Schematic drawing of the pressure measurement system in the MEKKA-facility.

While measuring pressures in three-dimensional MHD-flows a phenomenon appears which is not known in conventional hydrodynamics. Directly measured pressure differences do not represent the real pressure differences between two locations in the duct. A virtual pressure is superimposed on the real pressure in the duct. An MHD flow configuration which shows a situation where a virtual pressure appears is depicted in figure 9.6. This virtual pressure may reach significant values.

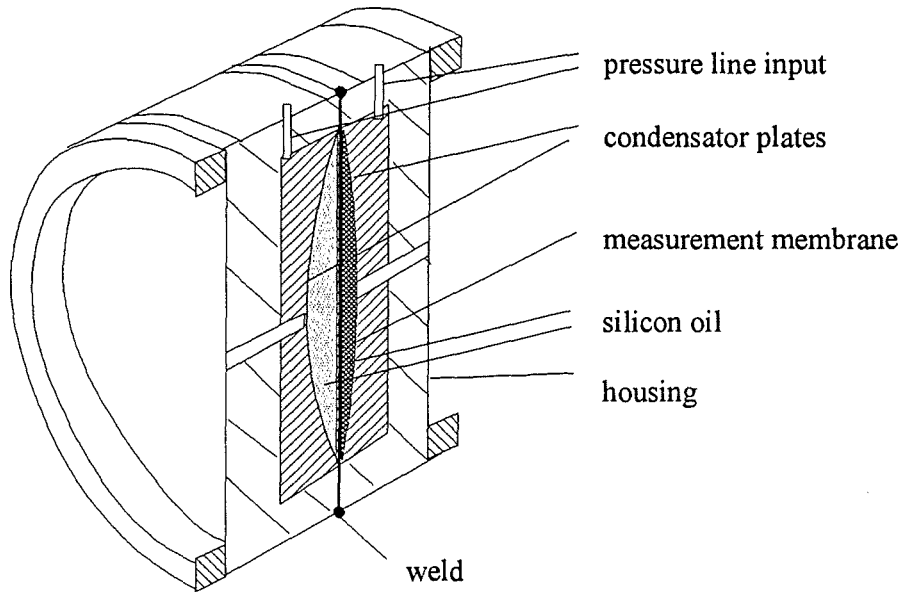


Figure 9.5: Measurement principle of a capacitive pressure transducer

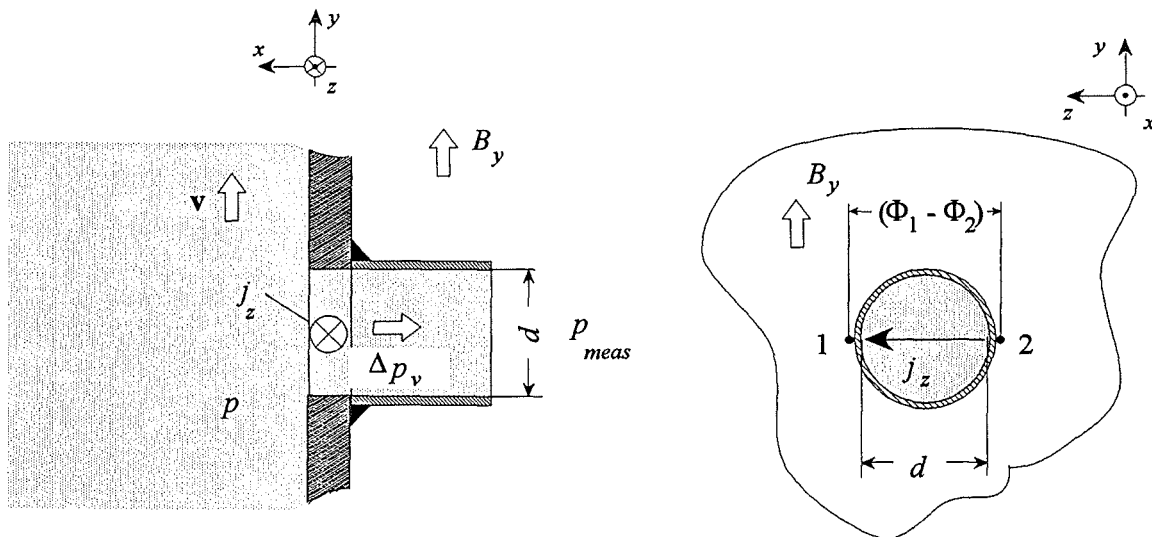


Figure 9.6: Virtual pressure appearing in strongly three-dimensional MHD duct flows.

But, by measuring the potential difference $\Phi_2 - \Phi_1$ by the potential probes directly at the stainless steel tube (figure 4) this virtual pressure can be estimated. Using simple considerations an analytical correlation for the pressure correction at the measuring hole can be deduced. The force balance at the pressure tap reads

$$\vec{n} \cdot \nabla p = \vec{n} \cdot (\vec{j} \times \vec{B}) \quad (9.2)$$

The Ohm's law formulates the relation between the current density and the wall potentials,

assuming a stagnant fluid in the tap ($\mathbf{v}=0$):

$$\vec{n} \cdot \nabla p = -\vec{n} \cdot (\nabla \Phi_w \times \vec{B}) \quad (9.3)$$

Integrating relation 9.3 over the thickness of the duct wall yields for the dimensionless virtual pressure jump p_v at the pressure tap equation 9.4. However, the obtained result assumes that the electric potential does not vary over the wall thickness.

$$\Delta p_v = -\frac{t_w}{d} (\Phi_2 - \Phi_1) \quad (9.4)$$

Herein, d denotes the gap of the pressure tap and t_w the wall thickness. $(\Phi_2 - \Phi_1)$ is the measured potential difference in the z -direction at the steel tube, see figure 9.6.

The pressure measurement lines from the test section to the measurement system end in a valve station, see figure 9.4. In this valve station the valves are arranged in ascending order, in order to allow a complete draining of the system in case of a shut down. If a gas bubble is in one of the lines the pressure lines can be degassed by opening the valves on top on the pressure system. The degassing has then to prolonged up to a point where a closed liquid metal jet is seen in the window.

By opening one valve on the high side and one on the low side the desired pressure difference can be measured. In case of large measurement campaigns the same pressure difference matrices has to measured very often and the operator has to open and close a lot of time the same valve configurations. In order to avoid this source of errors for the operator by the manual opening and closing an automatic switching of the measurement valves is available in the MEKKA-facility.

The operator activates this automatics by pushing a button in the control room. The second step performed by the operator is to write an ASCII file for the data acquisition system. This file must have the following form: first the desired number of the measurement combination (ordened in ascending numbers), as delimiter a comma and then nineteen characters. The characters are zero for a closed valve and one for an open valve.

```
1,000010000000000000000001
2,0000000000000000000000100
3,0000000000000000000000100
.
.
n,00000000010000000001
```

The file name must have the extension ".DAT". In the start-up of the data acquisition system the set-up can be loaded by the file name without the extension. The electronic equipment enabling the automatics is depicted in figure 9.7.

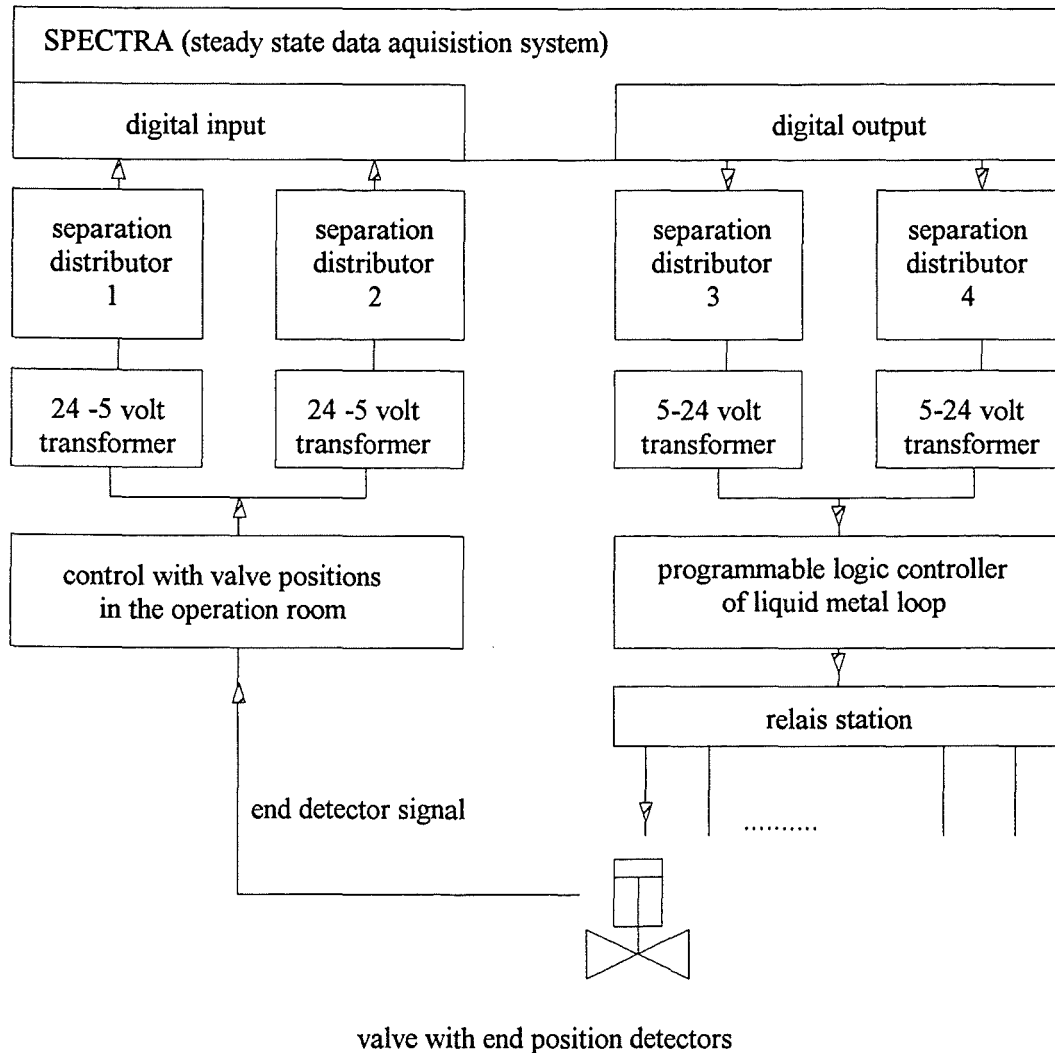


Figure 9.7: Schematics of the automatic valve switching in the MEKKA-facility.

9.4 Surface potential measurement method

Surface potential measurements are in principle possible in any kind of MHD duct flows. Due to the motion of the liquid in the magnetic field an electric potential is induced in MHD flows. The surface potential distribution on the ducts surface yields therefore a picture of the flow distribution inside the duct without any feedback or disturbance to the flow.

In order to measure the electric wall potentials spring loaded needles, mounted on fibreglass plates, are attached to the test section. But also wires welded or glued in or onto the

test section can be used.

The potential at a defined location is measured as a potential difference against a fixed reference potential. Since the measurement is currentless and the current source (MHD flow) is extremely low ohmic no corrections has to be taken into account while reducing the data. Only an electric contact of the needle with the wall (in case of electrically conducting walls) or with the liquid metal (electrically insulating ducts) has to be ensured.

The accuracy of this measurement type depends only on the resolution of the data acquisition system. In figure 9.8 a spring loaded needle, which is mostly used in the MEKKA facility is shown.

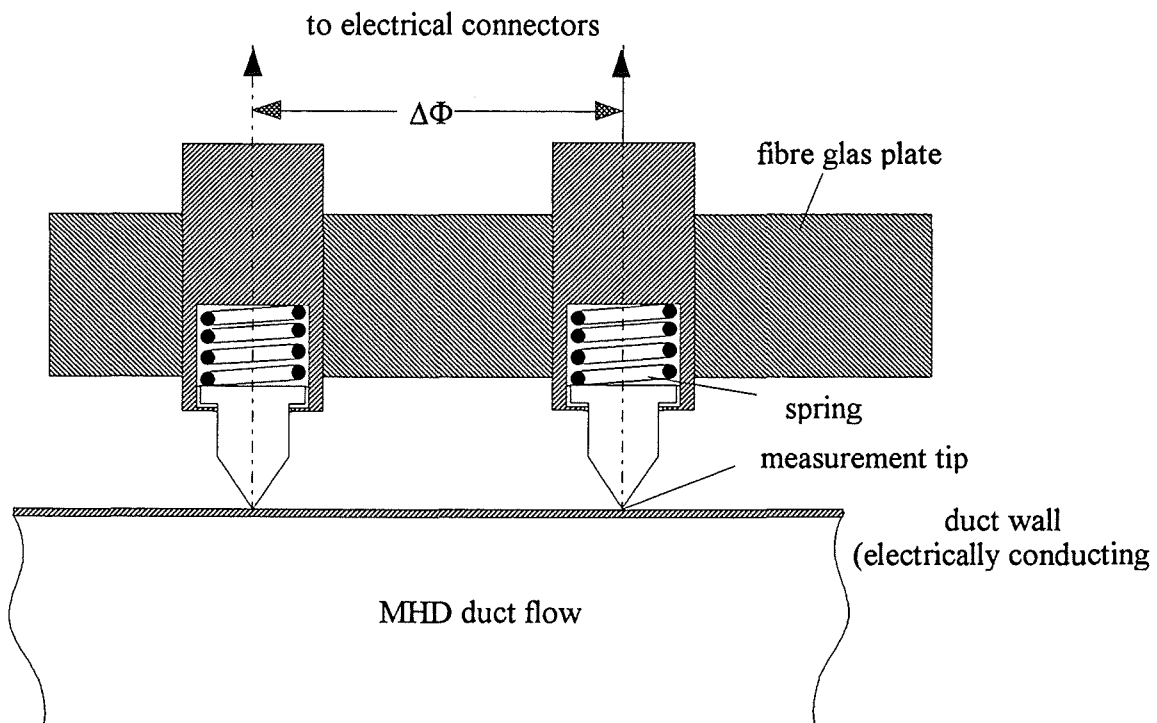


Figure 9.8: Surface potential difference measurement with a spring loaded needle.

9.5 Temperature measurement principle and error sources

The measurement of the temperature in the liquid metal is performed using thermocouples. The measurement of the temperature is necessary to determine the thermophysical data of the fluid, which depend strongly on the temperature. In contrary to ordinary hydrodynamics in magnetohydrodynamics the operator has to be extremely carefully what kind of thermocouple combination has to be used, because thermomagnetic effects can lead to tremendous measurement errors.

The temperature control far away from the magnets is performed by Ni-NiCr thermocouples. The dependence of the measurement signal against a reference ice point ($T=0^{\circ}\text{C}$) is shown in table 9.1.

The temperature measurements within the magnetic field is carried out using Cu-CuNi (copper-constantan) thermocouples, which dependence on the temperature is also shown in table 9.1.

temperature	Cu-CuNi	Ni-CrNi	temperature	Cu-CuNi	Ni-CrNi
0°	0.00	0.00	210°	9.74	8.54
10°	0.40	0.40	220°	10.29	8.94
20°	0.80	0.80	230°	10.85	9.34
30°	1.21	1.20	240°	11.41	9.75
40°	1.63	1.61	250°	11.98	10.16
50°	2.05	2.02	260°	12.55	10.57
60°	2.48	2.43	270°	13.13	10.98
70°	2.91	2.85	280°	13.71	11.39
80°	3.35	3.26	290°	14.30	11.80
90°	3.80	3.68	300°	14.90	12.21
100°	4.25	4.10	310°	15.50	12.63
110°	4.71	4.51	320°	16.10	13.04
120°	5.18	4.92	330°	16.70	13.46
130°	5.65	5.33	340°	17.31	13.88
140°	6.13	5.73	350°	17.92	14.29
150°	6.62	6.13	360°	18.53	14.71
160°	7.12	6.53	370°	19.14	15.13
170°	7.63	6.93	380°	19.76	15.55
180°	8.15	7.33	390°	20.38	15.98
190°	8.67	7.73	400°	21.00	16.40
200°	9.20	8.13	410°	21.62	16.82
Fitfunction polynom	A_0	A_1	A_2	temperature range	
Cu-CuNi.	3.4834965	23.22235	-0.21285	0°-410°C	
Ni-CrNi	-0.4179542	24.79475	-0.0201893	0°-380°C	

Table 8.1: Electric voltage of the thermocouples Cu-CuNi and Ni-NiCr in Milivolts as a function of the temperature in the range from 0°C to 400°C . The temperature function is calculated from the electric voltage produced by the thermocouple with the following polynom $T [^{\circ}\text{C}] = A_0 + A_1 \cdot U[\text{mV}] + A_2 \cdot U^2[\text{mV}]$.

In principle exist six (!) thermomagnetic effects which can influence the temperature measurement. An overview and a detailed description of these effects is given in the article of Kollie et al. 1977 and Eringen 1980. The effects can be categorised as

- (a) transverse effects Righi-Leduc -effect and Nernst-Ettingshausen effect
- (b) longitudinal effects in a transverse field and
- (c) longitudinal effects in a longitudinal field.

Both, (b) and (c) cause changes in the thermal conductivity and the Seebeck coefficient of a material. Of these effects the Righi-Leduc and the two longitudinal effects of the Seebeck coefficient are besides the Nernst-Ettingshausen effect the most important in thermocouple thermometry in a magnetic field. In general appropriate design considerations and material choices has to be made before instrumenting a test section. Only the consideration of the afterwards named effects and an order of magnitude estimates prevents from long term and exhausting calibration measurements.

9.5.1 The Nernst-Ettingshausen effect

If a temperature gradient ∇T is perpendicular to a magnetic field \vec{B} an electric field \vec{E} will be produced perpendicular to both quantities related to equation 9.5. The magnitude of the electric field is determined by the Nernst-Ettingshausen coefficient Q , which is a material property like the thermal conductivity of a material.

$$\vec{E} = Q(\nabla T \times \vec{B}) \quad (9.5)$$

The electromotive force EMF produced given by the integral along the wire from zero to the length l

$$EMF = \int_{s=0}^{s=l} [Q(\nabla T \times \vec{B})] ds \quad (9.6)$$

The Nernst-Ettingshausen factor Q for the four compounds appearing in the thermocouples Ni-NiCr and Cu-CuNi are shown in table 9.2.

material	Q [10^{-11} V/($^{\circ}$ C Gauss)]	μ_r magnetic permeability
copper (Cu)	0.27	1
copper-nickel (CuNi)	0.71	1
Ni (Alumel)	5.25	5
NiCr (Chromel)	27.00	1

Table 9.2: Nernst-Ettingshausen coefficient Q and magnetic permeability μ_r of different thermocouple materials.

Let us consider a configuration in which a temperature gradient of 50°C per mm exists, the thermocouple has a diameter of 0.5mm and the magnetic field strength is 2 Tesla ($2 \cdot 10^4$ Gauss). The thermocouple wires may have a length of 30mm perpendicular to the temperature

gradient and the magnetic field and they are insulated from each other by a magnesiumoxid ceramics. A calculation which includes the heat conduction in the thermocouple yields the following astonishing result. The measurement error for a copper-constantan thermocouple for this set-up yields 1.015°Kelvin; for Ni-NiCr, however, on such a short length an error of 33.2°Kelvin is measured. Of course, the big assumed temperature gradient has been chosen to outline the measurement errors. But in MHD flows with steep velocity gradients in the boundary layers such temperature gradients are likely to be expected, so that for investigating MHD the use of Ni-NiCr elements should be avoided.

9.5.2 The Righi-Leduc effect

If a temperature gradient ∇T is oriented perpendicular to a magnetic field \vec{B} a temperature gradient ∇T_t will develop transverse to ∇T and \vec{B} according to equation 9.7.

$$\nabla T_t = S(\vec{B} \times \nabla T) \quad . \quad (9.7)$$

Herein, S is the Righi-Leduc coefficient. However, equation 9.7 applies only if no heat flow occurs in direction of ∇T_t which is under adiabatic conditions. Similar to the Nernst-Ettingshausen effect a line integral for the temperature difference ΔT can be formulated, which reads to

$$\Delta T = \int_{s=0}^{s=l} S(\vec{B} \times \nabla T) ds \quad . \quad (9.8)$$

The Righi-Leduc effect results finally in a indicated temperature in a magnetic field that is different from that indicated without a magnetic field. However, for a 1m long Ni-NiCr wire in a magnesiumoxid mantle exposed to a magnetic field of 2 Tesla and a transverse temperature gradient of 50°C/1mm the error would be 45°C. The Righi-Leduc coefficient of Nickel is 10⁻⁷/gauss whereas the NiCr value was assumed to be infinitely small in the absence of data.

4.5.3 The Seebeck-effect

The Seebeck coefficient of metals is changed in the presence of magnetic fields. Such changes cause errors in the temperature measurement because the thermal electromotive force of a thermocouple E_t is defined as line integral

$$E_t = \int_{s=0}^{s=l_p} [S e_p \nabla T] ds - \int_{s=0}^{s=l_n} [S e_n \nabla T] ds. \quad (9.9)$$

along the length of the positive branch (l_p) and the negative branch (l_n) of the thermocouple. The positive and negative Seebeck coefficients $S e_p$ and $S e_n$ of non-ferromagnetic materials changes usually rather weak with the magnetic field, see Kollie et al. 1977. For ferromagnetic

materials the change is more expressed. The Seebeck coefficients for the two thermocouple pairs considered are shown in table 9.3.

material	Se [10^{-9} V/(°C)]
copper (Cu)	≤ 1
copper-nickel (CuNi)	3 ± 1
Ni (Alumel)	37 ± 1
NiCr (Chromel)	2 ± 1

Table 9.3: Seebeck coefficients Se from Kollie et al. 1977 and Powell et al. 1974.

9.5.4 Galvano-magnetic effects

Up to now only thermomagnetic effects are discussed. However, in MHD flows also galvanomagnetic effects may appear due to the interaction of electric and magnetic fields and lead to a miscellaneous reading of a temperature signal. For example the Ettingshausen galvano-magnetic effect, with the coefficient Pg , produces a transverse temperature gradient in a transverse magnetic field \vec{B} and a current density \vec{j} according to equation 9.10.

$$\nabla T = Pg (\vec{j} \times \vec{B}) \quad . \quad (9.10)$$

The coefficients Pg and the Nernst-Ettingshausen coefficient Q are related through the absolute temperature T and the thermal conductivity λ by relation 9.11:

$$\lambda Pg = T \cdot Q \quad . \quad (9.11)$$

9.6 Local measurements within the liquid metal

9.6.1 Some general remarks

In hydrodynamic flows around bodies boundary layers at the body surface develop due to the viscosity of the fluid. The form and thickness of the layers is determined by an equilibrium of pressure and viscosity. The influence of the body on the flow is mainly confined to an area behind the body if inertial flows are investigated. In case of MHD-flows in addition to the named forces electro-magnetic forces play a significant role. They may be even dominant and favour a development of a stagnant fluid area behind and in front of the body in magnetic field direction. This phenomenon is independent of inertia effects. Like for the discontinuous slope of a duct cross-section with respect to the magnetic field also in case of inserting a probe in a MHD-flow free shear layers (internal layers) appear separating different flow domains, see figure 9.9a. The length scale of the stagnant fluid domain upstream and downstream is directly

proportional to the Hartmann number of the body M_{body} (provided inertia effects are not dominant) and affects, like calculations of Kyrilidis et al. (1990) have shown, the flow in a quite large region. Order of magnitude arguments by Hasimoto 1960 or Chester 1961 express that disturbances in longitudinal flows may act over distances of the order $O(M)$.

Related to the appearing flow phenomena several aspects of probe measurements in duct flows and the conclusions, which one can draw from the data obtained are outlined.

The input of an arbitrary body in a duct flow affects the flow structure in the duct and thereby leads to different signals than for an undisturbed flow. The probe shaft Hartmann number for a probe with 3mm in diameter and a magnetic field of 3.6Tesla is about $M_{probe} \approx 3 \cdot 10^2$ (!). This Hartmann number can not be considered as small and thus electromagnetic disturbances originating from the shaft act in three-dimensional MHD flow over quite large distances. The order of magnitude argument then also holds for a sensing tip of a probe. Sensing tip diameters typically for probes are of about 0.5mm in diameter leading to a Hartmann number of about $M_{tip} \approx 50$.

Consider now a traversable probe consisting of a prong and two sensing tips within a duct of finite extensions, see figure 9.9b. At high M the zones, in which the flow is disturbed, may reach the duct walls. It is probably the case in the present experiment. Electrical currents flowing in the wall can short circuit through the zone from one duct wall to the other. As a result the global current path in the duct is changed and completely different flow patterns may be established compared to an undisturbed flow. This effect is most expressed for strongly three-dimensional flows.

If the shaft of the probe prong is electrically conducting electrical currents induced in the liquid metal can enter the prong and reduce the potential difference between wall and fluid. This also leads to local changes of the flow structure. In probes, in which the prong is non unidirectional (probes which have a 90°-bend) a shadowing of the sensing tips by the MHD-wake of the prong may also occur leading to irregular measurement results.

The wakes arising from the sensing tips equalises the potential in the stagnant columns in magnetic field direction. The measured potential gradients represent therefore some integral potential difference between the two columns in the flow. If the probe is near the wall, complex current paths between conducting walls, probe prong, sensing tips, different boundary and internal layers may appear, which lead to unpredictable current paths and thereby to misleading probe signals.

Besides these viscous-electromagnetic effects also inertial-electromagnetic effects may change the flow pattern locally and globally. In the appearing internal layers, which separate the flow domains, shear stresses may occur, which lead to a production of quasi-two-dimensional vortices. There are several indications, that these vortices may persist for quite a long distance, see Moreau (1990).

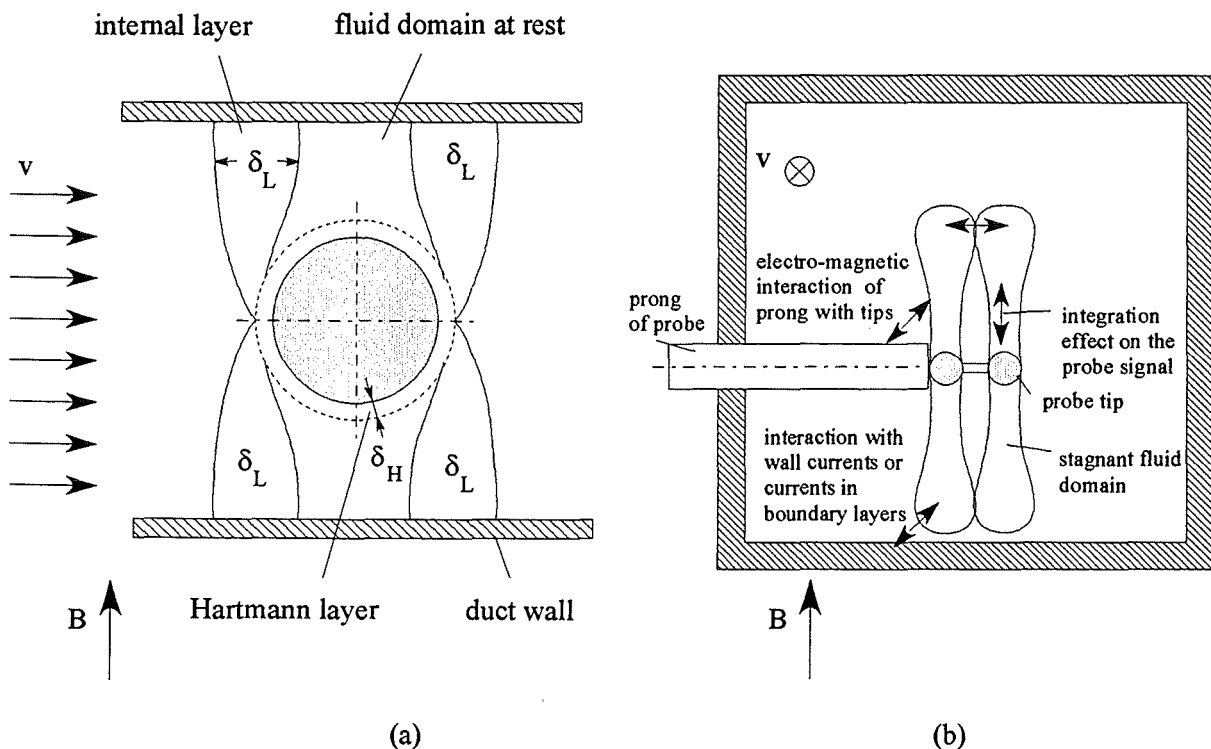


Figure 9.9: (a) development of different fluid areas in a MHD flow if a body is inserted in the duct.

(b) Sketch of the LEVI-probe inserted in the duct. Included in the graph are the possible electromagnetic interactions between the wall, the probe and the flow in a three-dimensional MHD-duct flow.

Generally the effects arising from this phenomena are small as long as the flow is two-dimensional or slightly three-dimensional as several experimentators have shown in the past, see e.g. Reed et. al (1987). But as soon as three-dimensional currents play a significant role the electromagnetic influence of the probe on the flow has to be considered. The lack of adequate theoretical background about the influence of the probe on the flow and moreover on the probe signal prevents clear analysis of the probe signals in three-dimensional MHD flows.

9.6.2 The potential probe (LEVI-probe) and the applicability in MHD-flows

The LEVI (liquid metal electromagnetic velocimetry instrument) is in principle a miniaturised local electromagnetic flow meter, which measures local electric potential gradients, being proportional to the local velocity and the applied magnetic field. The measurement signal yields from Ohms law for moving electrical conductors neglecting Hall effects according to relation 9.12.

$$\vec{j} = -\nabla\Phi + (\vec{v} \times \vec{B}) . \quad (9.12)$$

The equation 9.12 shows immediately one disadvantage of potential probes; they are not able to measure velocities in magnetic field direction. In duct flows, in which the wall conductance ratio c satisfies the inequation 9.13:

$$\frac{1}{M} \ll c \ll 1 , \quad (9.13)$$

the current density j can be neglected. This mostly holds for two-dimensional or quasi-two-dimensional flow as well as for flows with a high Hartmann number. In strongly three-dimensional flow like bend flows, discontinuous changes of the ducts cross section with respect to the externally applied magnetic field local areas of a high current density appear, in which the current density can not be neglected any more, see e.g. Stieglitz et al. 1996. If the current density \vec{j} can be neglected equation 9.12 may be reduced to

$$\Delta\Phi = (\vec{v} \times \vec{B}) \cdot \vec{s} , \quad (9.14)$$

where \vec{s} is the distance vector between the sensing tips and $\Delta\Phi$ is the measured potential gradient between the tips.

The signal detected with a potential probe is inertialess in contrary to hot film anemometers and the resolution of small fluctuations is only determined by the lower limit of the tip distance and by the data acquisition system.

The MHD remarks being made in section §9.6.1 lead to two contradicting design postulations for the probe. First the probe should be as small as possible in order to disturb the flow rather minimal. The other point is that a high mechanical stiffness has to be ensured to get a high reproducibility of the results. The sensing tips should be small, ideally a point, since otherwise the signal is integrated over the sensing length. Also no contact resistance between the sensing tip and the liquid should exist, which could lead to a measurement error. Finally the measurement lines has to be electrically insulated from the structural material of the prong, if this is electrically conducting (see Hunt et al. 1969).

It has been recently shown by Barleon et al. 1994 that also MHD in two-dimensional geometries at high Hartmann numbers may become turbulent for special flow parameters. Since not only momentum fluctuations are interesting for the nature of MHD turbulence but also the heat transfer characteristics a combined potential and thermal probe called TEMPO is available in the MEKKA facility. This probe is capable to measure velocity fluctuations as well as temperature fluctuations and thus allows to determine the oscillatory momentum and heat transport in a MHD flow.

In contrary to the pure potential probe the measured temperature signal in the TEMPO-probe is not inertialess. The resolution of a time dependent signal is given by the size of the thermocouple. In case if in both branches of TEMPO probe a 0.25mm thermocouple is used oscillations in the range up to 60Hz can be detected which is sufficient for most applications. A schematical drawing of a TEMPO probe is shown in figure 9.10.

This combined probe TEMPO can be built and used rather flexible. The possible configuration and the correlations, which can be measured with such a probe are outlined in the following sentences.

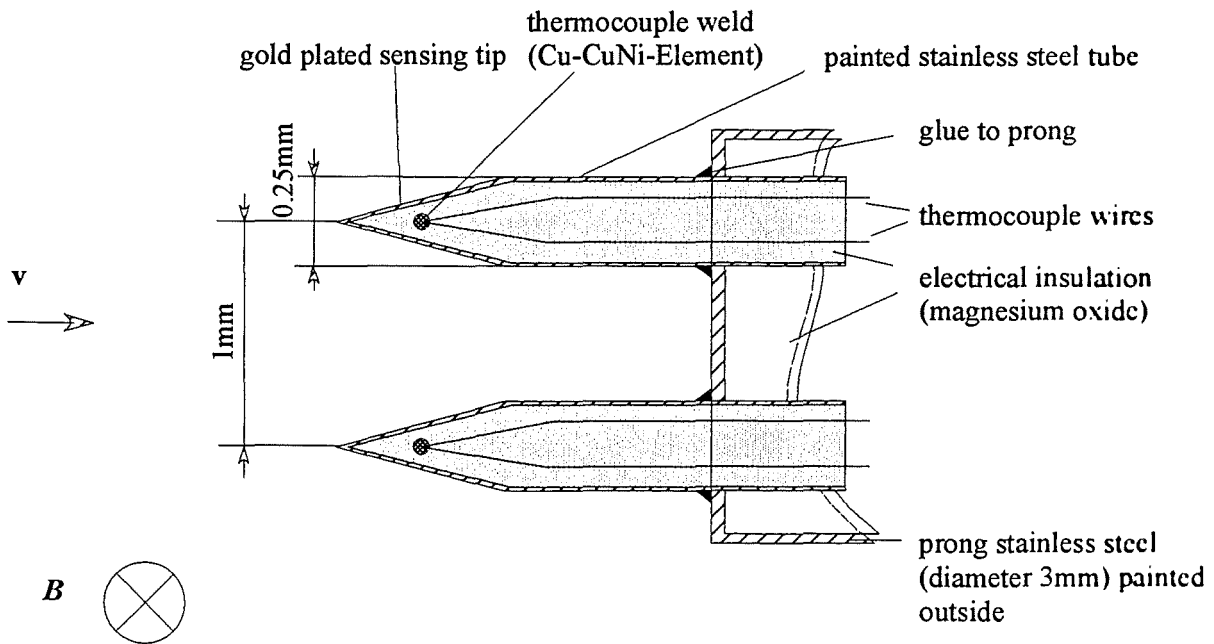


Figure 9.10: Schematical drawing of a two tip TEMPO probe

The planar 4-pole probe, shown in figure 9.11, is capable to measure the velocity component u in main flow direction, one velocity component perpendicular to the magnetic field, namely w and the fluctuations of these components.

If the 4-pole probe is made as a TEMPO probe also the turbulent heat transport quantities $u'T'$

and $w'T'$ can be calculated. The velocity components u and w are determined by the following equations:

$$u = \frac{\partial \Phi}{\partial z} + j_z \quad ; \quad w = -\frac{\partial \Phi}{\partial x} - j_x \quad ; \quad 0 = \frac{\partial \Phi}{\partial y} + j_y \quad . \quad (9.16)$$

Because is rather difficult to determine the local electric current densities j_i , the electric currents induced in the test section to be investigated should be rather small so that these current densities can be neglected.

An anti planar 4-pole TEMPO probe type is shown in figure 9.12. With this probe type the temperature gradient ∇T and all components of the potential gradient $\nabla \Phi$ can be measured. In contrary to the planar probe the measurement quantities obtained with this probe type allows some deduction about the characteristics of turbulent flow motion.

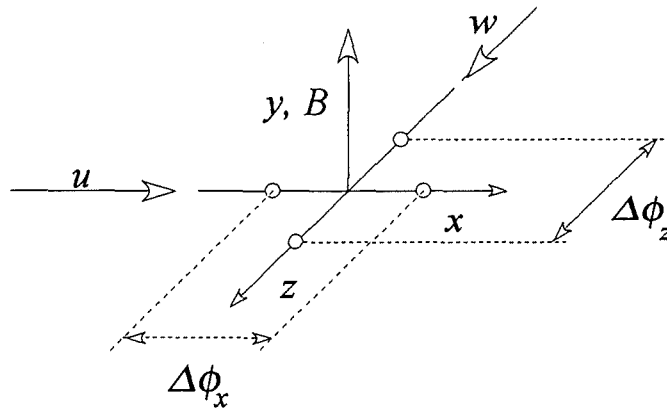


Figure 9.11: Measurable quantities in a planar 4-pole TEMPO probe $u, u', u'T', w, w', w'T'$.

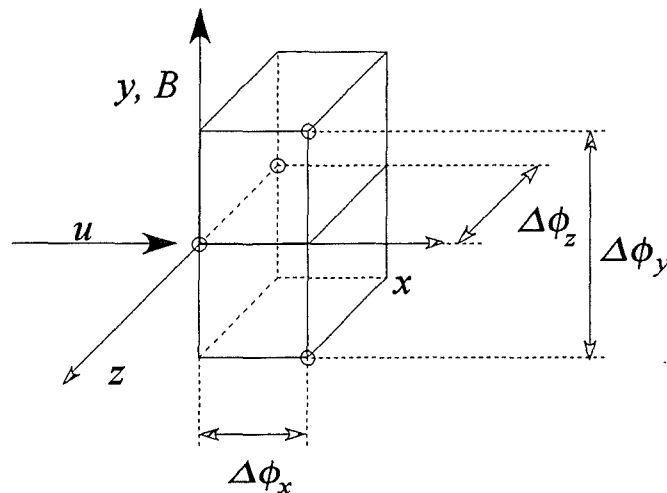


Figure 9.12: Measurable quantities $u, u', u'T', w, w', w'T', u'w', \nabla \Phi, \nabla T$.

An anti planar 7-pole probe is shown in figure 9.13. This probe type offers additionally to the previously named probes the possibility to determine the vorticity ω_B of the flow in direction of the magnetic field taking into account the conservation of charge ($\nabla \cdot \vec{j} = 0$). The vorticity ω_B in magnetic field direction is calculated via relation 9.17. The vorticity is the result of the Laplacian of the electric potential $\Delta\Phi$ on the probe tips.

$$\omega_B = \Delta\Phi \quad (9.17)$$

The vorticity of the flow in magnetic field direction is defined by

$$\omega_B = \frac{\partial u}{\partial z} - \frac{\partial w}{\partial x} \quad (9.18)$$

It should be mentioned in this context that for the derivation of the vorticity ω_B the local current densities must not be neglected. Therefore, it is possible to determine experimentally the vorticity ω_B of a strongly three-dimensional MHD-flow in which the local current densities are strong if a anti planar 7-pole probe is used.

A detailed description of the potential probes its capabilities and the results which can be deduced is given in Tsinober et al. 1987.

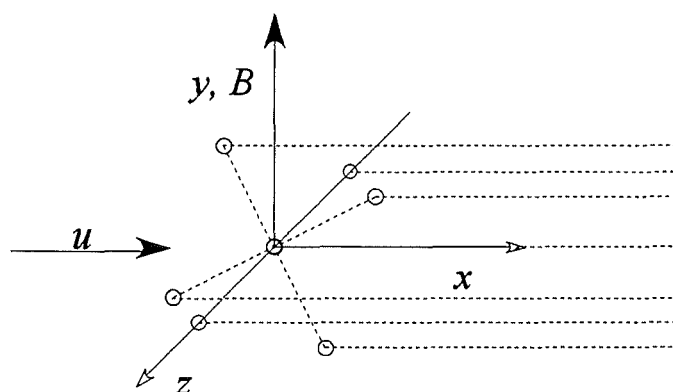


Figure 9.13: Measurable quantities $u, u', u'T', w, w', w'T', u'w', \nabla\Phi, \nabla T$.

9.6.3 The hot wire anemometer

Quite a lot problems arise using hot film anemometers in liquid metal flows. The main questions is the chemical compatibility of the liquid metal and the hot wire, in which surface tension and heat transfer aspects has to be considered. If alkali or earth alkali metals are used for the loop the compatibility of the wire with the liquid may become a killing issue. Up to now only silicium oxide plated wires of hot wire anemometers shows no degradation in connection with NaK, see Reed et al. 1986.

Surface effects which occur due to impurities in the liquid metal lead to reaction and change

the characteristics of the probe. Only by an appropriate cleaning of the probe such an effect can be avoided.

Another issue related to MHD has to be considered using hot wire probes. The hot wire probe measures in principle the heat transfer from the wire. The heat transfer in a MHD flow however is different to that of an ordinary hydrodynamic flow. The measurements of Lykoudis&Dunn 1973 show that the Nusselt number Nu strongly depends on the Hartmann number and the hydraulic Reynolds number, see figure 9.14. Thus, a calibration measurement of the hot wire anemometer for each measured magnetic field strength has to be performed.

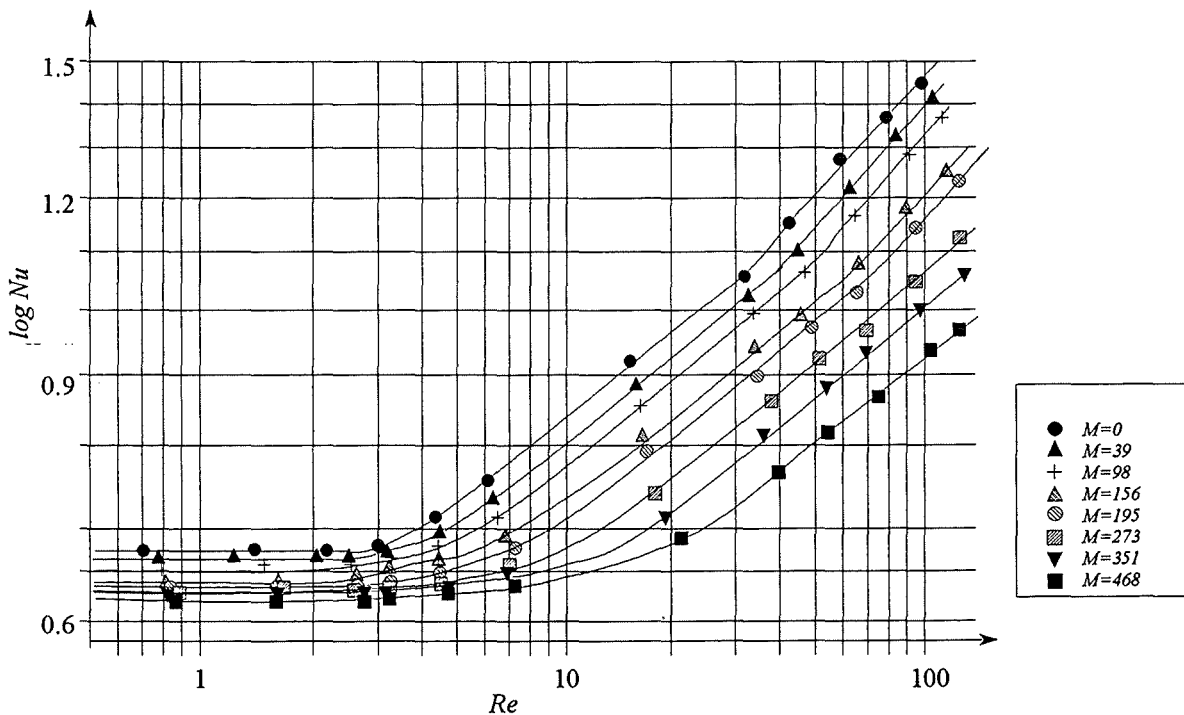


Figure 9.14: Dependence of the Nusselt number Nu on the Reynolds number Re and the Hartmann number M in a hot wire calibration measurement performed by Lykoudis&Dunn 1973.

In contrary to the potential probe the hot wire anemometer is not capable to detect the direction of the flow, because it measures the integral heat transfer at the wire. So using this probe type correlation measurements, which are necessary to determine vortex structures in turbulent flows can not be performed. Another disadvantage of the hot film probes originates from the low Prandtl numbers of the liquid metal leading to a drastic reduction of the resolution of the probe, because the conductive heat transfer in liquid metals is favoured compared to the convective one.

Like all other probe measurements in MHD flows the hot wire anemometer faces the same problems of a velocity reduction in front of the body. However, this probe type also shows two interesting features serving an crucial advantage compared to the potential probe. They are rather small, the wires are only some microns thin which affects the flow hardly but the probe is on the other side not very robust.

The second issue is that they are capable to measure flow components in magnetic field direction. Especially this application field is maintained by this probe type and measurements by Reimann et al. 1994 showed successful results. A schematical drawing of such a probe type is shown in figure 9.15.

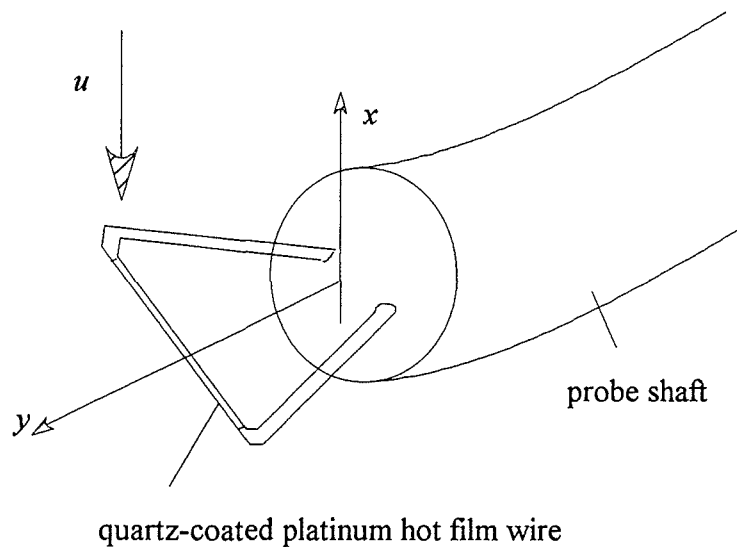


Figure 9.15: Schematical drawing of hot wire anemometer.

9.6.4 The temperature pulse method

The temperature pulse method is based on the measurement of the decay time of temperature pulses in a medium. The fluid velocity can be calculated from the propagation time of the temperature pulse.

The temperature waves are produced by a miniaturised heater, which is surrounded in defined positions by thermocouples. The propagation of a temperature pulse in a fluid at rest is shown in figure 9.16.

A drawing of the measurement instrument is shown in figure 9.17. A problem may arise with this measurement method in fluids with extremely low Prandtl numbers like in liquid metals, because there a temperature pulse diffuses rather fast. Therefore, high temperature pulses has to be brought in the liquid metal in order to enable a resolvable measurement of temperature changes in small distances from the mini heater. A determination of the velocity

temperature changes in small distances from the mini heater. A determination of the velocity vector is only possible if a grid of thermocouples is placed next to the heater. However, such a grid affects the flow non negligibly.

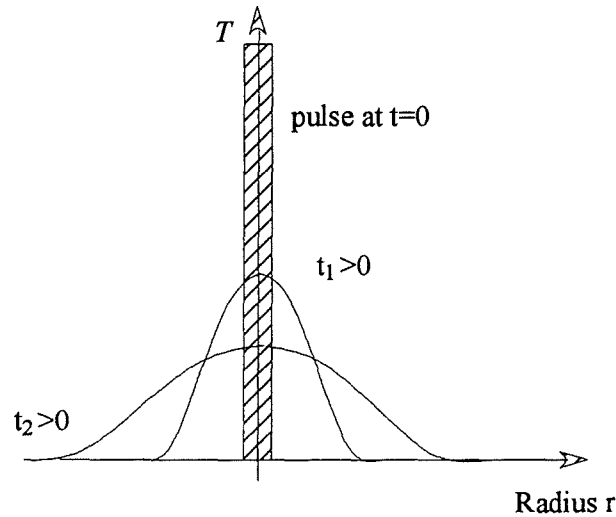


Figure 9.16: Temperature propagation of a temperature pulse as a function of the time t .

A second aspect which should be also considered is the choice of the thermocouples for this method, see therefore chapter §9.5. Casal et al. demonstrated the viability of this measurement method in water and also in liquid metals. Nevertheless, the resolution of this method in liquid metals is rather poor and the technical effort high.

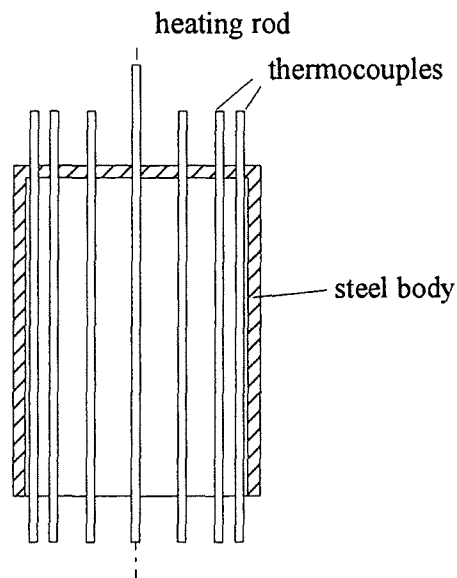


Figure 9.17: Schematical drawing of a temperature pulse measurement instrument to detect velocity vectors.

9.6.5 The pitot tube

Similar effects arising from a MHD flow around a body hold also for the Pitot tube. The Pitot tube measures the dynamic pressure difference Δp_{dyn} according to relation 8.16

$$\Delta p_{dyn} = \Delta p - \Delta p_{static} = \frac{\rho}{2} v^2 \quad (9.19)$$

Because the density of the alkali metals is rather low (e.g. NaK with 850kg/m^3) and the velocities to be measured are also low the measurement signal is rather small. Using NaK and assuming a velocity of 0.3m/s a pressure difference of only 38Pascal would be obtained.

The measurements of Hunt and Malcolm 1968 showed that Pitot tube measurement and potential probe measurements differ by more than 400% and even by a correction of the Pitot measurement, which accounts for all MHD effects, errors up to 150% appear. This is unacceptable for a measurement method.

9.6.6 Fibre-mechanical method

The fibre mechanical measurement principle is based on the mechanical bending of a light conducting fibre glass line. The mitigation of the light intensity of the light sent through the fibre glass line due to the bending is a measure for the fluid velocity. The measurements of Boyarevich et al. 1990 however, demonstrate that the measured quantity depends on the applied magnetic field strength. Hence, this method requires a calibration of the probe dependent on the magnetic field strength. The sensitivity of the probe also depends on the elastic behaviour of the fibre glass light conductor and the acquisition hardware. The experimental effort for this method is relatively high compared to a potential probe. Nevertheless also this method is capable to measure fluid velocities in magnetic field direction.

9.6.7 Ultrasonic measurement probes

The principle of this method is to utilise the pulsed echo technique of ultrasound and to detect the Doppler shift of the ultrasound wave reflected from moving particles suspended in the fluid., as a function of the time. The positions are obtained from the time after emission of the ultra sound pulse, and the values of the velocity come from the Doppler shift frequencies at each corresponding time forming a velocity profile. The details of the method and the apparatus may be taken from Takeda 1986 and 1987.

The experimental effort of this method is extremely high and the accuracy rather poor. Moreover, tracer particles have to be placed in the liquid, which may affect the thermophysical properties. Additionally the input of particles prevents a purification of the liquid using cold traps.

9.6.8 Traversing mechanisms

Each of the probe systems presented in the previous subsections has to be positioned within the duct to measure the local velocity distribution. Therefore, in the MEKKA facility two different traversing mechanisms are used. In both mechanisms the probe is screwed in via a metal bellow connected with a gear box. The gear mechanism has an accuracy of less than $\pm 0.05\text{mm}$. The gear box is connected via a shaft to a stepping motor. The stepping motor gets its pulses from an interface. The interface is activated itself from a personal computer via an RS232 line. The signal path from the computer to the probe is displayed in figure 8.18. The two different traversing mechanisms used are shown in the photos of figure 8.19a (NaK-loop) and 8.19b (GaInSn loop).

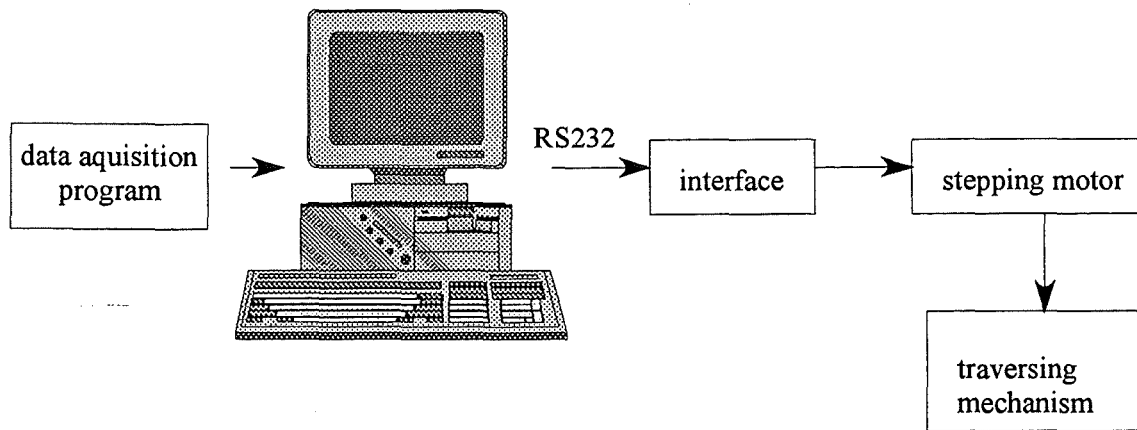


Figure 9.18: Signal path of the positioning of the traversing mechanisms.

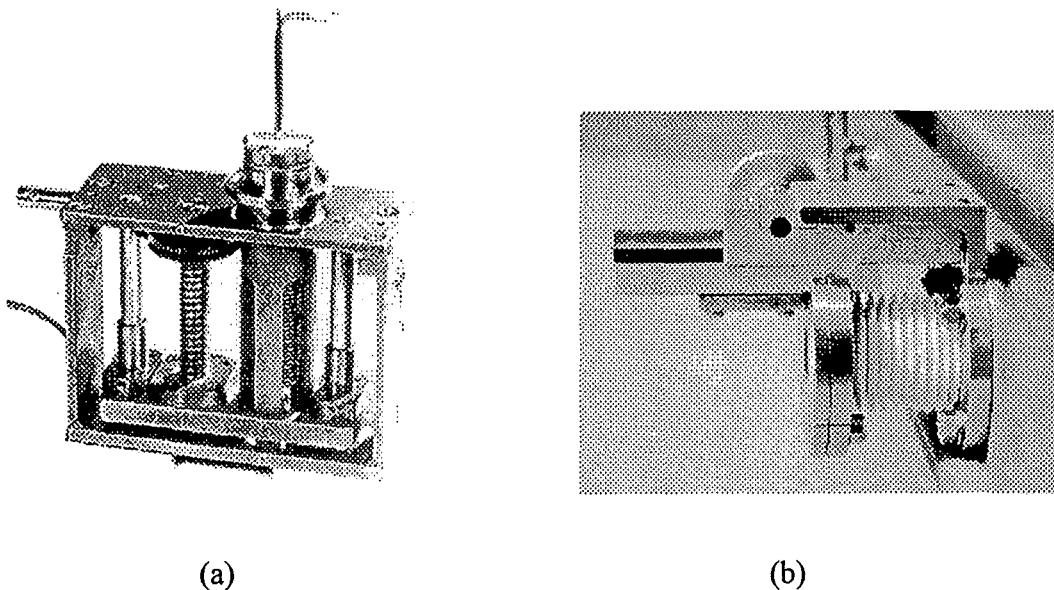


Figure 9.19: (a) Traversing mechanism used in the NaK-loop. (b) Traversing mechanism used in the GaInSn loop.

10 The data acquisition system

There are three data acquisition systems available in the MEKKA facility. All data acquisition systems are controlled by IBM compatible personal computers (PC's) and are communicating with the specific acquisition instruments.

- (1) Steady state data acquisition system SPECTRA.
- (2) Real time parallel acquisition system DT
- (3) Multi-channel acquisition system.

All three data acquisition systems can be operated independently and simultaneously. The following subsections give an overview about the organisation plans of the data acquisition systems, the instruments they contain and the specific features of the measurement accuracies of the instruments.

10.1 The steady state system SPECTRA

The organisation scheme of the steady state data acquisition system SPECTRA is shown in figure 10.1. The heart of this acquisition system is the SPECTRA data logger, which is a high precision microprocessor controlled data logger to measure steady state data.

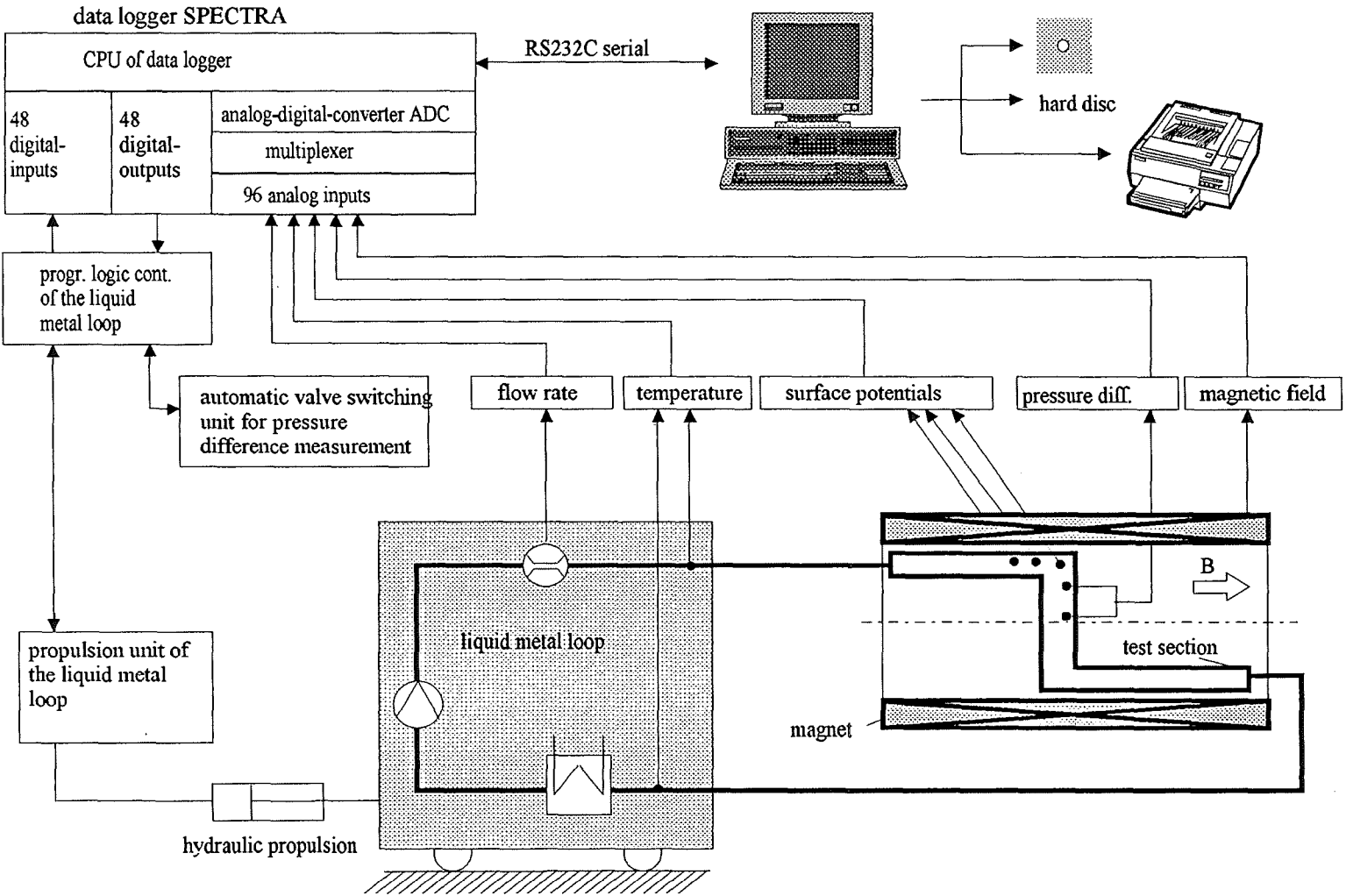
The communication with the data logger is done via a RS232 line connected to serial port of a IBM compatible personal computer (PC). The maximum transfer rate is 19200 Baud per second.

The SPECTRA has internally a central processing unit (CPU) which controls the multiplexer, the digital input and output cards and the different digital/analogue (DAC) and analogue/digital (ADC) converters. The measurement system of the SPECTRA consists of an amplifier, DACs and ADCs, read relays benches, autocalibration units and an electronics which allows to choose flexibly different measurement ranges and integration time steps.

The analogue system has 96 input channels and offers the choice to a voltage, current and ohmic resistance measurement. The integration time of each channel can be separately chosen in ten steps from 67 μ s to 4 seconds. The maximum accuracy of the 10 selectable measurement ranges is given by the accuracy of the ADC, which is a 16-bit device. The accuracy acc can be calculated by equation 10.1. The highest scan rate is limited to 110 channels per second. Measurement errors due to temperature shifts are compensated by an autocalibration electronics every 10 minutes.

$$acc = \frac{\text{selected measurement range}}{2^{(16-1)}} \quad [\text{physical unit}]. \quad (10.1)$$

The maximum allowed operation temperature range is 10°-80°C. Besides the analogue measurement system the SPECTRA has 48 digital output channels (O) and 48 digital input



channels (1). The signal strength set at the output is +5Volts; the input can detect voltages in the range down to 1Volt. With the digital I/O the automatic valve switching system and the propulsion unit of the movable liquid metal loop are controlled.

Figure 10.1: Organisation scheme of the data acquisition system SPECTRA.

The software realising the handshake between the devices is based on a set-up technique. Before a measurement campaign the user defines the channels and the related measurement ranges and save them in a set-up file. By calling the run-time module of the acquisition software the user has to specify the set-up file. The usage of the software is self-declaring on a graphical user interface which allows to stop and continue the measurement pressing function keys on the personal computer keyboard.

10.2 The fast acquisition system DT and DAS

An organisation scheme of the fast acquisition system DT is shown in figure 10.2. The data acquisition system DAS is similarly built up, so that it is not displayed here in detail.

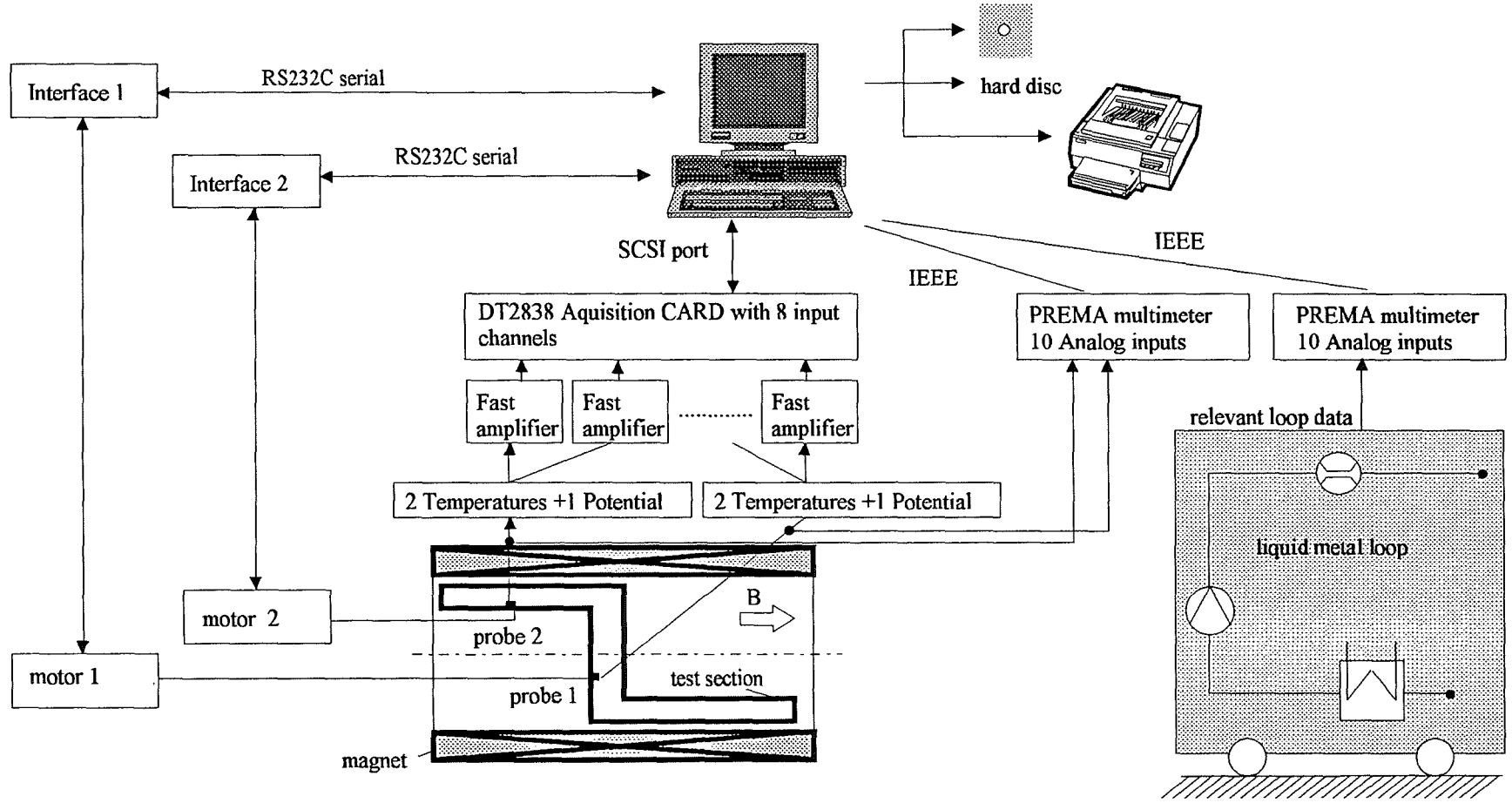
The acquisition system DT is controlled by the commercially available software package DIA/DAGO, which is also based on a set-up technique but additionally offers a large environment for data reduction and graphic sources.

The specific features of the DT data acquisition system is the DT2838 card. This plugin card is stuck into the computer and has 8 analogue inputs channels and 8 digital input/output channels. Each analogue input has a sample and hold memory which enables the card to get real time simultaneously the data from 8 channels. Using this mode (8 channels simultaneously measured) the scan rate is restricted to 20kHz. The analogue inputs have four selectable measurement ranges from $\pm 20\text{mV}$ to $\pm 10\text{V}$ with a resolution of 12 bit. So the smallest resolvable Voltage is $\pm 9\mu\text{V}$. In order to measure lower voltages an amplifier is preconnected to the analogue inputs. The amplifier gain can be selected by the user from 1 to 500 in four steps.

The multi-meter PREMA used is a high precision digital multimeter which is remote controlled via an IEEE488.2 interface from a PC. It allows variable integration times from 50ms to 10seconds and has a resolution of 16bits. The measurement quantities can be current, voltage and ohmic resistance. The measurement range can be selected in five steps from $\pm 0.2\text{Volts}$ to $\pm 1000\text{Volts}$. The highest scan rate is 7 channels per second. The offset drift is after a heating period of one hour less than 100nV and the long term stability is $\pm 3\mu\text{V}$ over 90 days.

The data acquisition system DAS is managed by the commercial software package TESTPOINT from Keithley. Also this system is based on a set-up technique and has similar options as the DIA/DAGO system. The difference in both systems is that the DAS system is capable of a high speed acquisition of 64 channels with up 330kHz. The responsible card plugged in a computer is the DAS1800 card from Keithley. In contrast to the DT2838 card from Data Translation is card is not capable of a real time acquisition, because it has no sample and hold memory elements.

Figure 10.2: Organisation scheme of the data acquisition system DT.



11 MHD-experiments performed in MEKKA

During the last seven years a large variety of MHD experiments have been conducted in the MEKKA-facility both in the NaK-loop and in the GaInSn-loop, which are documented in more than 40 publications. Since this report treats the main features of the MEKKA-facility and describes the design aims the authors followed while building up this laboratory only catchword like the main results obtained in experimental campaigns are described. For a more detailed information we suggest the readers to study the relevant papers. To get some order in the experimental results we firstly show some results obtained in two-dimensional flows then some exemplary results of three-dimensional flows investigated and finally a few results for "turbulent" MHD flows.

11.1 Fully-developed MHD-flows

The measurement campaigns in MEKKA started with one of the simplest problems, namely the investigation of the pressure drop and the electric potential distribution of an MHD-flow in an electrically conducting circular duct applied to a strong magnetic field perpendicular to the axis of the tube.

In figure 11.1b the measured dimensionless pressure drop of a circular pipe with a wall conductance ratio $c=0.036$ is shown for several Hartmann numbers M as a function of the interaction parameter N . These measurements performed by Barleon et al. (1989, 1991) show an excellent agreement between the analytical and the experimental results. In a second campaign a Flow-Channel Insert (FCI) has been inserted into same duct. The FCI was built up as shown in the principle sketch depicted in figure 11.a. The wall conductance ratio achieved has been $c=0.0039$. The pressure drop measured in the configuration with FCI agrees also rather good with the analytically calculated value. The pressure drop reduction achieved with the FCI is 95%. These measurements represent the first evidence of the viability and the effectiveness of FCI's to reduce the pressure drop in a piping system substantially.

In another experimental campaign performed in the GALINKA loop the pressure drop the pressure drop in an electrically insulating rectangular duct has been investigated. There also a perfect agreement between analytical and experimental values has been found. The experimentally obtained results compared to the theoretically ones are depicted in figure 11.2.

As a final example of pressure drop measurements in two-dimensional MHD-duct flows we present the results obtained in a rectangular duct with electrically conducting walls. The walls perpendicular to the magnetic field has been thin (1mm) and the walls aligned with

the field has a thickness of 6mm. The main flow direction is oriented perpendicular to the externally applied magnetic field. Here, like in the previous measurements the experimental data agree rather good with the calculated ones like the figure 11.3 demonstrates.

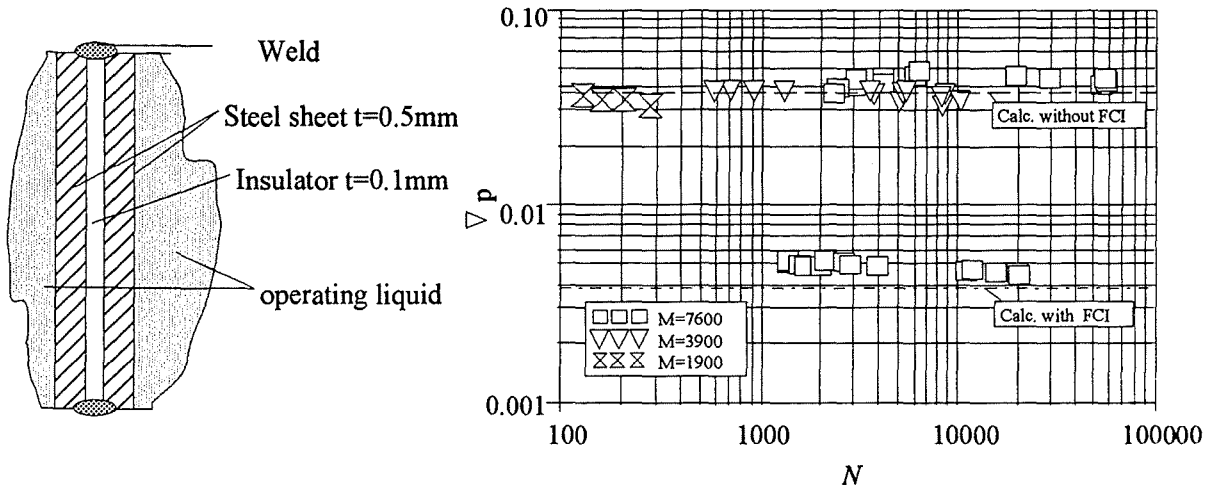


Figure 11.1: a.) Flow channel insert to reduce MHD-pressure drop. b.) Measured dimensionless pressure gradient in a circular duct without FCI ($c=0.036$) and with FCI ($c=0.0039$) as a function of the Interaction parameter for different Hartmann numbers.

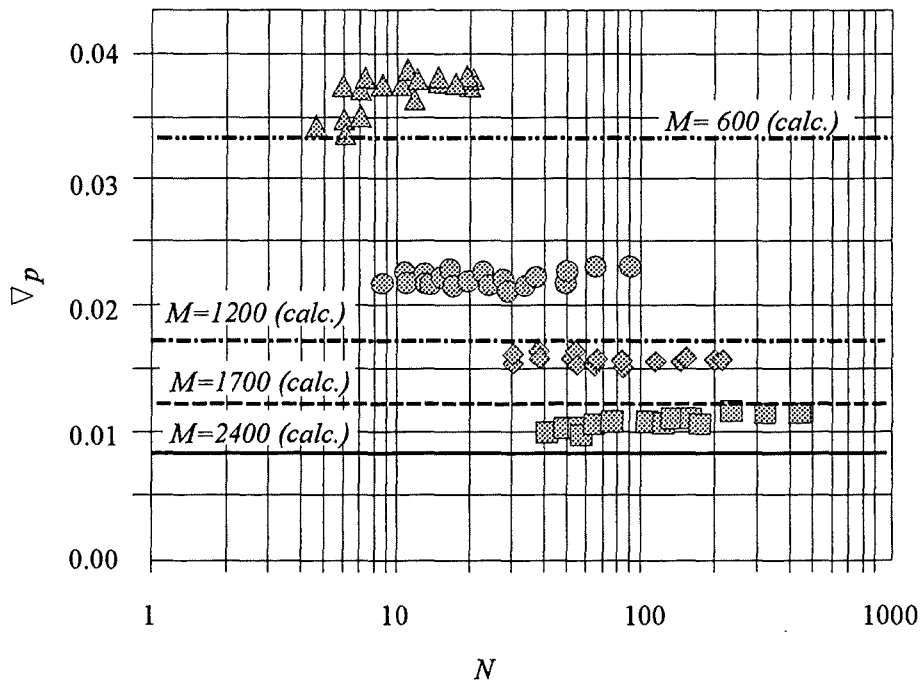


Figure 11.2: Measured dimensionless pressure drop in a rectangular electrically insulating duct as a function of the interaction parameter performed by Barleon et al. 1994. The symbols represent the experimental data (■) $M=2400$; (◆) $M=1700$; (●) $M=1200$; (▲) $M=600$.

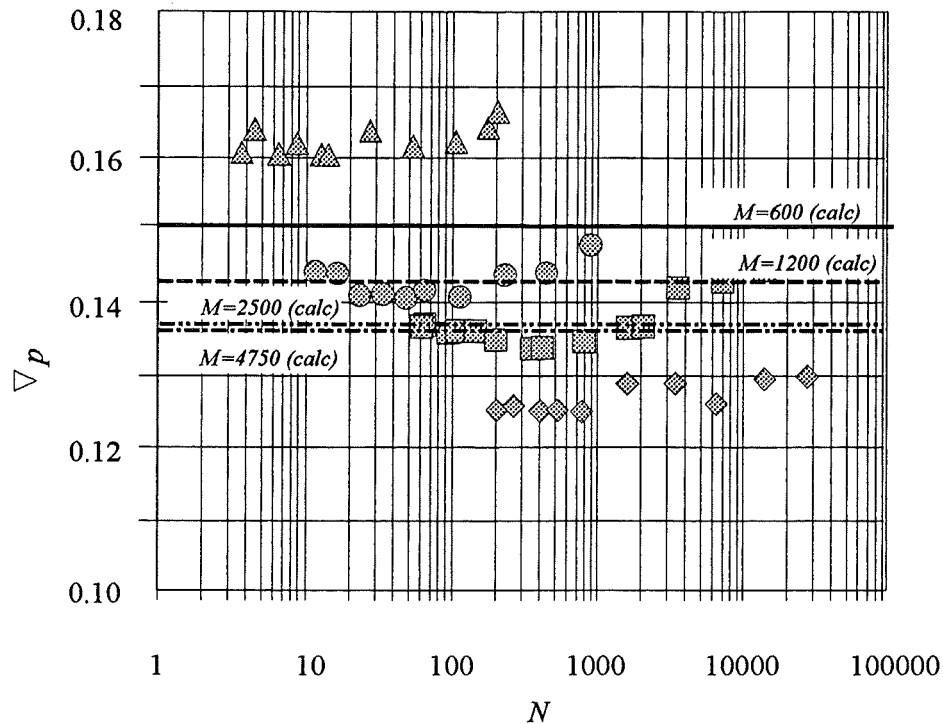


Figure 11.3 Measured dimensionless pressure drop in a rectangular electrically conducting duct as a function of the interaction parameter performed by Barleon et al. 1996. The wall properties are $c_H=0.0121$ and the side wall conductance ratios are $c_s=0.07247$. The symbols represent the experimental data (\diamond) $M=4750$; (\square) $M=2500$; (\circ) $M=1200$; (\triangle) $M=600$.

But not only such integral data like the pressure drop in a duct has been measured. Also the determination of the local velocity distribution within the duct is one of the major tasks, which has to be evaluated with respect to develop liquid metal cooled fusion reactor blanket.

The local velocity distribution is especially important for the heat transfer characteristics in a duct. The next figure (11.4) shows the velocity distribution in the midplane of a rectangular duct with thin electrically conducting walls. The shown velocity data are the time averaged data. Further measurements showed that the found inflection type profiles are not laminar throughout the whole investigated velocity range. The thickness of the wall adjacent side layers increase with increasing velocity and also the turbulence level increases at the inflection point. However, the pressure drop measured at flow velocities where a high turbulence level is found is the same as in laminar flows. An explanation for this behaviour is that the turbulence appearing in MHD flows is highly anisotropic. Both theoretical considerations and also previously performed experiments shows lots of indications that the turbulence in MHD flows is two-dimensional. The axis of the two-dimensional vortex structures are oriented in magnetic field direction, so that they minimise their dissipation. The electric currents flowing in that vortex structures are then negligibly small and thus produce no

pressure drop. However, this theory of two-dimensional is not proofed experimentally up to now and requires in the future some effort. The solution of such questions is required to describe the "turbulent" heat transfer characteristics in two-dimensional geometries especially for fusion relevant flows.

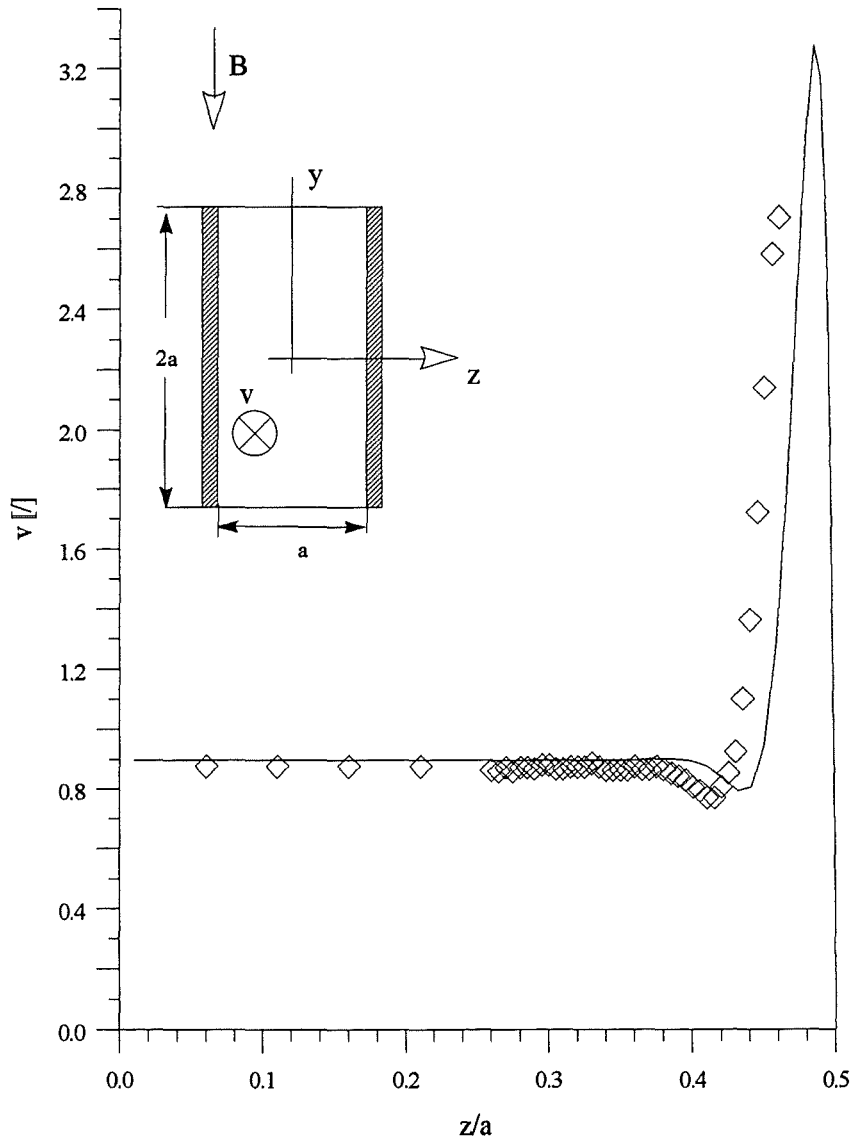


Figure 11.4: Measured dimensionless velocity profiles in a rectangular electrically conducting duct as a function of z/a with $c_H=0.0121$; $c_s=0.07247$; $M=4750$; $N=13200$. The solid line represents the calculated distribution.

11.2 Three-dimensional MHD-flows

In any blanket design bends appear, in which the flow changes the direction with respect to the magnetic field. In the blanket concept described by Malang et al. 1988, there are two bends forming an U-bend with radial-toroidal-radial orientation. Since in the toroidal part

which is perfectly aligned with the magnetic field the main flow direction coincides with the direction of the field the induced potential in this duct is zero. This part of the bend therefore serves as an additional current path and increases the total current and pressure drop in the radial leg. We consider here only one half of the U-bend (see figure 11.5) with appropriate boundary and symmetry conditions. In the toroidal plane of symmetry $y=y_s$ the symmetry conditions for the leading variables used in the analysis are

$$p = \Phi = 0 \quad \text{at} \quad y = y_s \quad . \quad (11.1)$$

If the toroidal duct is long enough $y_s \rightarrow \infty$ the resulting flow should approximate the flow near the junction in a single 90° bend. At large distance from the bend in the radial direction the flow should be fully developed, so that

$$\frac{\partial \Phi}{\partial x} = \text{const.}; \quad \frac{\partial \Phi}{\partial x} = 0 \quad \text{as} \quad x \rightarrow \infty \quad . \quad (11.2)$$

The detailed analysis of this problem based on inertialess, inviscid limit ($N, M \rightarrow \infty$) is described by Molokov & Bühler 1994. Here only the main results are summarised.

- ◆ The core of the toroidal duct has no component of velocity in the main toroidal direction.
- ◆ The flow in the toroidal duct is confined to thin boundary layers at all walls which are aligned with the field and which carry all flow rates Q_i . Even at the first wall there is a jet which carries a significant rate Q_1 of the total volume flux. The variations of flow rates in the layers along the toroidal coordinate y are shown in figure 11.5. At $y > 3.3$ the flow in the second wall layer becomes reversed because of the strong pumping and mass exchange via the toroidal core.
- ◆ The core in the toroidal duct is by no means stagnant. There is an intense exchange of fluid between the four layers which are aligned with the field. This exchange happens because of a direct interaction between neighbouring layers or even along larger distances if the core is involved.
- ◆ There is fluid motion in the core only in planes $y = \text{const.}$, and it does not contribute to an $O(1)$ volume flux in the toroidal direction. Nevertheless, this motion may lead to improved heat transfer conditions. The intensity of the flow in the core is most pronounced at the Hartmann wall of the toroidal duct and vanishes at the plane of symmetry. The flow behaves qualitatively like the flow analysed by Molokov & Bühler 1994, shown in figure 11.5.

The flow in the radial-toroidal bend has been intensively investigated experimentally (Stieglitz 1994, Barleon & Stieglitz and al. 1996) and compared with the results of the asymptotic model. The wall conductance ratio used in the experiment and in the analysis was

$c=0.052$. The main results are summarised next:

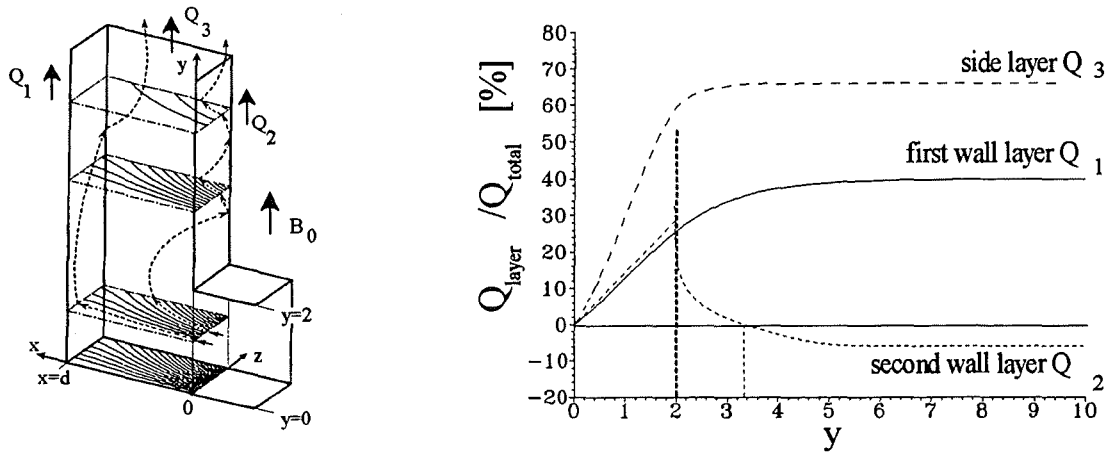


Figure 11.5 a) Isolines of potential at the bottom of the toroidal duct, streamlines in the toroidal core and sketch of flow path in the layers. (Molokov & Bühler 1994).
 b) Flow rates in the wall-adjacent boundary layers in the toroidal duct. Sketch of geometry, orientation of the magnetic field, and coordinates. $M \rightarrow \infty$, $c=0.052$. (Stieglitz 1994).

I. Wall potentials:

The electric wall potentials Φ have been measured at the positions A-Q. The distances between their positions and the outer corner are shown in dimensionless scale in figure 11.6. Only potential distributions at characteristic positions, along fat-solid lines, marked by the bigger letters are discussed below. The others, along thin-solid lines show quite the same tendency.

a) The measured values of the wall potential at different positions are shown for a relatively low interaction parameter $N=1920$ in figure 11.6 for a wide range of Hartmann numbers $M=1990-8177$. They are compared with the calculated potential distributions shown as solid lines. The excellent agreement of measured and calculated values of potential at the position A confirms the assumption of fully developed MHD flow, used as a boundary condition for calculation. A variation of the Hartmann number at all measured positions does not have an influence on the wall potential indicating that even flows at the lowest investigated Hartmann number $M=1990$ exhibit the asymptotic distribution of the wall potential, in good agreement with the theory.

b.) The influence of inertial effects was expected to have a significant effect on the wall potential in the vicinity of the bend where the main flow direction changes. Measured potentials at a high Hartmann number, $M=8177$, and for interaction parameters in the range of $1851 < N < 26930$ are compared with the calculated values in figure 11.7. The experimental data do not show a significant dependence on N since all measured values are spread only over a small range, which actually represents the experimental accuracy. Even bend flows at the

lowest investigated interaction parameter $N=1851$ show the asymptotic values of the wall potential. Small differences of measured and calculated potentials at positions G and H occur only close to the side wall ($z=-1$). Even at position I the agreement between experiment and theory is surprisingly good, although one would expect there some discrepancies caused by inertial effects. A more pronounced dependence of the wall potential on the interaction parameter N is obtained at the side walls of the toroidal duct (see figure 11.8). For increasing N the experimental data tend towards the calculated values of inertialess bend flow.

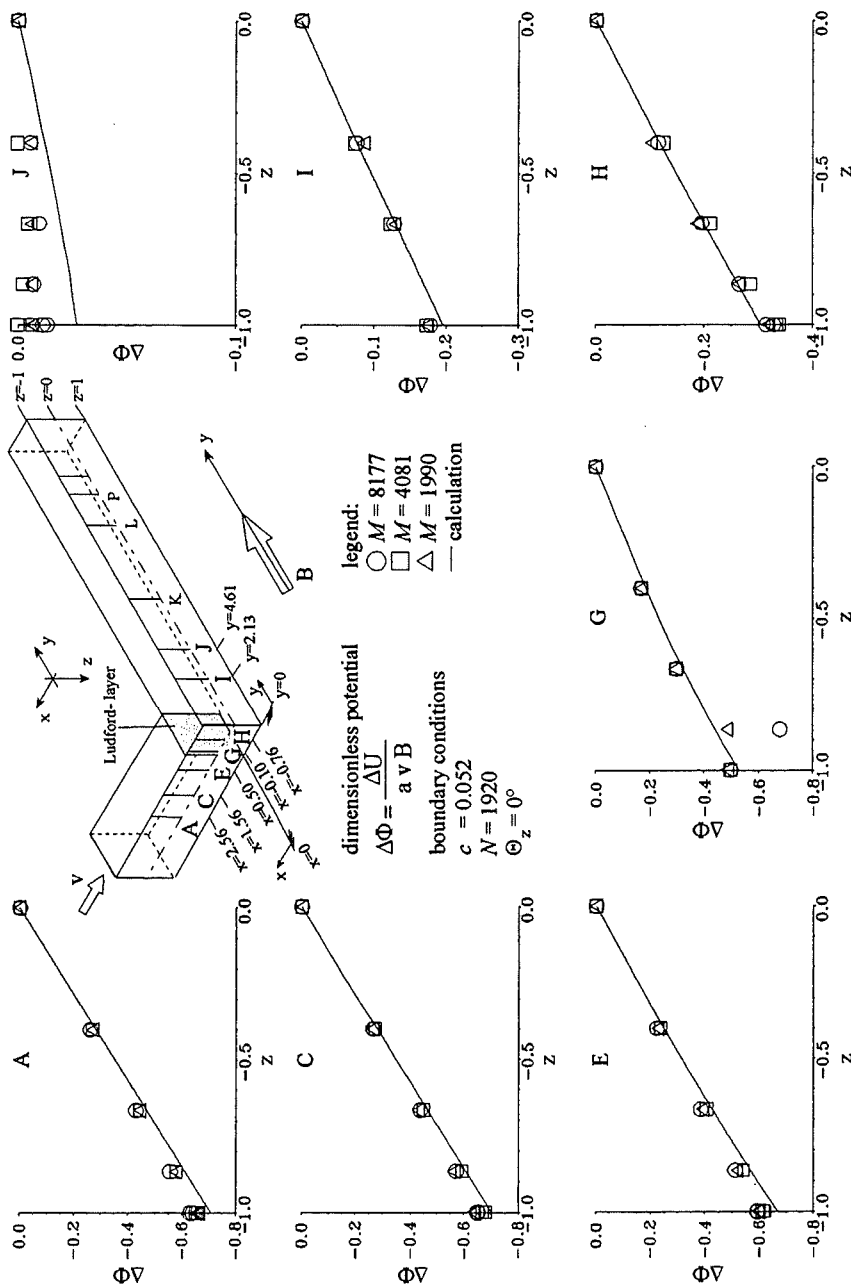


Figure 11.6: Positions where wall potentials are measured. At the Hartmann wall of the radial duct (A-E); at the Hartmann wall of the toroidal duct (G, H), at the first wall (I, J). (Stieglitz 1994, Stieglitz&Barleon 1996).

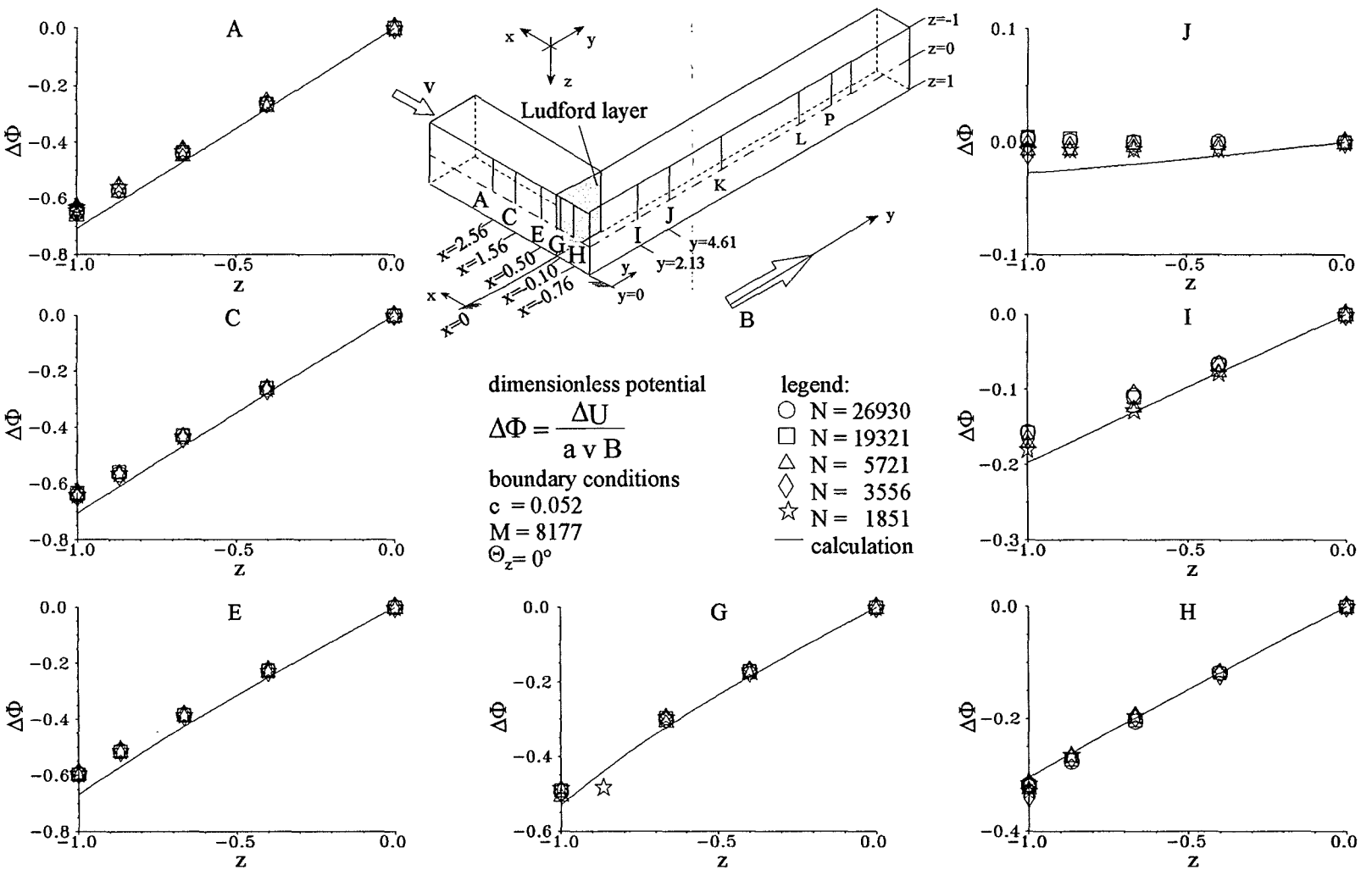


Figure 11.7: Wall potentials at different positions for different values of N at $M=8177$ compared to the asymptotic theory $N, M \rightarrow \infty$. (Stiegitz 1994).

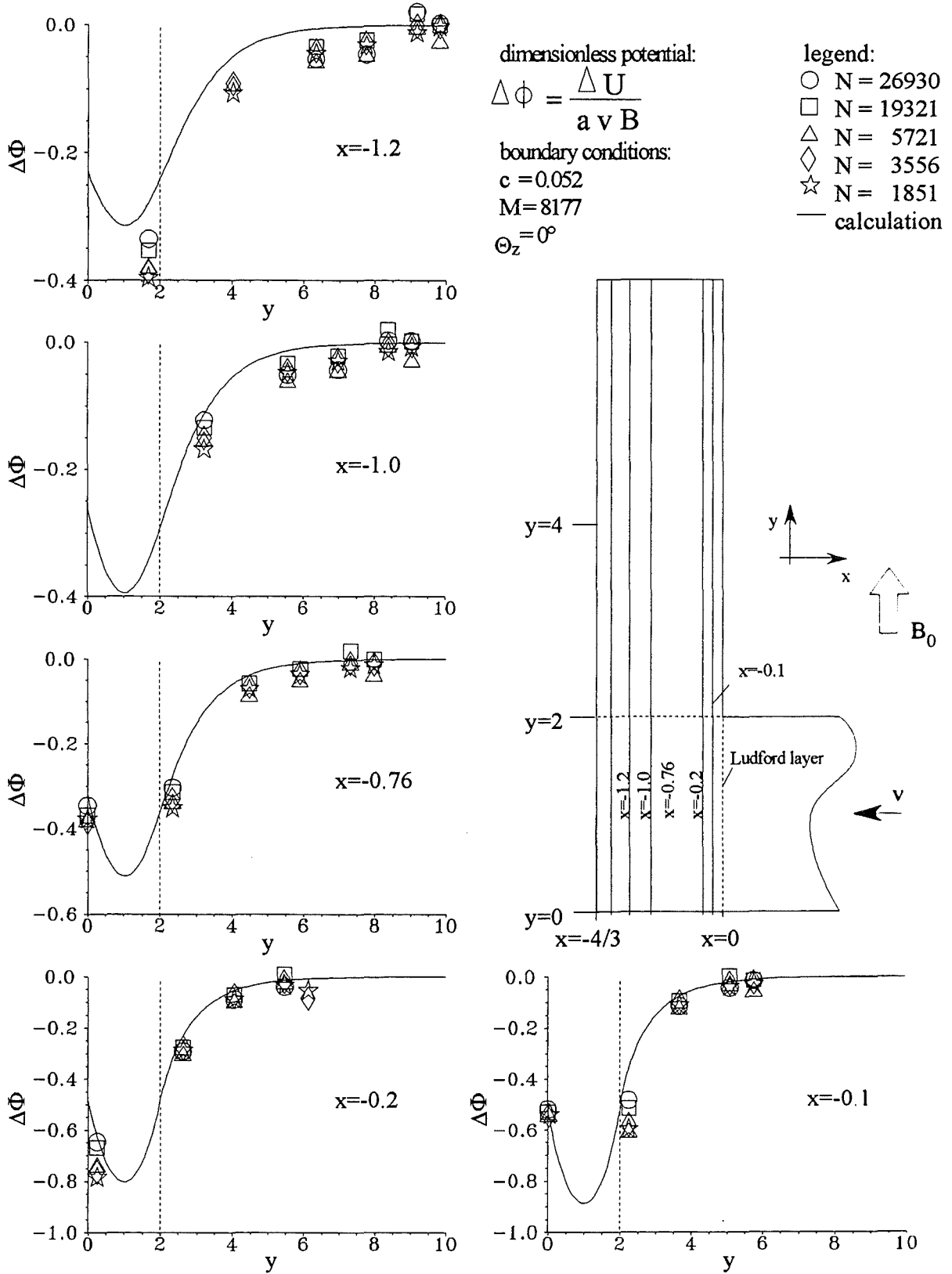


Figure 11.8: Wall potentials at the positions $x=-1.2-0.2$ for different values of N at $M=8177$, compared to the asymptotic theory $N, M \rightarrow \infty$. (Stieglitz 1994).

II. Pressure drop

Figure 11.9 shows experimental values of the total pressure drop over the whole bend. The calculated asymptotic limit is confirmed almost exactly by the experiment for high values of N . For $N < 2000$ the total pressure drop shows a significant dependence on N and M , which may be fitted by the following correlation:

$$\Delta p_{total} = \Delta p_{asymptotic} + 0.406 N^{-0.337} + 0.0939 M^{-0.565} \quad (11.3)$$

The expression has been obtained by a statistical analysis of the experimental data. The exponents -0.337 and -0.565 are very close to theoretically predicted values $-1/3$ and $-1/2$, respectively. This means that in the inertial flow regime the layers are characterised by inertial-electromagnetic interaction. The asymptotic value $\Delta p_{asymptotic}$ for high M and N is that obtained for the inertialess limit at $N \sim M^{3/2}$ and may be further split in a part of fully developed MHD flow perpendicular to the field and an additional contribution of inertialess 3D effects like:

$$\begin{aligned} \Delta p_{asymptotic} &= \Delta p_{fd} + \Delta p_{3D} \\ \text{or} \\ \Delta p_{asymptotic} &= (l_{rad} + l_{3D}) \left. \frac{\partial p}{\partial x} \right|_{fd} \end{aligned} \quad (11.4)$$

The equivalent length l_{3D} characterising the additional pressure drop Δp_{3D} in the considered bend flow is $l_{3D} = 0.563$, which is for sure not critical for blanket applications. l_{rad} is the length of the radial duct. Since some blanket elements require flows with $N < 2000$, the above named equation can be used as inertial correction to the theoretically obtained asymptotic solution for pressure drop.

The U-bend flow-problem represents in principle a coupling between the flow in two 90° -bends. Most of the flow features are similar. In the ducts oriented in magnetic field direction a zero potential is induced, whereas in the ducts perpendicular to the field a potential due to $\vec{v} \times \vec{B} \neq 0$ is induced. Therefore, these toroidal ducts act as a shortcut for the electric current, forcing the flow in the radial ducts towards the side walls and moreover producing a 3D pressure drop.

If the distance of the two 90° -bends is not of the order $l \sim \sqrt{M}$ an electric current between the two bends can circulate because of an opposite induced potential in the radial ducts (see figure 11.10). This additional global current leads to an amplified 3D effect compared to a single 90° -bend and as a consequence to a higher 3D-pressure drop in the U-bend compared to two 90° -bends.

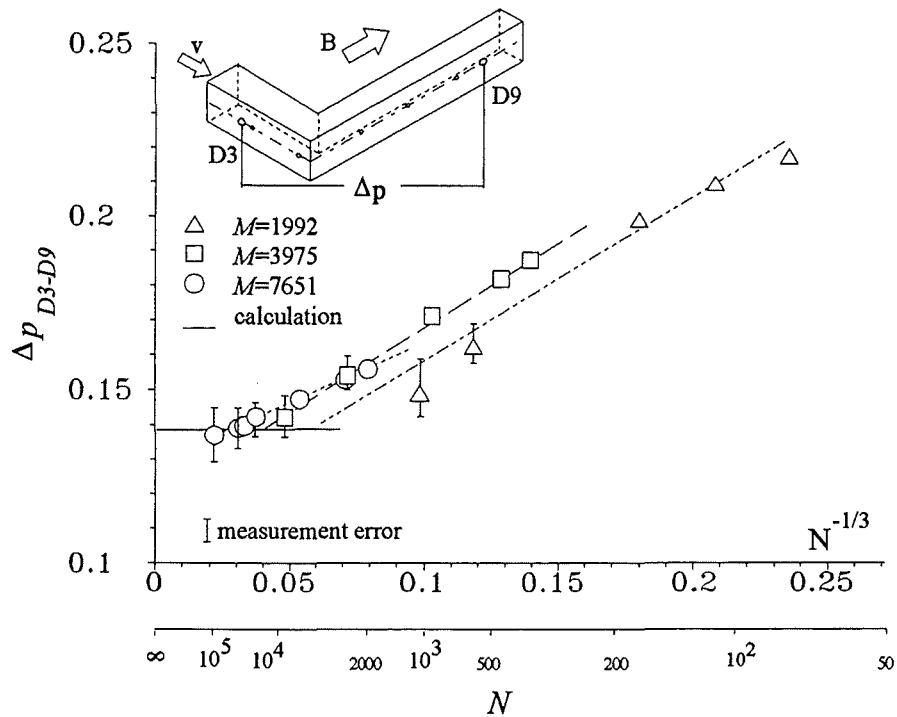


Figure 11.9: Pressure differences between D3-D9 for different values of N at varying M compared to the asymptotic theory $N, M \rightarrow \infty$ (Stieglitz 1994).

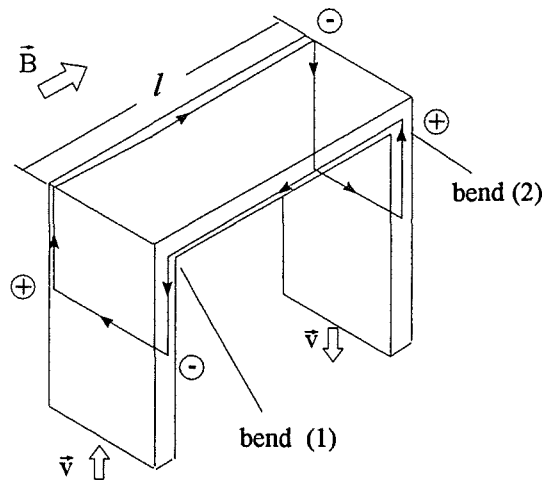


Figure 11.10: Sketch of the additional global current path in a radial-toroidal-radial U-bend.

The U-bend flow has been experimentally investigated in the context of the multi-channel U-bend flows by Stieglitz (1994).

A comparison of the measured wall potentials and the calculated ones showed an excellent agreement like in the 90° -bend. The potentials on the Hartmann walls are independent of the Interaction parameter in the range $1001 \leq N \leq 32390$ and independent of the Hartmann number in the range $600 \leq M \leq 2365$. Slight deviations in the potential measurement between the calculations and the experiment are confined to the immediate vicinity of the bend. In a

distance of four characteristic length after the bend the flow reaches the fully developed flow regime which is expressed by the pressure gradient of the fully developed MHD-flow in a rectangular duct, see figure 11.11, and the related potential distribution.

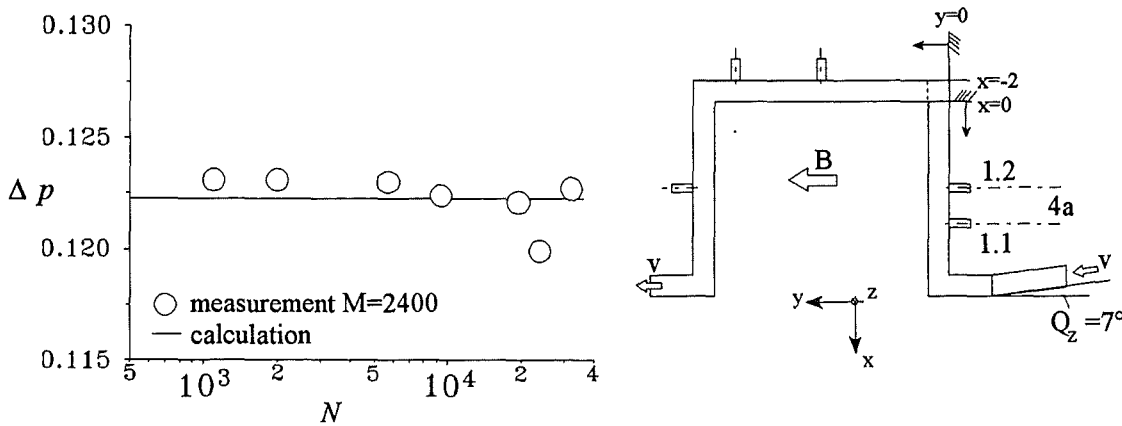


Figure 11.11: Dimensionless pressure difference Δp between the taps 1.1-1.2 in a single U-bend flow for $M=2400$, $c=0.038$ and $\Theta_z=0^\circ$.

The flow in the U-bend itself is affected by inertial effects. At high Interaction parameters the pressure drop in each of the two 90° -bends is the same but it still 8% higher than that calculated with the inertialess, inviscid asymptotic model, indicating that inertia effects are still present at Interaction parameters beyond $N \geq 40,000$ (see figure 11.12). At higher flow velocities (decreasing Interaction parameters) discrepancies in the pressure drop between the two 90° -bends appear, which are caused by the different effects of the electric current path due to the formation of recirculation areas in the bends, for detailed discussion see Stieglitz 1994. The total pressure drop in a U-bend flow is shown in figure 11.12b. The additional pressure drop originating by inertial effects $\Delta p_{3D,N}$ in the U-bend scales like in the 90° -bend with $\Delta p_{3D,N} \sim N^{-1/3}$.

Of course, also multi-channel problems have been measured in the frame of the MEKKA program. We restrict here our small presentation to the multi-channel U-bend problem. To give the reader an insight what one has to understand by a multi-channel-flow problem, short MCF we like to start with the Multi channel flow in straight ducts.

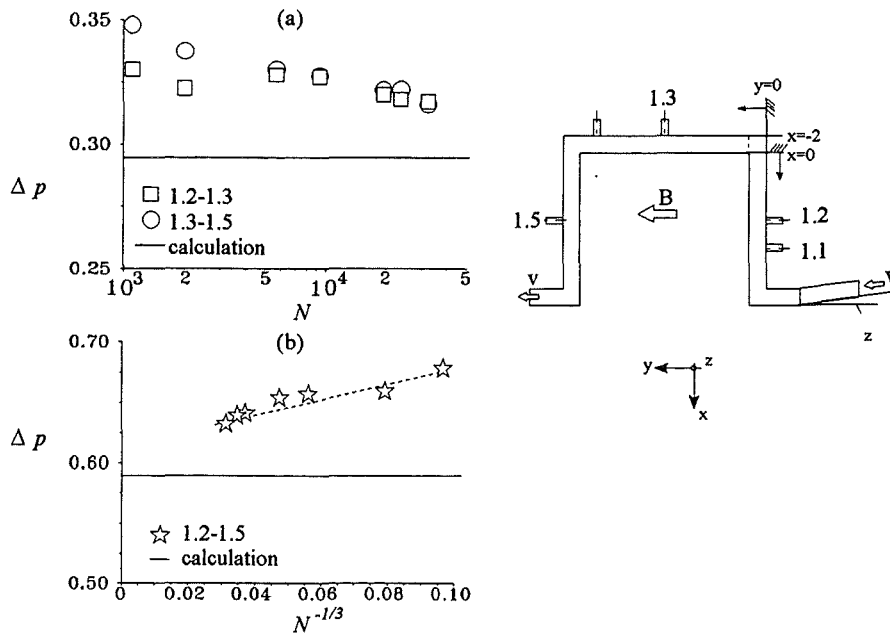


Figure 11.12: a) Dimensionless pressure losses for 90°-bend flows in the radial-toroidal (O) and the toroidal-radial (□) direction for $M=2400$, $c=0.038$ and $\Theta_z=0^\circ$.
 b.) Dimensionless pressure drop in a U-bend for $M=2400$, $c=0.038$ and $\Theta_z=0^\circ$.

MCFs have been considered e.g. by McCarthy & Abdou (1991) for an array of three channels as shown in figure 11.13. In this arrangement the potentials along the side wall have almost the same values at the junction of two ducts if the flow rates in the sub-channels are the same. Therefore no significant effects in MCFs are observed. Only for strongly different flow rates in the sub-channels or for different wall conductance ratios an influence due to MCFs is observed. With respect to applications in the radial-toroidal blanket concept (Malang et al. 1988) the arrangement of channels as shown in figure 11.13 is more interesting as it represents the radial duct configuration. Here the potentials at dividing conducting walls can sum up along the whole array of sub-channels. The current can cross the walls and pass via all sub-channels, thus causing a strong electromagnetic coupling. Especially this case is investigated by the following considerations in more detail.

The MHD flow in an array of sub-channels as shown in figure 11.13b with conducting dividing walls has been analysed by Molokov (1993a, b). In his calculations he used the flow variables \vec{v} , \vec{b} which correspond to the fluid velocity and to the induced magnetic field or the stream function for current, respectively. Since this approach leads to results only for fully developed flow conditions we do not refer to this formulation in more detail. To keep the notation introduced before using v , Φ , the velocity and the potential, Molokov's basic ideas are expressed using these quantities, which can also serve for calculations in more complex 3D geometries.

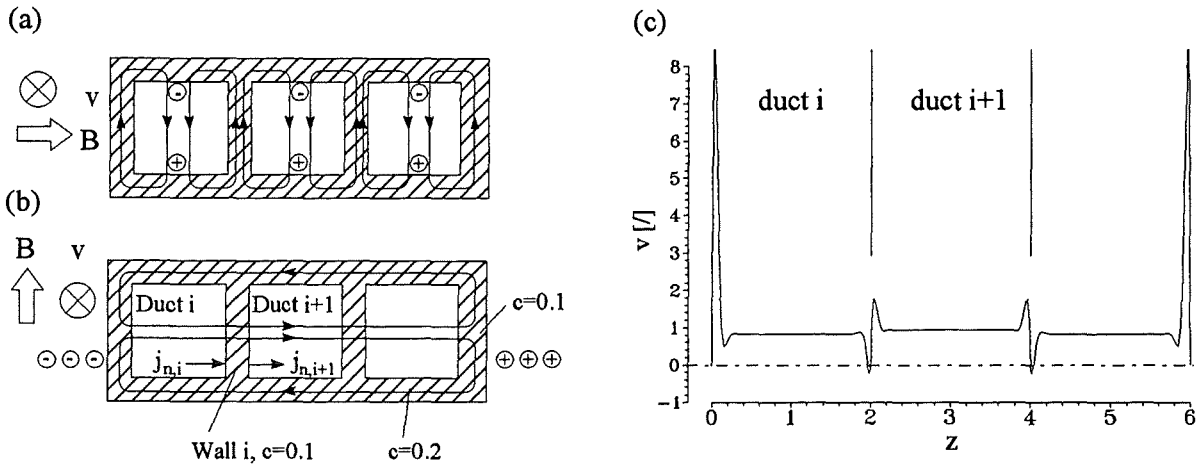


Figure 11.13: Current path in 2D multi-channel duct flows (a, b). c.) Velocity distribution of a 2D MHD-flow in the configuration (b) for $M=800$ [Molokov 1993].

The flow in each sub channel is considered to be fully developed. The walls are assumed to be thin and to have perfect contact with the liquid metal so that the thin-wall condition (see theory chapter §2) can be directly applied at all the outer walls. At conducting dividing walls this condition needs some modification. Since only a part of the current \vec{j}_i which enters the wall i from the duct i at one side turns in the tangential direction and produces there a distribution of wall potential $\Phi_{w,i}$. The rest of the current entering the wall at one side may leave it at the other side towards the adjacent sub-channel $i+1$ (see figure 11.13b).

$$\vec{j}_{n,i} - \vec{j}_{n,i+1} = c_i \Delta_t \Phi_{w,i} . \quad (11.5)$$

This coupling condition allows the global current path across all sub-channels. The above named equation shows immediately some interesting features.

- ◆ If the pressure gradient $\nabla p = \vec{j} \times \vec{B}$ (in the asymptotic limit $M, N \rightarrow \infty$) is constant in each sub-channel the currents entering and leaving the side walls have to be equal $\vec{j}_{n,i} = \vec{j}_{n,i+1}$. There is no net current flux into the wall so that the potential $\Phi_{w,i}$ becomes the same linear function between the two Hartmann walls as for the core potentials $\Phi_{C,i}$. Flow rates $Q_{i,R,L}$ of $O(1)$ carried by high-velocity jets along the right and the left side of the wall i occur only if there exists potential differences between the cores and the walls. For the same pressure gradients in each channel they do exist only at the outer sides but they do not exist along the dividing walls. Thus the MCF in this case is comparable to a single channel flow in a duct with a width of the whole multi channel array.

- ◆ More interesting is the case when instead of the pressure gradients the flow rates are equal in all the sub-channels. This case is even more desirable because it ensures a homogeneous convective heat removal by the array of channels in a technical application. Equal flow rates result mostly not in equal pressure gradients and thus cause different currents at both sides of the dividing walls. The equation leads for this case to a parabolic variation of potential Φ_w along the dividing wall. Since the potential differences across the right and left side layer at the dividing wall, $\Phi_{w,i} - \Phi_{C,i}$, $\Phi_{C,i+1} - \Phi_{w,i}$, respectively, are the same but with opposite sign (since $\Phi_{C,i} = \Phi_{C,i+1}$) the high-velocity jets in the layers have different directions. In one duct the flow rate carried by the layer contributes to the total flow rate while in the adjacent duct it acts in opposite direction.

If the wall conductance ratios of the sub-channels vary and the volumetric flow rate in the sub-channels is identical the velocity profiles may become even more peculiar. There may appear reversed flows and high velocity jets at the side walls, as depicted in figure 11.13c.

Lets now explain the features of a multi-channel bend flow. In the blanket concept proposed by Malang et al. (1988) a large number of parallel toroidal ducts is fed by the radial ones. At the opposite toroidal end of the blanket segment the flow direction turns again to the radial direction. Thus, the front part of the blanket is formed by an array of radial-toroidal-radial U-bends. As explained already in the previous paragraph conducting dividing walls lead to an overall current path and a summation of potentials induced in the radial sub-channels where the flow direction is perpendicular to the applied strong magnetic field. Here only the most important results of this work are summarised. The high resulting voltage may cause now extreme 3D effects leading to high pressure drop near the radial-toroidal junction. There exists in addition the possibility of a current short-cut between one radial leg and the other one via the toroidal ducts. Such a current path becomes possible since the high voltages in both radial legs are induced with opposite sign. That this may lead to severe design problems has been realised already years ago (Madarame 1984).

In order to investigate the MHD flow in a number of parallel U-bends a test section of five sub-channels as shown in figure 11.14 has been used. A more detailed description of the test section as well as of all obtained experimental results is given by Stieglitz 1994. The channels are numbered starting from the inner one which contains the plane of symmetry $z=0$. The weak inclination of the entrance part by the small angle of $\Theta_z=7^\circ$ was needed to study the sensitivity with respect to small inclinations of the whole test section in the available test volume of the laboratory magnet. The part of the test section in which the flow is analysed with prior interest is the upper half with $x < 10$ (see figure 11.14).

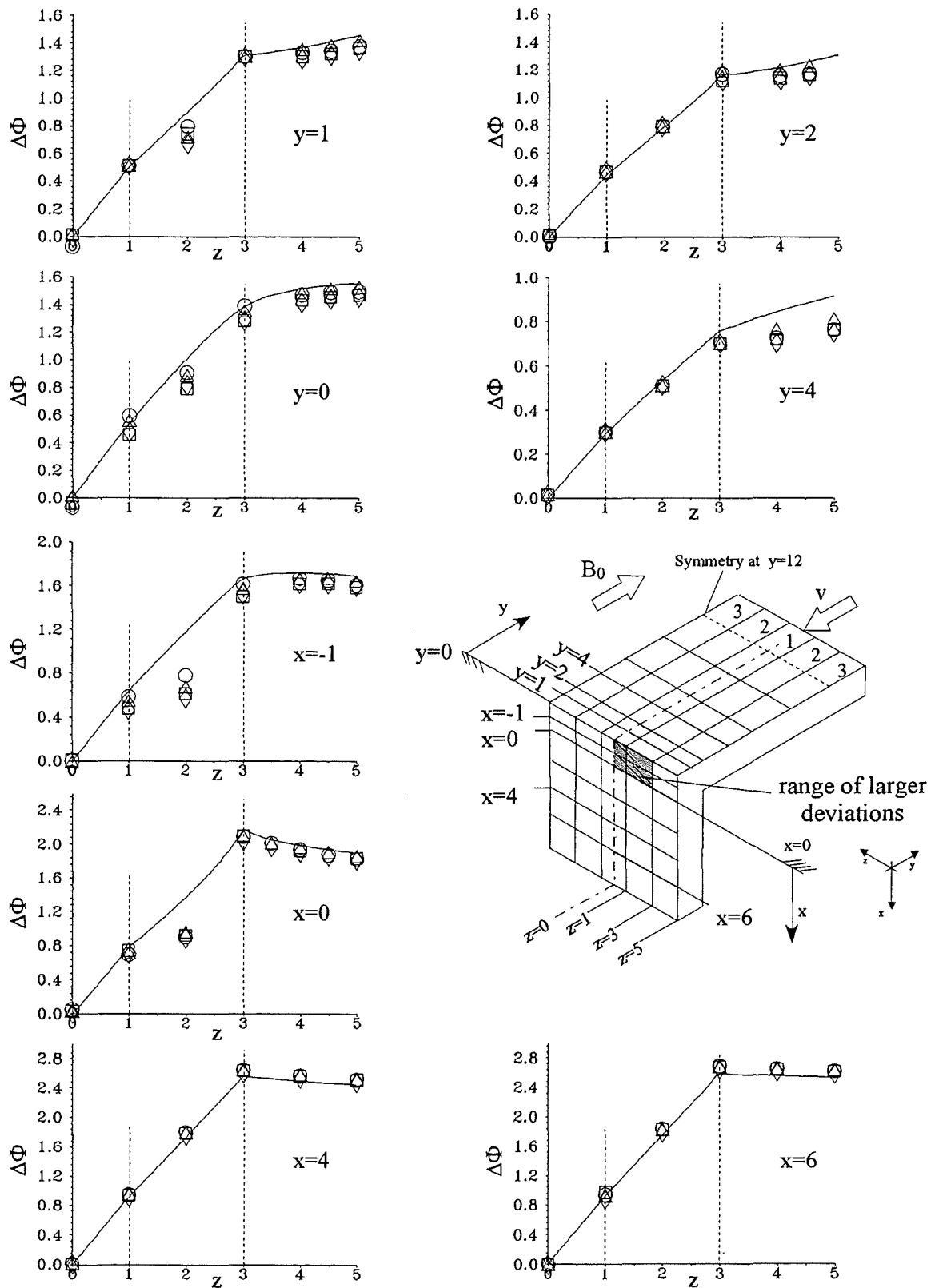


Figure 11.15: MHD flow in the inner bends 1, 2, bends 3 are empty. Wall potentials at different positions as indicated in the graph. $N=1034$, $c=0.038$. $M=2431$ (O), $M=1910$ (\square), $M=1211$ (Δ), $M=634$ (\diamond), calculation(—); (Stieglitz 1994).

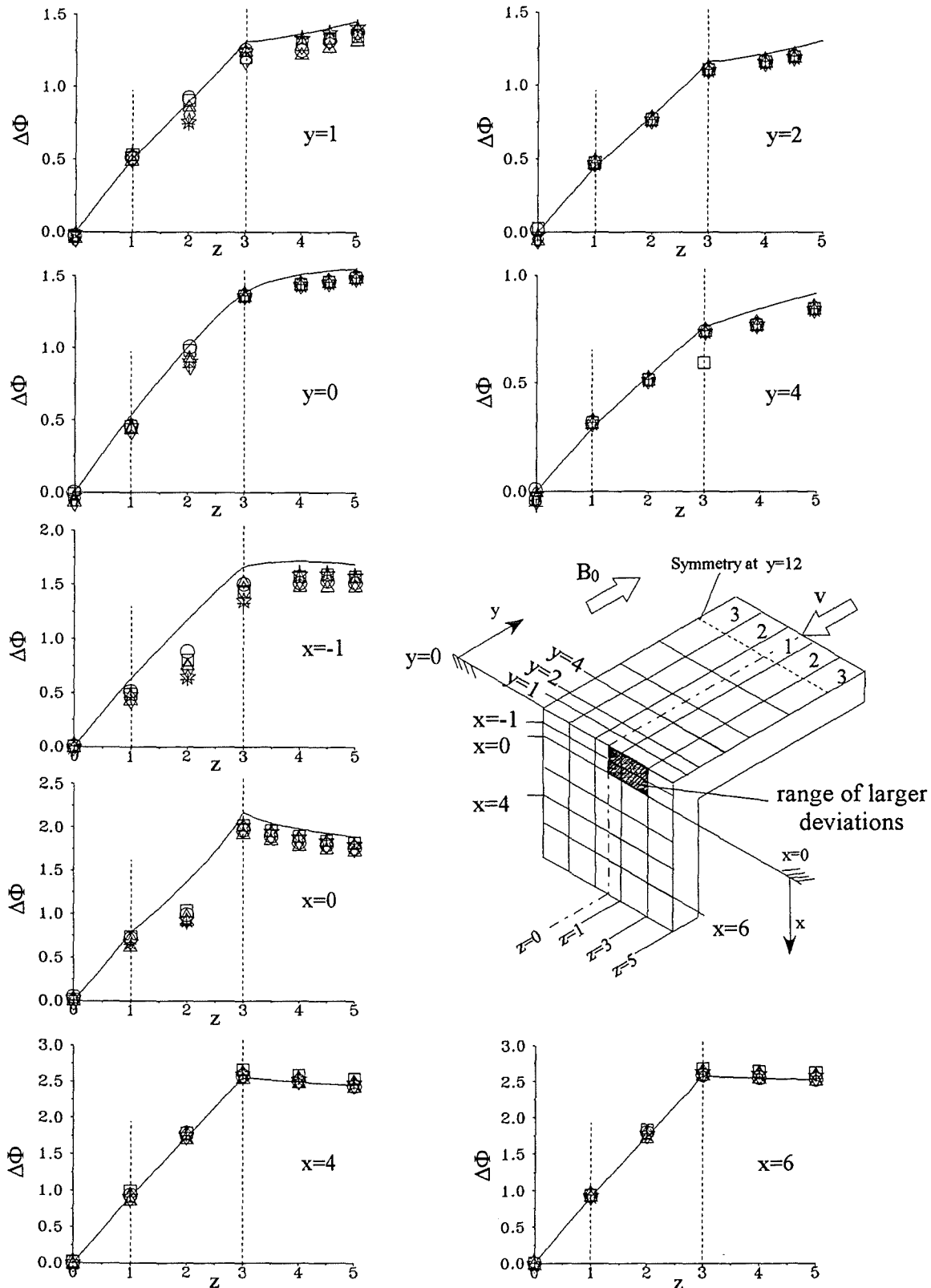


Figure 11.16 MHD flow in inner bends $i=1,2$, bends $i=3$ are empty. Wall potentials at different positions as indicated in the sketch of geometry. $M=2431$, $c=0.038$, $\Theta_z=0$. $N=37436$ (O), $N=20355$ (□), $N=10457$ (Δ), $N=4153$ (◇), $N=1827$ (*), $N=1034$ (+), $N, M \rightarrow \infty$ calculation (—) (Stieglitz 1994).

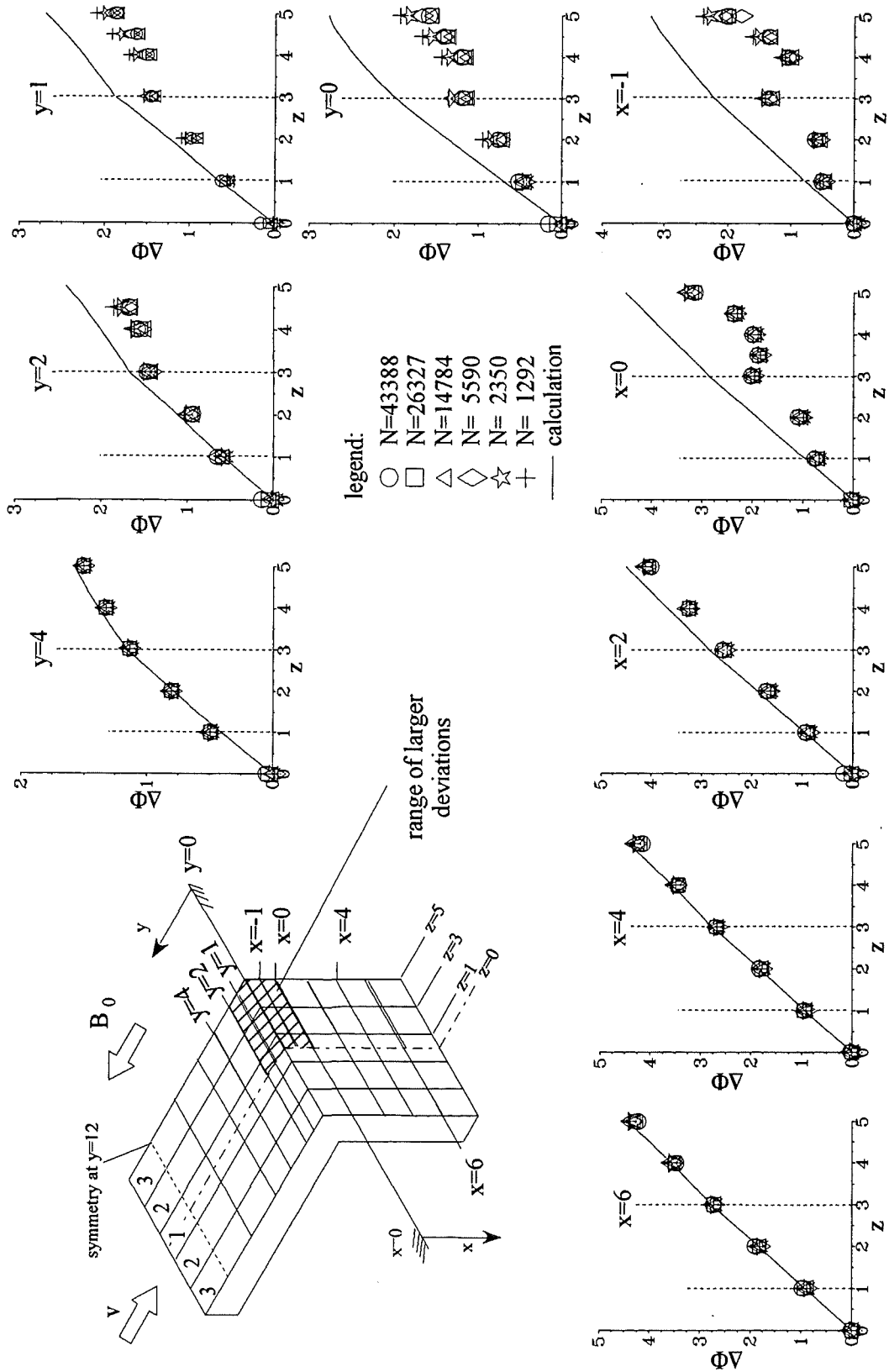


Figure 11.17: MHD flow in all bends $i=1,2,3$. Wall potentials at different positions as indicated in the sketch of geometry. $M=2372$, $c=0.038$, $\Theta_z=0^\circ$. $N=43388$ (O), 26327 (□), 14784 (Δ), 5590 (◇), 2350 (*), 1292 (+), calculation (—). Stieglitz 1994.

In all cases considered the agreement between theoretically and experimentally obtained potentials is surprisingly good even if the used asymptotic theory does not account for inertia or for viscosity. Only near the radial toroidal junction at the positions $x \leq 0$ for 3BF or at the positions $x \leq 0, y \leq 2$ for 5BF larger differences are measured. The range of positions where the disagreements occur is small and indicated by the hatched surface of the geometry in figure MCF5. Although the strongest inertia effect are expected in this part of the bend the discrepancy between theory and experiment does not disappear even for the highest investigated values of N so that it can not be explained by inertia forces only.

II. Pressures:

Measurements of the pressure differences between the positions (i,k) have been performed for a number of different cases. Here the first index i denotes the channel number, the second one k stands for the position along the U-bend.

Figure 11.18 shows the pressure drop in the centre of the duct $i=1$ between the positions $k=1$ and $k=2$. A comparison of the experimental data with the asymptotic model (AM) results for fully developed 2D flows shows good agreement for the single bend flow, see figure 11.18b, indicating that the radial part used in the experiment has been long enough to provide fully developed conditions between the positions 1.1 and 1.2.

In the case of a 3BF the results of fully developed 2D pressure drop and the measured pressure data do not agree, even for the highest value of N , indicating that the radial length is too short for the flow to become fully developed (see figure 11.18c). This can be confirmed by detailed 3D calculations including the entrance part of the geometry and, in addition, the wall conductivity of the empty channels. If all these effects are taken into account the AM predicts the experimental findings almost exactly for high values of N . The same tendency is observed for the 5BF, which is shown in figure 11.18d.

A comparison of all measured radial pressure differences show that the pressure differences 1.1-1.2 increases with the number of filled channels (compare figures 11.18b-d). Inertialess conditions are already reached for the 1BF at moderate N of 10^3 . In the 3BF inertialess flow is reached at $N \geq 10^4$, while for 5BF it has been not yet reached even at the highest investigated value of N . In all cases considered the inertia effects increase the pressure drop.

In figure 11.19 the pressure drop along the whole U-bend between the positions i.2-i.5 is shown as a function of the interaction parameter. The pressure drops are shown versus the $N^{-1/3}$ -axis to demonstrate the dependence $p_{3D} \sim N^{-1/3}$ by the linear behaviour of the experimental data for all cases considered (1BF, 3BF, 5BF). The agreement in the inertialess limit as $N^{-1/3} \rightarrow 0$ with the results obtained by inertialess analysis is good for 1BF and also for 3BF. In case of the 5BF the pressure drop in the outer channels is comparable to the predicted values.

The inner channels 1 and 2 show differences of about 30% in comparison to the theoretically obtained pressure data. Although the dependence $\Delta p_{3D} \sim N^{-1/3}$ is confirmed for different numbers of bends (1,2,3) the influence of inertia effects is more pronounced for higher channel numbers. It can reach two times (3BF) or three times (5BF) the value of inertialess flow.

At smaller values of N i.e. $N^{-1/3} > 0.25$ the pressure drop correlation $p_{3D} \sim N^{-1/3}$ is changed to a weaker dependence due to turbulent effects.

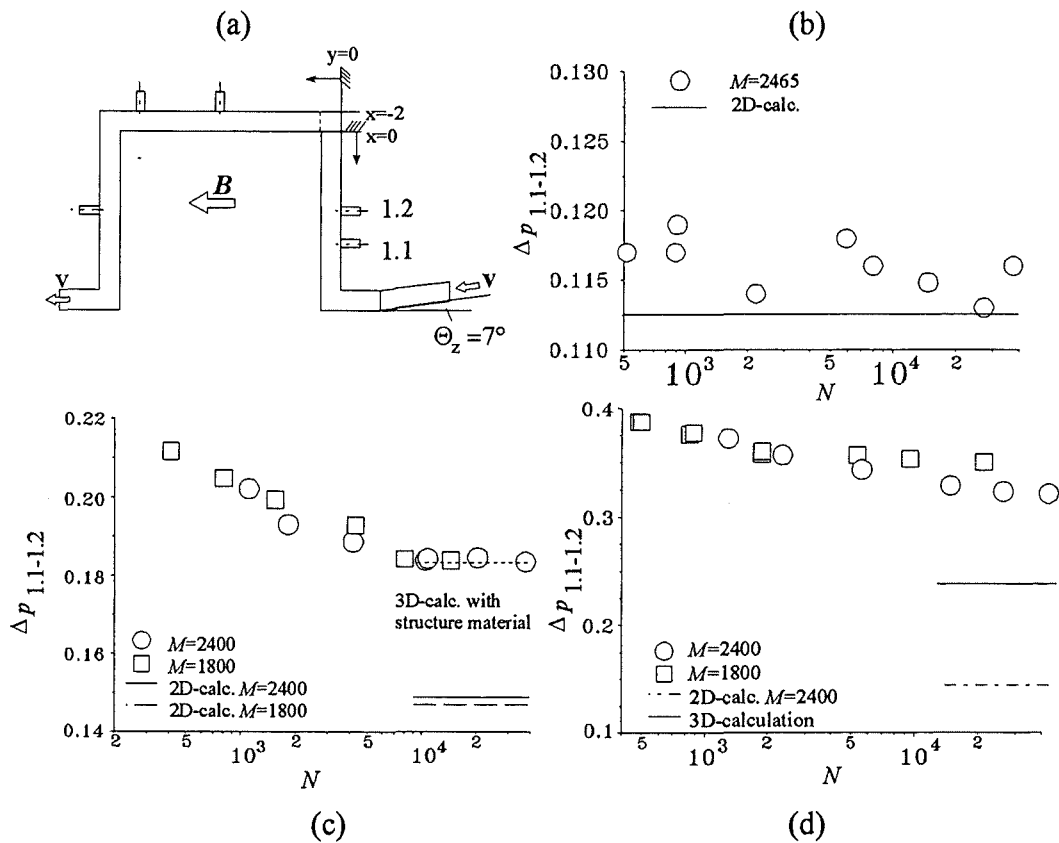


Figure 11.18: Pressure drops in the radial part of multi-bend flows as a function of N . $c=0.038$. a) Sketch of geometry, b) 1BF, c) 3BF, d) 5BF (Stieglitz 1994).

In all cases considered the highest pressure drop has been observed in the inner channel $i=1$. It decreases continuously with higher N , but increases with the number of filled channel linearly up to the number of five bends considered, see figure 11.20.

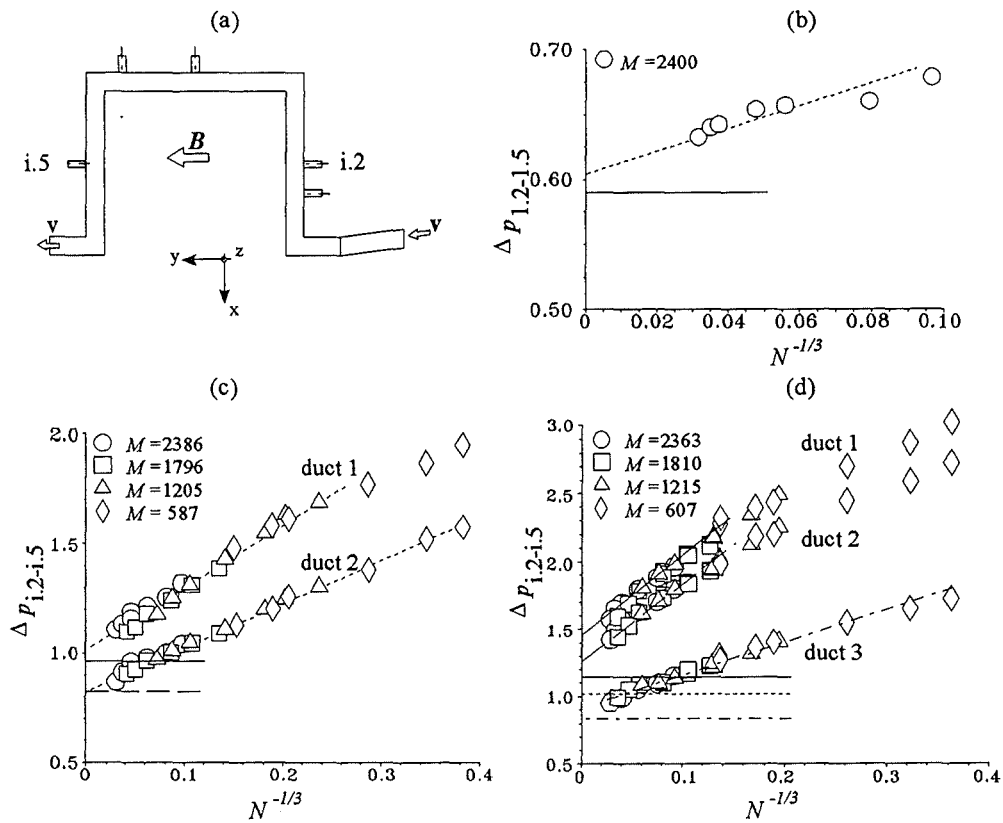


Figure 11.19: Total pressure drops in multi-bend flows as a function of N ; $c=0.038$, $\Theta_z=0$.
 a) Sketch of geometry, b) 1BF, c) 3BF, d) 5BF. 3D calculations bend 1 (—), bend 2 (- - -), bend 3 (- · - · -). (Stieglitz 1994).

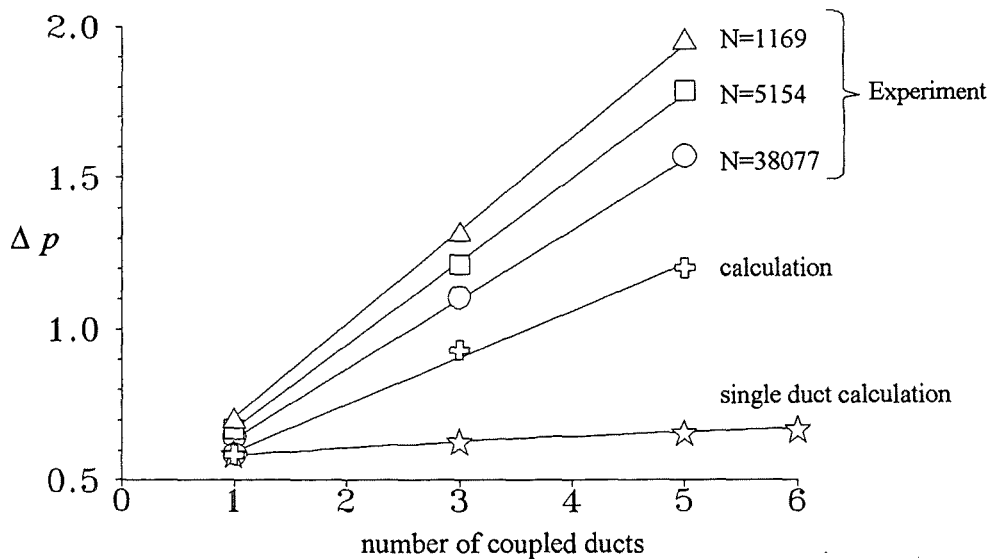


Figure 11.20: Total pressure in the bend $i=1$ for different interaction parameters as a function of the number of filled channels. $M=2402$, $c=0.038$, $\Theta_z=0$. (Stieglitz 1994).

12 Summary and future program

The authors described in the beginning some fundamental phenomena appearing in magnetohydrodynamic duct flows. Afterwards the link of these flow problems to the liquid metal cooled fusion reactor blanket has been outlined.

The following chapters dealt the choice of the model liquid, the magnets and the liquid metal loops designed and built up in the MEKKA-laboratory of the Forschungszentrum Karlsruhe. Within these sections the authors followed the aim to make the readers the chosen design and the required tools to construct the main components transparent.

One of the most important chapters especially to experimentalists is §9, where most of the rather specific effects related to measurement methods in magnetohydrodynamic flows are discussed. There, the relevant equations for each problem are given and the limitation of the particular methods are discussed.

Finally some of the results obtained in the MEKKA-laboratory being far of completeness are shown.

The main research has been focused up to now on the investigation of isothermal MHD-flows. The results obtained up to now confirmed the analytical and the numerical solutions obtained for the laminar MHD-flows. But as discussed in the previous section MHD-flows reveal for certain flow parameters a time-dependent flow characteristic or even a fully turbulent flow behaviour. Especially for fusion reactor applications and also many applications in industry the flow is far of being fully laminar in all flow domains. Some of experimental results show that the turbulence in MHD-flows is highly anisotropic and it seems to be that the turbulence is two-dimensional. The experimental problems to be investigated in the future related to this field can be formulated as follows.

When, how and why turbulence becomes two-dimensional in MHD flows ?

In order to investigate this quite simple but rather complex question one has to start with the simplest problems of the stability of two-dimensional MHD-flows. Similar to hydrodynamics we intend to start the experimental research with the investigation of the stability of a shear flow. The figure 12.1 shows a configuration where the flow is oriented perpendicular to the applied magnetic field. The duct walls are electrically insulating except for a thin copper film glued to the walls in the ducts centre. The fluid velocity under the copper film is drastically reduced due to this jump of the wall conductivity as the schematics in the graph shows. The shear flow caused by the electromagnetic obstacle gets instable at certain Hartmann numbers and interaction parameters. The instability can be measured by electric potential probes located on the duct walls.

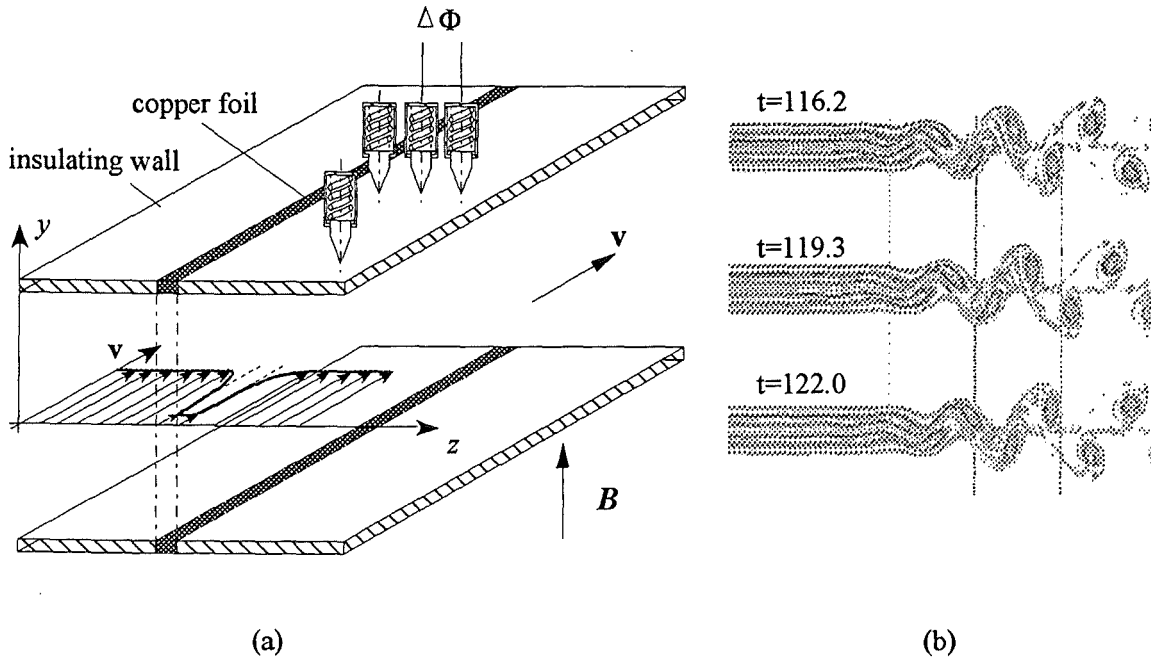


Figure 12.1: a.) Sketch of a test section to investigate the stability of a two-dimensional MHD shear flow. The figure shows the velocity profile and the measurement method. b.) The figure on the right shows the calculated vorticity distribution of the flow problem for different times and a $M=1100$.

Of course, the investigation of the stability problem forms only the start of investigations into the field of time-dependent MHD-flows. The next step of research has to investigate the transition problems from laminar flow to two-dimensional turbulence and from 2D-turbulence to 3D-turbulence. These investigations require rather sophisticated probes in order to measure the velocity fluctuations in the duct cross sections. Especially the knowledge of the correlations $u'v'$, $u'w'$, $v'w'$ are important to describe the flow state (laminar, 2D-turbulent, 3D-turbulent) and they are necessary to develop turbulence models for MHD-flows.

Up to now the major task of the investigations related to the development of liquid metal cooled fusion reactor blankets has not been discussed, namely the heat transfer behaviour of MHD-flows. In order to investigate this problem the test section shown in figure 11.4 is radiation heated in the way depicted in graph 12.2. The Peclet number range attainable is of $O(10^1)$ to $O(10^3)$. Besides the velocity fluctuations named above also temperature fluctuations ($u'T'$, $v'T'$) are measured with a TEMPO probe (explained in §9.6.2; figure 9.10) in order to determine the turbulent heat fluxes. A characteristic preliminary result of the temperature distribution in z -direction is displayed in figure 12.2. This result obtained for a specific parameter configuration demonstrate, that the heat which can be removed from a heated wall is higher than the values calculated using a laminar heat transfer and is significantly higher than the heat conduction model with a slug flow velocity profile, which has been used in the

thermohydraulic design studies for the fusion reactor blankets.

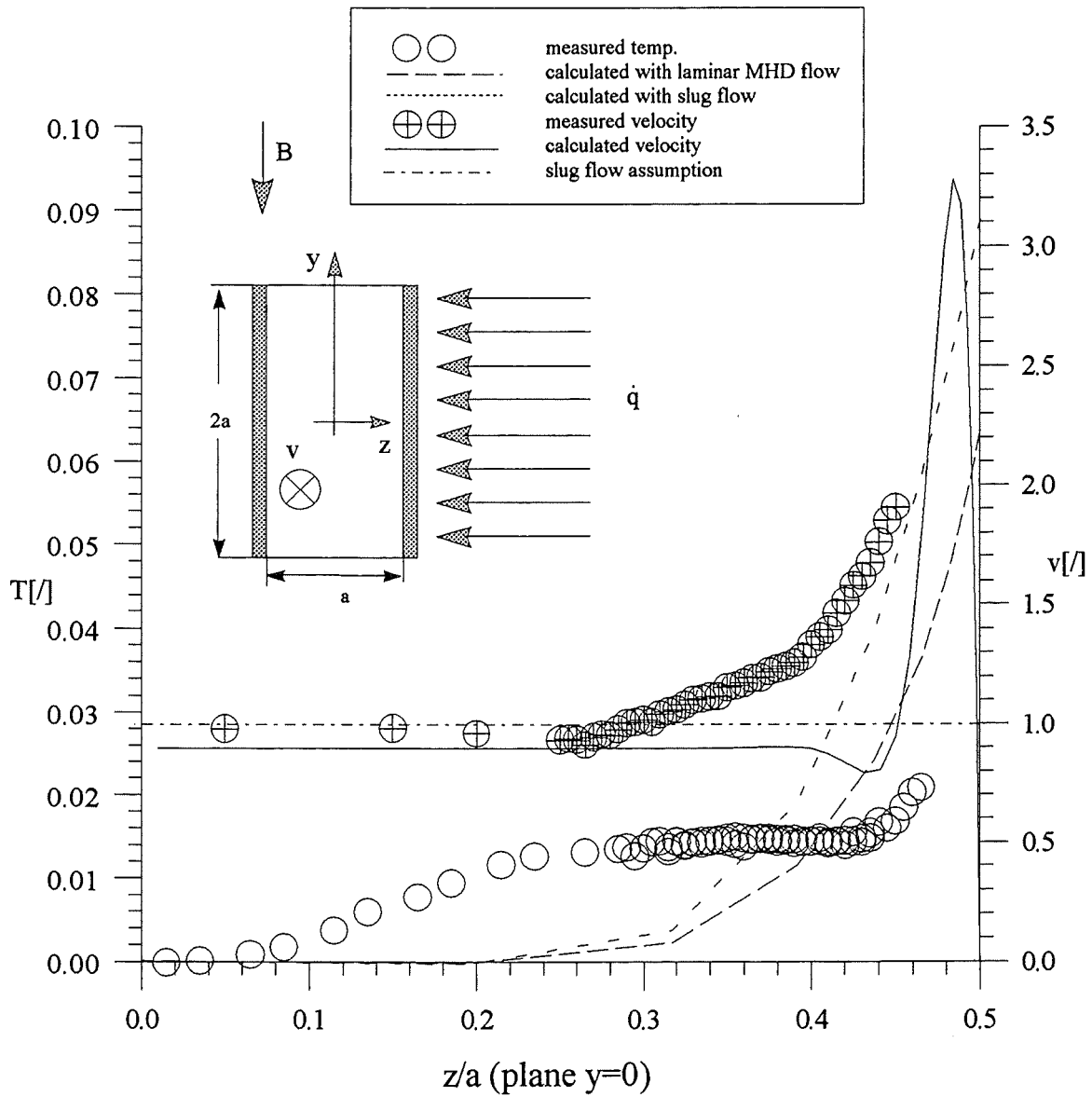


Figure 12.2: Measured dimensionless temperature T and measured dimensionless velocity in a rectangular duct with thin electrically conducting walls ($c_H=0.0121$; $c_s=0.07247$) at $M=4750$, $Pe=1898$, $Re=78909$ as a function of z compared to theoretically predicted data.

Another field of research is actually in discussion with respect to the development of liquid metal fusion blankets, namely the natural convection of liquid metals in a strong magnetic field, which is called often magnetoconvection. For this purpose a convection test section has been already designed, which can be inserted in the normal-conducting MA-Magnet (magnetic field direction parallel to gravity vector) as well as in the super-conducting CELLO-

magnet (magnetic field perpendicular to gravity vector) of the MEKKA-facility. It is expected that the flow patterns as well as the measured Nusselt number for both cases is considerably different. The test section itself is already fabricated and the measurement will latest start in the beginning of next year.

A more academic field of research, which should not be omitted in this context since it may gain more importance in the future in terms of flow control is the problematics of MHD flows around obstacles. In order to investigate this field in a first state a test channel for the GALINKA-loop has been designed, in which cylindrical as well as rectangular obstacles oriented in direction of the magnetic field can be inserted at different positions in the channel. It is foreseen to measure the electric wall potentials at the walls normal to the magnetic field, the velocity and the velocity fluctuations in the ducts cross section.

Acknowledgement

This work has been performed in the framework of the Nuclear fusion project of the Forschungszentrum Karlsruhe and is supported by the European Union within the European Fusion Technology Program. The authors are grateful to all workers of the Institute for Applied Thermo- and Fluidynamics of the Forschungszentrum Karlsruhe. We thank especially Prof. Dr. U. Müller, Dr. L. Bühler, Dr. S. Molokov and many other unnamed guest scientist and students for their help in planning, designing, performing the experiments and many hours of constructive discussions interpreting the experimental results. Without the help of these people and lots of their overtime successful measurement campaigns would not be performable.

13 References

- Addison, C.C. (1984);** The chemistry of the liquid alkali metals; John Wiley&Sons Ltd; ISBN0471905089.
- Barleon, L.; Casal, V.; Mack, K.-J.; Kreuzinger, H.; Sterl, A.; Thomauske, K. 1989** Experimental and theoretical work on MHD at the Kernforschungszentrum Karlsruhe -the MEKKA-program-; Liquid Metal Magnetohydrodynamics (Lielpeteris, J.; Moreau, R. editors); Kluwer Academic Publishers; pp. 55-61.
- Barleon, L., Lenhart, L., Mack,,K.J., Sterl, A., Thomauske, K. 1989** Investigations on liquid metal MHD in straight ducts at high Hartmann numbers and interaction parameters. Proceedings of Fourth International Topical Meeting on Nuclear Reactor Thermal-Hydraulics NURETH-4, Karlsruhe, 2, pp. 857-862.
- Barleon, L., Casal, V., Lenhardt, L. 1991** MHD-flow in liquid metal cooled blankets. Fusion Engineering and Design, 14, 401-412.
- Barleon, L.; Mack, K.-J.; Kirchner, R.; Frank, M.; Stieglitz, R. 1994** MHD heat transfer and pressure drop in electrically insulated channels at fusion relevant parameters; Proceedings of the 18th Symposium on Fusion Technology (SOFT); Karlsruhe; August 1994, Elsevier Science Publishers; Volume 2, ISBN 0 444 82220 8; p.1201-1204.
- Barleon, L.; Mack, K.-J.; Kirchner, R.; Stieglitz, R. 1994** MHD heat transfer and pressure drop in electrically insulated channels at fusion relevant parameters; Proceedings of the 2nd Internat. Conf. on Energy Transfer in Magnetohydrodynamic Flows (PAMIR); Aussois; France; 1994; p. 381-390.
- Barleon, L., Bühler, L., Mack, K.-J., Stieglitz, R., Picologlou, B.F., Hua, T.Q., Reed, C.B. 1992** Investigations of liquid metal flow through a right angle bend under fusion relevant conditions; Proceedings of the 17th Symposium on Fusion Technology (SOFT), Rom; Elsevier SCIENCE Publishers B.V., Vol.II, p.1276-1280.
- Birzvalks, J. 1986;** Streifzug durch die Magnetohydrodynamik; VEB Deutscher Verlag für Grundstoffindustrie; Leipzig;1986; ISBN3-342-001 14-3.
- Bochkarev, E.P. 1977** Technological instructions for Gallium Indium Tin alloy usage in liquid metal loops; GIREDMET Institute Moscow; Translated from Russian by I. Buceniks; Latvian Academy of Sciences, Riga, Latvia.
- Boyarevich, A.V. 1990** Measurement of averaged local velocities in magnetohydrodynamic experiments; Magnetohydrodynamics; Vol. 26; pp. 133.
- Branover, H. 1986** Turbulence and the feasibility of self-cooled liquid metal blankets for fusion reactors; Fusion Techn., Vol. 10; pp. 822-829.
- Bühler, L. 1993** Convective-diffusive transport in laminar MHD flows; KfK-5241.
- Bühler, L.; Molokov, S. 1994** Magnetohydrodynamic flows in ducts with insulating coatings; Magnetohydrodynamics; 30; No. 4; pp. 439-447.

- Bühler, L.; Müller, U. 1994** MHD channel flow related to self-cooled liquid metal blanket development; KfK-5407.
- Casal, V., Arnold, G. 1988** Velocimeter for local measurement in liquid metals; 1st World Conf. on Experimental Heat Transfer in Fluid Mech. and Thermodyn.; Dubrovnik; Yugoslavia; September 4-9.
- Chester, W. 1961** The effect of a magnetic field on the flow of a conducting fluid past a body of revolution; J. Fluid. Mech.; Vol. 3; S.459-465.
- Eringen, C.A. 1980** Mechanics of continua; Robert E. Krieger Publishing Comp.; New York; pp. 459ff.
- Foust, O.J.; 1972** Sodium-NaK engineering Handbook; Vol.1; Sodium chemistry and physical properties; Gordon and Breach SCIENCE Publishers; ISBN0677030204.
- Gold, R. 1962** Magnetohydrodynamic pipe flow; Part 1; J. Fluid Mech.; Vol. 13; pp. 505-512.
- Grinberg, G.K.; Kaudze, M.Z.; Lielausis, O.E. 1985** Local MHD-resistances on a liquid sodium circuit with a superconducting magnet; Magnetohydrodynamics; No.1; Vol.21; pp.99-103.
- Hartmann, J. 1937** The theory of the laminar flow of an electrically conductive liquid in a homogeneous magnetic field; Det. Kgl. Danske Videnskabernes Selskab, Matematisk-fysiske Meddelelser, Vol. XV, p. 1-45.
- Hasimoto, H. 1960** Steady longitudinal motion of a cylinder in a conducting fluid; J. Fluid. Mech.; Vol.8; S.61-81.
- Holroyd, R.J.; Mitchell, J.T.D. 1984** Liquid Lithium as a coolant for Tokamak Reactors; Nuclear Engineering and Design/Fusion; Vol.1; pp. 17-38.
- Holroyd, R.J.; Walker, J.S. 1978** A theoretical study of the effects of wall conductivity, non-uniform magnetic fields and variable area ducts on liquid metal flows at high Hartmann number; J. Fluid Mech.; Vol.84; part 3; pp.471-495.
- Hua, T.Q.; Picologlou, B.F. 1991** Magnetohydrodynamic flow in a manifold and multiple rectangular coolant ducts of self-cooled blankets; Fusion Technology, 19, p. 102-112.
- Hua, T.Q.; Gohar, Y. 1995,** MHD pressure drops and thermal-hydraulic analysis for the ITER breeding blanket design; Fusion Eng. and Design, 27, p. 696-702.
- Hunt, J.C.R.; Stewartson, K. 1965** Magnetohydrodynamic flow in rectangular ducts-Part II; J. Fluid Mech.; Vol. 22; pp. 563.
- Hunt, J.C.R.; Malcolm, D.G. 1969** Some electrically driven flows in magnetohydrodynamics; J. Fluid Mech.; Vol. 33; pp. 775ff.
- Kollie, T.G.; Anderson, R.L.; Horton, J.L.; Roberts, M.J. 1977** Large thermocouple thermometry errors caused by magnetic fields; Rev. Science Instrum.; Vol.48; No. 5; pp.501-511.
- Kyrlidis, A.; Brown, R.A.; Walker, J.S. 1990** Creeping flow of a conducting fluid past axis-symmetric bodies in the presence of an aligned magnetic field; Phys. Fluids A, 2; 2230-2239.

- Lehmann, W.; Barth, W.; Augustin, W. 1979** Auslegung und Ausführung kryotechnischer Anlagen für die beiden supraleitenden Kompensationsspulen des CELLO-Detektors in DESY; Internal Report of the Research Center Karlsruhe; KfK-Primärbericht 08.01.01P06A.
- Lykoudis, P.S.; Dunn, P.F. 1973** Magneto fluid mechanic heat transfer from hot film probes; Int. Journal Heat and Mass Transfer; Vol. 16; pp 1439ff.
- Lyon, R.N. 1952** Liquid metals handbook; Navexos P-733; Second edition.
- Malang, S., et al. 1988**, Self-cooled liquid-metal blanket concept, Fus. Techn., Vol.14, p. 1343.
- Malang, S.; Dalle Donne, M.; Anzidei, L.; Giancarli, L.; Proust, E. 1994**, European blanket development for a DEMO reactor, Fusion Technology, **26**, p. 1069ff. .
- Malang, S.; Tillack, M.S. 1995** Development of Self-Cooled Liquid Metal Breeder Blankets; FZKA 5581; November 1995.
- Mauer, W. 1989** Der PUMA und sein Feld, Internal Report of the Research Center Karlsruhe, KfK-Primärbericht 12.03.01P45A.
- McCarthy, K.A. Abdou, M.A. 1991**, Analysis of liquid metal MHD flow in multiple adjacent ducts using an iterative method to solve core flow equations. Fusion Engineering and Design, Vol. 13, p.363-380.
- Miyazaki, K; Inoue, S.; Yamaoak, N. 1986** Magnetohydrodynamic pressure drop of lithium flow in rectangular ducts; Fusion Techn.; Vol. 10; pp. 830-836.
- Miyazaki, K; Konishi, K.; Gonno, Y. 1991** Reduction of MHD pressure dop of liquid metal flow by insulation; part II; insulated circular ducts; Fusion Techn.; Vol. 19; pp. 961.
- Molokov, S. 1993a** Fully developed liquid metal flow in multiple rectangular ducts in a strong uniform magnetic field; KfK report, KfK5075.
- Molokov, S. 1993b** Fully developed liquid metal flow in multiple rectangular ducts in a strong uniform magnetic field. Eur. J. Mech. B/Fluids, Vol. 12, No.6, p.769-787.
- Molokov, S. Shishko, A. 1993** Fully developed Magnetohydrodynamic flows in rectangular ducts with insulating walls. KfK report, KfK5247.
- Molokov, S.; Stieglitz, R. 1995** Liquid metal flow in a system of electrically coupled U-bends in a strong uniform magnetic field; Journal of Fluid Mechanics; Vol. 299; p. 73-95.
- Moon, T.J.; Walker, J.S. 1990** Liquid metal flow through a sharp elbow in the plane of a strong magnetic field; J. Fluid Mechanics; Vol. 213; pp. 397-418.
- Moreau, R. 1990** Magnetohydrodynamics; Kluwer Academic Publishers; Dordrecht-Boston-London; ISBN 0-7923-0937-5.
- Morley, N.B., Tillack, M.S., Abdou, M.A. 1991** Development of an analytic core flow approximation for a square duct in an oblique magnetic field. Report UCLA-FNT-46, University of California Los Angeles.
- Picologlou, B.F. 1985** Magnetohydrodynamic Considerations for the Design of self-cooled liquid-metal Blankets; Fusion Technology, Vol.8, N^o. 1, pp. 276-282.

- Powell; R.L.; Hall, W.I.; Hyink, C.H.; Sparks, L.L.; Burns, G.W.; Scroger, M.G.; Plumb, H.H. 1974** Thermocouple reference tables; IPTS-68; U.S. Department of commerce.
- Rademacher; Ebert; Pickert 1976** Einführung in die Chemie; Verlag W. Girardet; Essen; 4.Auflage; pp. 205 ff.; ISBN 3-7736-2162-0.
- Rebhahn, E. 1992** Heisser als das Sonnenfeuer; R. Piper GmbH&Co. KG; München Zürich; ISBN 3-492-03109-9.
- Reed, C.B. & Picologlou, B.F. 1986** Techniques for Measurements of Velocity in Liquid Metal MHD-Flows; Proc. 7th Top. Meeting on Fusion Technology; Nevada, 1, p 297ff. .
- Reed, C.B.; Picologlou, B.F. & Walker, J.S. 1987** ALEX-Results-A comparison of measurements from a round and a rectangular duct with 3D-code predictions; IEEE No. 87CH2507-2; Vol. 2; 1267- 1270.
- Reed, C.B. & Picologlou, B.F. 1989** Side wall flow instabilities in a liquid metal MHD-flow under blanket relevant conditions; Fusion Technology; 15; 705-715.
- Reimann, J.; Molokov, S.; Platnieks, I.; Platancis, E. 1993** MHD-flow in Multichannel U-bends: Screening tests and theoretical analysis; KfK 5102.
- Reimann, J.; Buceniaks, Dementev, S.; Flerov, A.; Molokov, S.; Platnieks, I. 1994** MHD velocity distributions in U-bends partly parallel to the magnetic field, Proceedings of the 2nd Internat. Conf. on Energy Transfer in Magnetohydrodynamic Flows (PAMIR); Aussois; France; pp. 391-402.
- Schulz, B. (1986)** Thermophysical properties in the system LiPb; KfK-4144.
- Shercliff, J. A. 1956** The flow of conducting fluids in circular pipes under transverse magnetic fields; J. Fluid Mech. Vol. 1; pp. 644
- Smith, D.L. et al. (1984)** Blanket comparison and selection study; Final report; ANL/FPP-84-1; Volume 2, Chapter 6.
- Smith, D.L. et al.**, Blanket comparison and selection study, Fus. Techn., Vol.8; p.1, 1985.
- Stieglitz, R. 1994** Magnetohydrodynamische Strömungen in Ein- und Mehrkanalumlenkungen. Dissertation, Universität Karlsruhe.
- Stieglitz, R., Molokov, S., Barleon, L., Reimann, J., Mack, K.-J. 1994** MHD-flows in electrically coupled bends; 2nd Int. Conf. on Energy Transfer in Magnetohydrodynamic Flows; PAMIR, 26th-30th Sept. 1994; Aussois, France; Vol. 1; p.403-413.
- Stieglitz, R., Barleon, L., Reimann, J., Mack, K.-J., 1994** MHD flows in partially decoupled parallel U-bends at high Hartmann numbers, Proceedings of the 18th Symposium on Fusion Technology (SOFT), Karlsruhe, Vol. 2, p.1209-1212.
- Stieglitz, R.; Barleon, L.; Bühler, L.; Molokov, S. 1996** Magnetohydrodynamic flow in a right angle bend in a strong magnetic field; to be published in J. Fluid Mech.
- Stieglitz, R.; Müller, U. 1996**, GEODYNAMO - Eine Versuchsanlage zum Nachweis des homogenen Dynamoeffektes, FZKA 5716.

Takeda, Y. 1986 Velocity profile measurement by ultrasound doppler shift method; Int. J. Heat Fluid Flow; Vol. 7; pp. 313ff.

Takeda, Y. 1987 Measurement of velocity profile of mercury flow by ultrasound doppler shift method; Nuclear Technology; Vol. 79; p. 120-124.

Tillack, M.S. 1990 Magnetohydrodynamic flow in rectangular ducts. Design equations for pressure drop and flow quantity; UCLA-FNT-41.

Toschi, R.; Albanese, R.; Biggio, M.; Borrás, K. and the NET Team 1985 NET- status report December 1985; Commission of the European Communities-Directorate General XII-Fusion programme; Brussels; NET-Report 51.

Tsinober, A.; Kit, E.; Teitel, M. 1987 On the relevance of the potential difference method for turbulence measurements; Journal Fluid Mech.; Vol. 175; pp. 447-462.

Walker, J.S. 1981 Magnetohydrodynamic duct flows in rectangular ducts with thin conducting walls, Part I; Journal de Mécanique; 20; N° 1; pp.79-112.

APPENDIX A

event	7.00 open/ close	7.01 open /close	1.01 open/ close	NaK pump off	EM- pump off	Oil pump off	NaK cooler off	Cold trap cooler off	1.04	1.05 off	Alarm on	4.02 close	4.03 close	1.09 open	5.06 open	Magnet off
Shut down		open	open	x	x	x	x	x		x	x					x
loop leak		open	open	x	x	x	x	x			x					x
power off		open	O						O	x						
E5 max.		open		x	x	x	x	x	O	O						x
E4 min.		open*1		x	x	x	x	x	O	O						x
temp. NaK max.		O	O	x	x	x	x	x	O	O	x					x
temp. oil max.		O	O	x	x	x	x	x	O	O	x					O
argon min											x					
flow rate coolant water min.						x	x	x	O	O	x					O
temp. cold trap max												x	x			
airpres. min.		open	open	x	x	x	x	x	O	O	x					x
water flow rate magnet min.																x
E1 contact															x	
E2 contact	open															
E3 contact														x		

- x action
- O remain in current position
- *1 ignore Electrode E4 during filling procedure

Table A1: Operational/security program of the logic controller of the NaK1-loop.

Abbreviations, Variables and characteristic numbers

Abbreviations used

2D	two-dimensional
3D	three-dimensional
ADC	Analogue-Digital-Converter
AM	Asymptotic Model
ANL	Argonne National Laboratory
CELLO	name of the super-conducting magnet in MEKKA
CPU	Central Processing Unit (Zentralrecheneinheit)
Cu	Copper
CuNi	Copper-Nickel alloy, often called Constantan
DAC	Digital-Analogue-Converter
DIA/DAGO	Data acquisition software used in MEKKA
DNS	Direct numerical simulation
DEMO	planned Fusion reactor which should demonstrate the viability of fusion technology
DPA	displacements per atoms, a measure of the destruction of a material by neutrons
EM	electro-magnetic
FCI	Flow channel insert
FZK	Forschungszentrum Karlsruhe
Ga	Gallium
GALINKA	Gallium-Indium loop Karlsruhe
GEODYNAMO	Experimental facility being built up in FZK to demonstrate the development of the earth magnetic field
GIREDMENT	State Research and Design Institute of Rare Metals Industry of Russia
Hg	mercury
IATF	Institute for Applied Thermo- and Fluidynamics
ITER	planned experimental fusion reactor
K	potassium
LAS	Latvian Academy of Sciences (Lettische Akademie der Wissenschaften)
Li	Lithium (alkali metal)
MA	name of the normal-conducting magnet in MEKKA
MEKKA	Magnetohydrodynamic experiments in sodium potassium (in german: Kalium) Karlsruhe
MHD	magnetohydrodynamic

Na	Sodium
NaK	eutectic sodium-potassium alloy Na ²² K ⁷⁸
NaK1	name of the sodium-potassium loop
Ni	Nickel
NiCr	Nickel-Chrom alloy often called Chromel in terms of thermocouples
Pb	Lead
PC	Personal Computer
RS232	serial communication line of a personal computer
Sn	Tin
SIKKA	Experimental facility which demonstrates the flow control by means of steady and oscillating magnetic fields.
SPECTRA	steady state data acquisition system in MEKKA
TEMPO	combined temperature- and potential probe
TOKAMAK	operation principle of a fusion reactor

Vectors used

\vec{B}	magnetic induction
\vec{E}	electric field
\vec{j}	electric current density
\vec{n}	normal unity vector perpendicular to an area
\vec{v}	velocity vector

Variables in latin symbols (large fonts)

<u>Abbreviation</u>	<u>phys. Unit</u>	<u>Explanation</u>
A	[m ²]	Area of a specified domain
B_0	[Tesla]	magnetic field strength
$F_{Lorentz}$	[N]	Lorentz-force
I	[A]	electric current
H	[m]	pumping height of a pump
L_{COIL}	[Henry]	inductivity of a coil
P_{mech}	[Watt]	mechanical power
P_{ohmic}	[Watt]	ohmic dissipation in a domain
Q	[Watt]	source term in energy equation
Q	[/]	Nernst-Ettingshausen coefficient
P_g	[/]	galvano-magnetic coefficient
R_i	[Ω]	inner ohmic resistance
R_w	[Ω]	ohmic resistance of the wall

Abbreviation	phys. Unit	Explanation
S	[/]	Righi-Leduc coefficient
S_{al}	[Nm ⁻²]	maximum tolerable material stress
Se_i	[/]	Seebeck-coefficient
T	[K]	Temperature
U_{ind}	[Volt]	induced electric potential
\dot{V}	[m ³ /s]	volumetric flow rate in a duct

Variables in latin symbols (small fonts)

Abbreviation	phys. Unit	Explanation
a	[m]	half of duct height in magnetic field direction
acc	[unit]	accuracy of a measurement system
b	[m]	duct width perpendicular to magnetic field direction
c	[/]	wall conductance ratio
c_H	[/]	wall conductance ratio of the Hartmann wall
c_p	[J/(kg K)]	specific heat capacity of a fluid
d	[m]	diameter of circular duct
c_s	[/]	wall conductance ratio of side wall
j	[Am ⁻²]	electric current density
l	[m]	length of a duct
l_{dev}	[m]	developing length from 3D-flow to 2D-flow
p	[Pascal]	pressure
\dot{q}	[Wm ⁻²]	surface heat flux
r	[m]	radius
s	[m]	curved line coordinate
t	[s]	time
t_w	[m]	wall thickness of a duct
v_0	[m/s]	average flow velocity in a duct
x, y, z	[m]	cartesian coordinates

Greek symbols large

Abbreviation	phys. Unit	Explanation
Φ	[/]	dimensionless electric potential
Φ_w	[/]	dimensionless electric wall potential
χ	[m ² /s]	thermal diffusivity

Greek symbols small

<u>Abbreviation</u>	<u>phys. Unit</u>	<u>Explanation</u>
α	[W/(mK)]	heat transfer coefficient
α	[N/cm]	surface tension
β	[°]	inclination of a duct with respect to an axis
δ	[m]	thickness of a boundary layer
λ	[W/(mK)]	molecular thermal conductivity of a material
κ	[/]	dimensionless contact resistance at an interface
μ_r	[Vs/(Am)]	magnetic permeability of a material
μ_0	[Vs/(Am)]	magnetic permeability of vacuum
η	[/]	stretched boundary layer coordinate
η_{pump}	[/]	effectiveness of a pump
π	[/]	circle constant
ν	[m ² /s]	kinematic viscosity
ρ	[kg/m ³]	specific density of a fluid
σ	[A/(Vm)]	specific electric conductivity of a fluid
σ_w	[A/(Vm)]	specific electric conductivity of the duct wall
ω_B	[s ⁻¹]	vorticity of a flow in magnetic field direction

mathematical Operators

∇	gradient of a vector
∂	partial derivative of a vector
∂_i	partial derivative in direction i
Δ	laplacian $\Delta = \partial_{xx} + \partial_{yy} + \partial_{zz}$
$(\nabla \cdot)$	divergence of vector
$(\nabla \times)$	rotation applied to a vector
\times	cross product of two vectors

characteristic numbers

Bi	Biot number
M	Hartmann-number
N	Interaction parameter
Nu	Nusselt-number
Pe	Peclet-number
Re	hydraulic Reynolds number
Re_m	magnetic Reynolds number